

# Molecular functions of cell plate-associated phosphoinositides during plant somatic cytokinesis

## Dissertation

zur Erlangung des  
Doktorgrades der Naturwissenschaften  
„*doctor rerum naturalium*“  
(Dr. rer. nat.)

der

Naturwissenschaftlichen Fakultät I  
– Biowissenschaften –  
der Martin-Luther-Universität Halle-Wittenberg,



vorgelegt

von Herrn Feng Lin

geboren am 1. April 1986 in Jiangsu, China

Gutachter:

1. Prof. Dr. Ingo Heilmann
2. Prof. Dr. Bettina Hause
3. Prof. Dr. Karin Schumacher

Halle (Saale), September 5<sup>th</sup>, 2018

## Table of Contents

1. Introduction .....	1
1.1 Plant cell division .....	1
1.2 Membranes as structural barriers with regulatory roles .....	5
1.2.1 Synthesis of PtdIns4P .....	6
1.2.2 Membrane trafficking accompanied by PtdIns4P signaling .....	8
1.3 Endocytosis in plants .....	13
1.3.1 Common chemicals used for studying endocytosis .....	19
1.3.2 Endosomal compartments and their specific markers in plants .....	20
1.4 Mitogen activated protein kinase (MAPK) cascades in plants .....	24
1.5 Microtubules, MAPs and MAPKs .....	26
1.5.1 Control of microtubule dynamics by MAPs .....	28
1.5.2 Phosphorylation mediated regulation on microtubule dynamics .....	30
1.6 Cytokinesis requires membrane trafficking and cytoskeletal rearrangement .....	31
1.7 Aims and objectives .....	36
2. Material and methods .....	38
2.1 Plant materials .....	38
2.2 Sterilization of seeds .....	38
2.3 Plant growth conditions .....	38
2.4 Genotyping .....	38
2.5 DNA separation and purification .....	39
2.5.1 Agarose DNA gel electrophoresis .....	39
2.5.2 Extraction of DNA from gels .....	39
2.6 PCR strategies .....	39
2.6.1 Standard PCR .....	39
2.6.2 Colony PCR .....	40
2.6.3 Restriction free (RF) cloning .....	40
2.7 Manipulation of DNA constructs .....	41
2.7.1 Preparation of <i>E. coli</i> competent cells .....	41
2.7.2 Transformation of plasmids into <i>E. coli</i> .....	42
2.7.3 Extraction of plasmids from <i>E. coli</i> .....	42
2.7.4 Restriction enzyme digestion .....	42
2.7.5 DNA sequencing .....	42
2.8 Gateway LR reaction .....	43
2.9 Electrophoretic separation of proteins by sodium dodecyl sulfate polyacrylamide gel electrophoresis (SDS-PAGE) .....	43
2.10 Immunodetection of specific proteins (Western blotting) .....	44
2.11 Molecular cloning and plant transformation .....	44
2.12 Staining of cell walls .....	46
2.13 Generation of the Rabbit anti-AtPI4K $\beta$ 1 antibody .....	46
2.14 Whole-mount immunostaining .....	46

2.15 Determination of MAPK activity by immunocomplex kinase assays	47
2.16 Co-immunoprecipitation (Co-IP) from <i>A. thaliana</i>	48
2.17 Protein interaction analysis based on yeast two-hybrid (Y2H)	49
2.17.1 Yeast competent cells preparation	49
2.17.2 Yeast transformation	50
2.17.3 Yeast two-hybrid tests	50
2.18 Chemical treatments	51
2.19 Analysis of PtdIns4P levels by thin layer and gas chromatography	51
2.20 Phosphorylation assay	52
2.20.1 Protein expression and purification	52
2.20.2 In vitro phosphorylation assay	53
2.20.3 In vitro catalytic activity of PI4K $\beta$ 1 assay	53
2.21 Microscopy usage and data analysis	54
2.21.1 Confocal laser scanning microscopy (CLSM) and data analysis	54
2.21.2 Spinning disc microscopy and data analysis	56
2.21.3 Structured illumination super-resolution microscopy (3D-SIM)	57
2.22 Quantification of BFA bodies and dynamic microtubule parameters	57
3. Results	58
3.1 PI4K $\beta$ 1 is involved in cytokinesis and localizes to the cell plate	58
3.2 <i>pKNOLLE</i> -driven expression of PI4K $\beta$ 1 rescues the <i>pi4k<math>\beta</math>1 pi4k<math>\beta</math>2</i> double mutant phenotype	61
3.3 Endocytosis is impaired in the <i>pi4k<math>\beta</math>1 pi4k<math>\beta</math>2</i> double mutant	63
3.4 The <i>A. thaliana pi4k<math>\beta</math>1 pi4k<math>\beta</math>2</i> double mutant displays multinucleated cells and aberrant phragmoplasts	65
3.5 The microtubule-associated protein MAP65-3 mislocalizes in <i>pi4k<math>\beta</math>1 pi4k<math>\beta</math>2</i> double mutants, concomitant with phragmoplast stabilization	67
3.6 PI4K $\beta$ 1 and MPK4 interact genetically and physically in <i>A. thaliana</i>	70
3.7 MPK4 colocalizes with PI4K $\beta$ 1 at the cell plate but may precede PtdIns4P formation during somatic cytokinesis	73
3.8 Possible control of PI4K $\beta$ 1 by MPK4	75
3.9 Possible control of MPK4 by PI4K $\beta$ 1	77
3.9.1 MPK4 associates with BFA-sensitive membrane compartments	79
4. Discussion	82
4.1 Functional complementation of the <i>pi4k<math>\beta</math>1 pi4k<math>\beta</math>2</i> double mutant aids the analysis of PI4K $\beta$ s	82
4.2 PI4K $\beta$ 1/PtdIns4P at the growing cell plate is required for somatic cytokinesis in <i>A. thaliana</i>	82
4.3 Characterization of cytokinetic defects of the <i>pi4k<math>\beta</math>1 pi4k<math>\beta</math>2</i> double mutant	85
4.4 Regulatory interplay of MPK4 and PI4K $\beta$ 1	85
4.5 MPK4 activity is not a determinant for phenotypes of the <i>pi4k<math>\beta</math>1 pi4k<math>\beta</math>2</i>	

double mutant.....	88
4.6 MPK4 recycling from the cell plate associates with a BFA sensitive membrane trafficking pathway .....	89
4.7 Loss-of-function of <i>PI4Kβ1</i> and <i>PI4Kβ2</i> affects endocytosis .....	90
4.8 Unsuccessful transition of MAP65-3 in the <i>pi4kβ1 pi4kβ2</i> double mutant .....	91
5. Summary .....	93
6. References .....	94
7. Appendix .....	116
8. Abbreviations .....	129
Publications .....	134
Acknowledgements.....	135
<i>Curriculum vitae</i> .....	138
Erklärung/Declaration under Oath.....	140

## **1. Introduction**

Eukaryotic cells are complex structures and contain numerous subcellular compartments. These compartments enable the coordination of independent metabolic processes, including the processing of genetic information in the nucleus, the formation of proteins in the cytoplasm, and of secretory proteins in the endoplasmic reticulum, protein modification in the Golgi, energy metabolism in mitochondria, and - in plants - photosynthesis in chloroplasts. In the living cell, subcellular compartments maintain strictly controlled avenues of contacts, by which substance and information are exchanged between compartments. An important aspect of organellar function is their interaction, which involves the exchange of substances by vesicle trafficking as well as organelle movement. Both these processes are controlled by the cytoskeleton. This complex structure, consisting in plants mainly of actin and microtubules, provides a network of protein fibers, which can associate and dissociate in a dynamic manner, according to cellular requirements, thereby enabling the controlled movement of cellular components, their contacts and polarized distribution. In plants, the interplay of cytoskeletal dynamics and membrane trafficking are not well studied to date. In this thesis, the interplay of microtubule dynamics and membrane trafficking is elucidated in the context of complex cellular processes taking place during plant somatic cytokinesis.

### **1.1 Plant cell division**

Cell division is a process by which daughter cells inherit components such as cytosol matrix or chromosomes, from their mother cell. The division of somatic cells differs somewhat from that of generative cells. In generative cells, meiosis produces gametes with half of chromosomes from the parent cell, because only one round of DNA replication occurs during two rounds of cell divisions. During sexual reproduction, the number of DNA in the zygotes is recovered. In contrast to meiosis, the mitosis of somatic cells features one

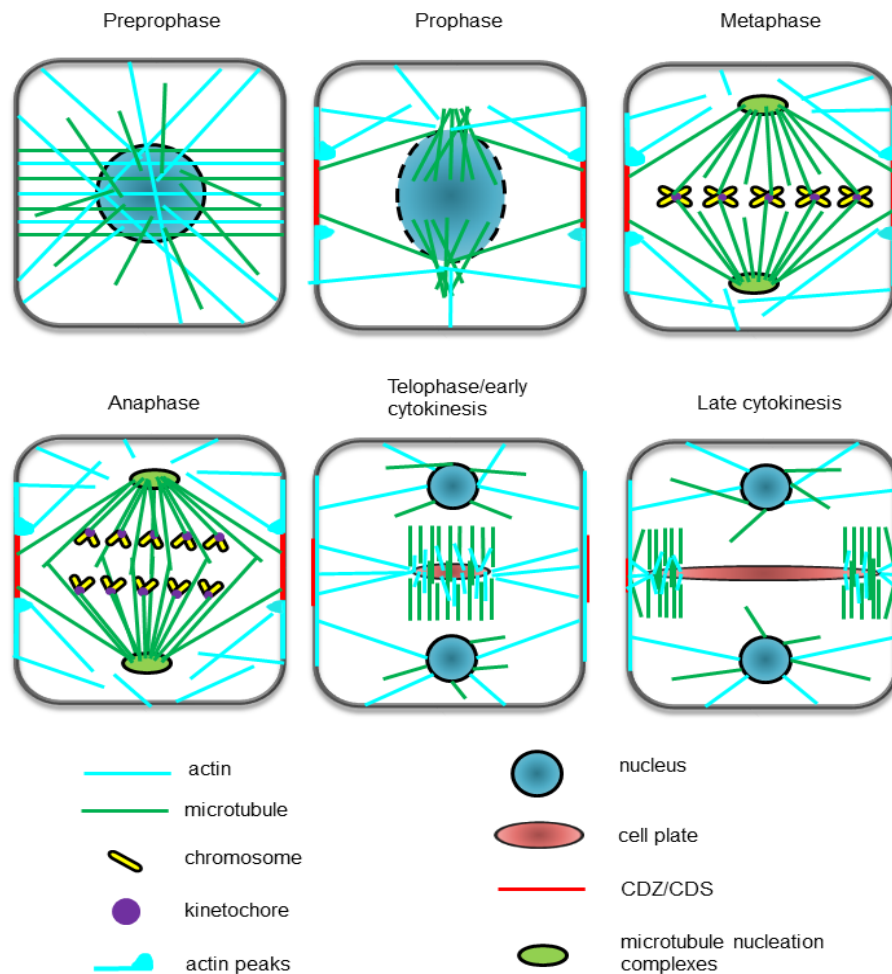


**Fig 1.1. Schematic of the stages of plant cell division.** Preprophase is characterized by a robust anti-parallel alignment of cytoskeletal elements, named the preprophase band (PPB). The PPB is composed of microtubules and actin. The PPB may recruit PHRAGMOPLAST-ORIENTING KINESIN 1 (POK1) and POK2 to establish the cortical division zone (CDZ), which will persist throughout mitosis. In addition, microtubules are also nucleated from the nuclear envelope, and actin bundles spread throughout the entire cell. In prophase, actin fibers are removed from the CDZ to form the actin depleted zone (ADZ), which is flanked by zones of F-actin enrichments to form actin peaks, and the PPB also disappears, leaving only few microtubules still contacting the CDZ. During nuclear envelope breakdown (black dashed line), perinuclear microtubules reach out from the spindle poles. Subsequently, chromatids are condensed to form chromosomes. The chromosomes are moved to the equator of the cell and attached to spindle microtubules by kinetochores. During anaphase, the spindle microtubules separate chromatids to the opposite poles of the cell. In telophase, the chromatids reach the poles of the cell and loosen again. The nuclear membrane is reformed. In the meantime, the cell plate initializes between mirrored microtubule arrays, termed the phragmoplast, which contains IMTs, nIMTs and actin. Actin reappears also at the CDZ, and contacts the cell plate. In late cytokinesis, the phragmoplast forms a ring-like structure, which radially expands outwards with the growing cell plate. The CDZ is narrowed down to give rise to the CDS which is connected by microtubules and actin to mediate the insertion of the cell plate. The figure is created based on review articles by Lipka et al., 2015; Müller and Jürgens, 2016.

round of DNA replication for each cell division. Therefore, somatic mitosis and cytokinesis absolutely increase the number of cells with faithful copies of the parental chromosomes. In contrast to other eukaryotes where mitosis consists of prophase, metaphase, anaphase, and telophase, in plant cells there is one additional stage, termed "preprophase" prior to prophase (Fig. 1.1).

Preprophase is the first stage of mitosis in plant cells in which a preprophase band (PPB) consisting of densely assembled anti-parallel actin and microtubules is formed underneath the plasma membrane (PM) (Müller and Jürgens, 2016; Vos et al., 2004). The PPB defines the cortical division zone (CDZ), which will form cortical division sites (CDS) that mark insertion sites for future cell plates (Van Damme et al., 2007). PPB microtubules form a belt-like band originating from cortical microtubules likely due to the involvement of phosphorylation-regulated activities of microtubule-associated proteins (MAPs) that alter microtubule dynamic instability (Müller and Jürgens, 2016). A critical protein complex for PPB formation is the TTP complex which contains the proteins TONNEAU1 (TON1) with similarity to a human centrosome protein and an essential role for microtubule organization at the cortex, TON1-recruiting motif proteins (TIRMs) that target TON1 to cortical microtubules, and the protein phosphatase 2A (PP2A) characterized by its unique B subunit TON2/FASS (Drevensek et al., 2012; Müller and Jürgens, 2016; Spinner et al., 2013). The TTP complex may thus act on downstream MAPs such as MICROTUBULE ORGANIZATION (MOR)1 in a phosphorylation dependent manner (Kirik et al., 2012) and malfunction of TTP complex components disrupts PPB formation (Rasmussen et al., 2013). The PPB is a transient marker for the plane of cell division and disassembles during prometaphase (Müller and Jürgens, 2016). How CDZs/CDSs are remembered after metaphase has commenced is still a matter of debate. It is plausible that the PPB serves as a platform to recruit proteins to the CDZ to mark sites for future insertion throughout mitosis. In favour of this model, some MAPs including kinesin-12 proteins

PHRAGMOPLAST-ORIENTING KINESIN (POK) 1 and POK2 are recruited to PPB in a microtubule-dependent manner and mark CDZ/CDS throughout mitosis and cytokinesis (Lipka et al., 2014; Müller and Jürgens, 2016; Rasmussen et al., 2011; Stöckle et al., 2016).

Prophase is the second stage of mitosis in which duplicated chromatins are gradually condensed to form chromosomes. During early prophase, the PPB disappears, and at late prophase, the nuclear envelopes and nucleoli are broken down. Concomitant with the disappearance of PPB microtubules, cortical actin is removed at the CDZ to form the actin-depleted zone (ADZ), which persists through the anaphase/telophase transition (Lipka et al., 2015; Müller and Jürgens, 2016; Van Damme et al., 2007).

The following metaphase is characterized by chromosomes moving to the equator of the dividing cell, and by the formation of the spindle microtubular structure. Spindle microtubules are attached to kinetochores of chromatids. The formation of the PPB is not the prerequisite for the spindle apparatus, as plant cells undergoing meiosis and even some somatic cells naturally lack a PPB but still are able to form bipolar spindles (Bannigan et al., 2008; Chan et al., 2005; Zhang and Dawe, 2011).

Anaphase is the next step, in which chromosomes are separated toward the poles of the cell by spindle microtubules (Lipka et al., 2015).

Telophase is the last stage of mitosis, in which the chromosomes reach the poles and form chromatids with some modifications. In the meantime, the nuclear envelopes reappear to encircle a set of chromatids and nucleoli also reform. A plant-specific microtubular structure containing interdigitating microtubules (IMTs) and noninterdigitating microtubules (nIMTs), termed the phragmoplast, is also formed, which derives from the mitotic spindle and serves as a track for vesicle delivery to give rise to the cell plate (Lipka et al., 2015; Müller and Jürgens, 2016). This thesis focuses mainly on events controlling the assembly of the phragmoplast.

After somatic mitosis, cytokinesis is the final step to separate the mother cell into two daughter cells, a process involving vesicle trafficking and cytoskeletal rearrangements (also see section 1.6).

## **1.2 Membranes as structural barriers with regulatory roles**

The body of each cell is defined by membranes. In plant cells, as in other eukaryotic cells, different membranes define compartments to execute specific functions without affecting other compartments. Thus, membranes are important elements of compartmentation and provide native barriers for the exchange of substances and information between inside and outside of cellular compartments. Membranes are formed in aqueous environments as bilayers of amphipathic lipids containing hydrophobic fatty acid tails and polar hydrophilic head groups. The body of plant membranes is mainly composed of structural glycerophospholipids, such as phosphatidylcholine or phosphatidylethanolamine, sphingolipids, such as inositolphosphorylceramides, and sterols, such as phytosterol. Thylakoid membranes of chloroplasts are predominantly formed by glycolipids, such as mono- or digalactosyldiacylglycerol. In addition to the structural components forming the membrane bilayer, membranes also contain minor amounts of phospholipids with regulatory functions. An example are polyphosphoinositides (PPIs), the phosphorylated derivatives of the membrane glycerophospholipid, phosphatidylinositol (PtdIns), which make up < 1 % of membrane phospholipids (Munnik and Nielsen, 2011) and play crucial roles in cellular activities. PtdIns contains the cyclitol, *D-myoinositol*, as a head group, which is attached via a phosphodiester bond to the C1 position of the lipid's glycerol backbone. PtdIns is synthesized by phosphatidylinositol synthase (PIS) from *D-myoinositol* and cytidine diphosphate diacylglycerol (CDP-DAG). The *Arabidopsis thaliana* genome encodes two PIS isoforms, PIS1 and PIS2 (Löfke et al., 2008), which are integral membrane proteins with four predicted transmembrane helices. PtdIns serves as a substrate for PPI biosynthesis (Gerth et al., 2017). The phosphorylation of hydroxyl groups at

positions D3, D4, and D5 of the inositol ring is catalyzed by specific lipid kinases, giving rise to different PtdIns monophosphates or PtdIns bisphosphates (Heilmann, 2016). The D2 and D6 positions of the head group cannot be phosphorylated, likely due to steric constraints (Gerth et al., 2017). The abundance of PPI species varies to a great extent between animals and plants, and only five of the seven PPIs known from other eukaryotes have been found in plants so far. These include the PtdIns-monophosphates, PtdIns 3-phosphate (PtdIns3P), PtdIns 4-phosphate (PtdIns4P) and PtdIns 5-phosphate (PtdIns5P); and the PtdIns bisphosphates, PtdIns 3,5-bisphosphate (PtdIns(3,5)P<sub>2</sub>) and PtdIns 4,5-bisphosphate (PtdIns(4,5)P<sub>2</sub>). The presence of PtdIns(3,4)P<sub>2</sub> and PtdIns(3,4,5)P<sub>3</sub> in plants has not been confirmed (Fig. 1.2) (Heilmann, 2016). Experiments in this thesis mainly address new functions of

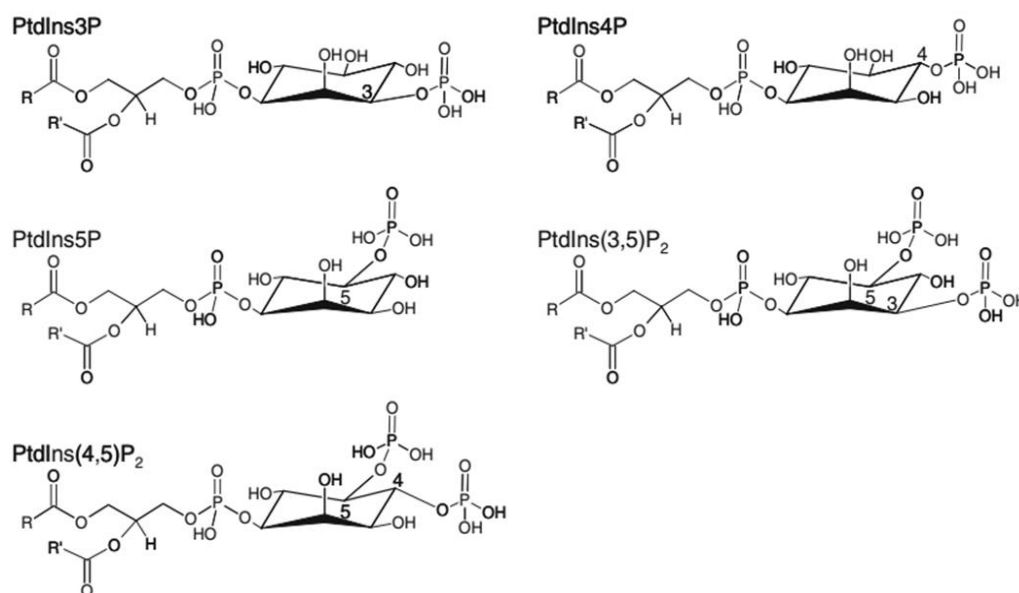


**Fig 1.2. Structure of PPIs in plants.** PPIs derive from PtdIns, a glycerophospholipid carrying an inositol head group. Phosphorylation of the D3, D4 or D5 positions of the inositol ring by different lipid kinases generates PtdIns3P, PtdIns4P, PtdIns5P, PtdIns(3,5)P<sub>2</sub> and PtdIns(4,5)P<sub>2</sub> in plants. The figure is modified from Ischebeck et al., 2010a.

the PPI, PtdIns4P, and this lipid will be introduced in more detail in the following paragraphs.

### 1.2.1 Synthesis of PtdIns4P

In plants, PtdIns4P is the most abundant PPI, accounting for ~ 80 % of total

plant PPIs (Munnik and Nielsen, 2011; Munnik and Vermeer, 2010). PtdIns4P is formed from PtdIns by enzymes of the phosphatidylinositol 4-OH kinase (PI4K) family, which in *A. thaliana* is comprised of the isoforms PI4K $\alpha$ 1, PI4K $\alpha$ 2, PI4K $\beta$ 1, and PI4K $\beta$ 2 (Heilmann, 2016). Eight further sequences with similarity to genes encoding PI4K $\alpha$  and PI4K $\beta$  families in the *A. thaliana* genome, namely PI4K $\gamma$ 1-PI4K $\gamma$ 8, do not encode gene products harboring lipid kinase activities. While no lipid substrate has been identified, PI4K $\gamma$ 3, PI4K $\gamma$ 4, PI4K $\gamma$ 5 and PI4K $\gamma$ 7 from *A. thaliana* show protein kinase activity *in vitro* (Akhter et al., 2016; Galvão et al., 2008; Tang et al., 2016), raising doubt whether PI4K $\gamma$ s are in fact lipid kinases. Based on their sensitivity to the inhibitors, adenosine and wortmannin, PI4Ks can be classified as type-II and type-III, respectively (Balla and Balla; Szumlanski and Nielsen, 2010). Based on these criteria, the PI4K $\alpha$ - and PI4K $\beta$ -families of Arabidopsis belong to the type-III PI4Ks (Balla and Balla, 2006; Ischebeck et al., 2010a; Mueller-Roeber and Pical, 2002). The yeast PI4Ks, Stt4p and Pik1p are homologous to the PI4K $\alpha$ - and PI4K $\beta$ -groups from *A. thaliana*, respectively. Interestingly, complementation studies in yeast have shown that Stt4p cannot be substituted by the Pik1p, and vice versa (Audhya et al., 2000), indicating that these enzymes are not functionally redundant. The PI4K $\alpha$  proteins from *A. thaliana* contain a pleckstrin homology (PH) domain that separates the lipid kinase unique (LKU) and the catalytic domains (Fig. 1.3) (Stevenson-Paulik et al., 2003; Stevenson et al., 1998). The PH domain of *A. thaliana* PI4K $\alpha$  is capable of binding several anionic lipids *in vitro*, including PtdIns4P and PtdIns(4,5)P<sub>2</sub>, but also phosphatidic acid (PtdOH) (Stevenson et al., 1998). Deletion of the PH domain results in the inhibition of AtPI4K $\alpha$ 1 activity and mislocalization of the AtPI4K $\alpha$ 1, suggesting a role for lipid-binding of the PH domain in regulating localization and activity of PI4K $\alpha$ 1 (Stevenson-Paulik et al., 2003). In contrast to PI4K $\alpha$ 1 with a length of 2028 AA, PI4K $\alpha$ 2 is smaller, only possessing 525 AA. The  $\beta$ -family of PI4Ks is comprised of PI4K $\beta$ 1 and PI4K $\beta$ 2, which are 1121 and 1116 AA in length, respectively, and contain an additional unique domain termed novel homology (NH) domain, which is

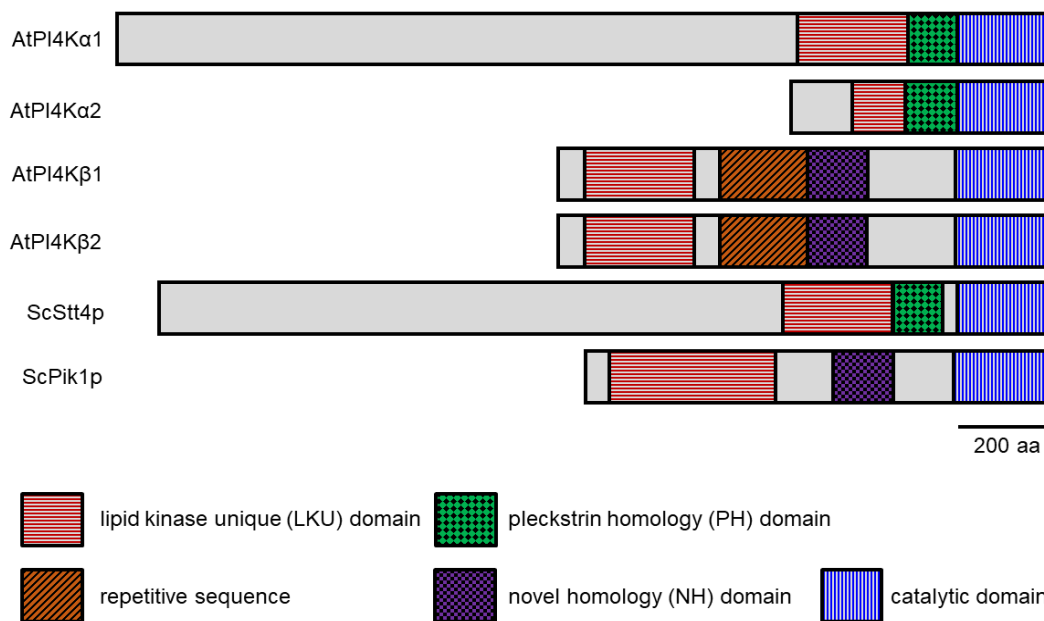


**Fig 1.3. Overview of the domain structures of PI4Ks from *A. thaliana* and yeast.** Sequence homology comparison among PI4Ks of *A. thaliana* and yeast (*Saccharomyces cerevisiae*) including AtPI4Kα1, AtPI4Kα2, AtPI4Kβ1, AtPI4Kβ2, ScStt4p, ScPik1p. Various domains are annotated, as indicated. The figure is created based on published descriptions (Heilmann and Heilmann, 2015; Stevenson-Paulik et al., 2003; Xue et al., 1999; Yamamoto et al., 2018).

conserved in yeast, animals and plants. The *A. thaliana* PI4Kβ isoforms also contain a repetitive motif unique to the PI4Kβs in *A. thaliana*, but lack a PH domain (Mueller-Roeber and Pical, 2002; Xue et al., 1999). The NH domain binds to a small GTPase-RabA4b, and the repetitive motif (also called plant PI4K charged (PPC) domain) is responsible to target PI4Kβs to the PM, possibly via binding to PtdOH, PtdIns, or PtdIns4P (Lou et al., 2006). The LKU domain of the yeast Pik1p (Fig. 1.3) associates with the frequenin homologue, Frq1, a 190-residue *N*-myristoylated calcium-binding protein (Hendricks et al., 1999). Likewise, the Ca<sup>2+</sup> sensor, AtCBL1, also interacts with the NH<sub>2</sub> terminus of PI4Kβ1 in *A. thaliana* (Preuss et al., 2006).

### 1.2.2 Membrane trafficking accompanied by PtdIns4P signaling

PPIs function as platforms to recruit proteins to specific membrane compartments or subdomains, giving rise to membrane identity. Furthermore, PPIs directly influence the biophysical properties of membranes, such as rigidity (unsaturated lipids), curvature (endocytosis), and the charge of the cytosolic

membrane leaflet (negative charge of PPIs) (Gerth et al., 2017; Santiago-Tirado and Bretscher, 2011). Several protein domains have been identified that bind to PPIs either specifically or with a broad affinity. Examples for PPI-binding protein domains with high selectivity include the PtdIns3P-specific FYVE domain, named after the yeast proteins: Fab 1 (yeast orthologue of PIKfyve), YOTB/ZK632.12, Vac 1 (vesicle transport protein), and EEA1 (early endosome antigen 1) (Gaullier et al., 1998; Jensen et al., 2001); the PH domain of human phospholipase C  $\delta$ 1 (PLC $\delta$ 1), which specifically binds to PtdIns(4,5)P<sub>2</sub> (Garcia et al., 1995); the PH domain of human phosphatidylinositol-four-phosphate adaptor protein-1 (FAPP1), which only binds to PtdIns4P (DOWLER et al., 2000). In *A. thaliana*, PtdIns4P can be visualized by specific biosensors based on the selective PtdIns4P-binding of the PH domain of FAPP1. Using such reporters, PtdIns4P has been found to be enriched at the PM, the trans-Golgi-network (TGN) and the cell plate (Simon et al., 2014; Simon et al., 2016; Vermeer et al., 2009). In yeast, PtdIns4P has been demonstrated to reside at the PM and the Golgi and additionally in transient membrane compartments involved in secretion and endocytosis (Audhya et al., 2000). The observation of PtdIns4P residing partially at the TGN (Simon et al., 2014), which in plants is a transitory compartment for secretion and endocytosis (Viotti et al., 2010), is consistent with several studies demonstrating that PtdIns4P is involved in the control of both secretion and endocytosis in plants (Fujimoto et al., 2014; Preuss et al., 2006).

### **1.2.2.1 The PtdIns4P pathway affects membrane trafficking in plants**

In yeast, Stt4p and Pik1p function nonredundantly in regulating membrane dynamics. While the PM-bound Stt4p is required for maintaining vacuole morphology, the Golgi-associated Pik1p regulates secretion, Golgi and vacuolar morphology, and endocytosis (Audhya et al., 2000; Walch-Solimena and Novick, 1999). Furthermore, in yeast PtdIns4P is also present in late

secretory vesicles to mediate vesicle association with and their transport by the myosin-V Myo2p (Santiago-Tirado et al., 2011). Similarly, in mammals the expression of a catalytically inactive variant of the mammalian Pik1p counterpart, PI4KIII $\beta$ , also alters the Golgi integrity and secretion (Godi et al., 1999). In mammals, PI4K $\beta$ /PtdIns4P appears to function in concert with small GTPases to regulate membrane trafficking (Di Paolo and De Camilli, 2006; Santiago-Tirado and Bretscher, 2011). The best-known case is the monomeric GTPase, ADP-ribosylation factor 1 (ARF1), which recruits and activates PI4KIII $\beta$  at the Golgi, thereby boosting PtdIns4P formation to maintain the structural integrity of the Golgi (Godi et al., 1999). ARF1 activation for PI4KIII $\beta$  recruitment may be mediated by a guanosine nucleotide exchange factor (GEF), for instance because the yeast Pik1p does not interact with ARF1 directly, but rather interacts with the ARF1-specific GEF Sec7p to control the recruitment of clathrin at the Golgi (Gloor et al., 2010). Later, Pik1p was found to be functionally involved in another GTPase-dependent signaling pathway to regulate the secretion of cargoes that require recycling through the early endosomes (EEs) (Sciorra et al., 2005). A functional link between PI4K and monomeric GTPases of the Rab family is further supported by evidence that PI4KIII $\beta$  binds physically to and recruits active Rab11 to the Golgi to mediate secretion at the PM (Burke et al., 2014; de Graaf et al., 2004). Functional interactions between PI4K $\beta$  and monomeric GTPases have also been reported for plants. For example, the TGN-localized small GTP-bound GTPase, RabA4b (a paralog of mammalian Rab11) interacts with AtPI4K $\beta$ 1 and AtPI4K $\beta$ 2 and recruits them to the TGN, mediating the formation of PtdIns4P for polarized secretion in growing root hairs of *A. thaliana* (Kang et al., 2011; Preuss et al., 2006). The involvement of PtdIns4P in the polarization of growing root hairs is further corroborated by knockdown of *root hair defective4 (RHD4)/suppressor of actin 7 (SAC7)*, which leads to abnormal morphologies of root hairs likely owing to elevated levels of PtdIns4P (Thole et al., 2008). Similarly, PtdIns4P synthesized de novo from PtdIns derived from the PIS2 is also involved in the

control of polarized growth of tobacco pollen tube via functional interplay with PI4K $\beta$ 1 and phosphatidylinositol-4-phosphate 5-kinase 5 (PIP5K5) to mediate pectin secretion (Ischebeck et al., 2010b).

In addition to their interplay with small GTPases, Arabidopsis PI4K $\beta$ s and PtdIns4P are also involved in other membrane trafficking pathways with unknown mechanisms, influencing the abundance of proteins, or through PtdIns4P binding directly to various proteins (Gronnier et al., 2017; Löffke et al., 2015; Naramoto et al., 2009; Stanislas et al., 2015; Tejos et al., 2014; Wu et al., 2017). PtdIns4P has also been shown to bind to the Arabidopsis EXOCYST subunit, AtEXO70A1, which is involved in exocytosis, and to Patellin 3 (PATL3) (Wu et al., 2017). The plant ARF-specific GTPase activating protein (ARF-GAP), VAN3, is localized to the TGN, and regulates auxin signal transduction via a TGN-mediated vesicle transport system, influencing the formation of the vascular network in leaves (Koizumi et al., 2005). Interestingly, PtdIns4P can bind to VAN3 and enhance the ARF-GAP activity, which is required for the continuity of plant vascular tissues (Naramoto et al., 2009). Eukaryotic membranes can contain membrane microdomains that are enriched in particular lipids, such as sterols and sphingolipids, together with some specific proteins. These membrane microdomains are thought to be involved in the control of diverse processes, including signal transduction, membrane trafficking, pollen tip growth, or intracellular virus movement (Brown and London, 2000; Lingwood and Simons, 2010; Liu et al., 2009; London and Brown, 2000; Raffaele et al., 2009; Simons and Toomre, 2000). In plants, PtdIns4P has been shown to be enriched in detergent-resistant membranes (DRMs) and form microdomains enriched in proteins such as plant REMORIN (REM), a membrane-bound protein involved in responses to biotic and abiotic stimuli (Furt et al., 2010; Gronnier et al., 2017; Gui et al., 2014; Jarsch and Ott, 2011).

PI4K $\beta$ s and PtdIns4P also regulate vacuolar trafficking. The abundance of

the vacuolar R-soluble NSF (N-ethylmaleimide-sensitive factor) attachment protein receptors (R-SNARE), vesicle-associated membrane protein 711 (VAMP711) is decreased upon auxin treatment and in the *pi4kβ1 pi4kβ2* double mutant (Löffke et al., 2015), suggesting that PI4Kβs and/or PtdIns4P are functionally involved in the control of dynamic vacuolar morphology and of its role in the generation of turgor pressure.

In contrast to intense studies focusing on the PtdIns4P involvement in secretion, a role in endocytosis is less well studied. Invaginations of the PM observed in pollen tube tips in consequence of overexpression of the PI4P 5-kinase isoform PIP5K6 and excessive clathrin-mediated endocytosis (CME) were partially rescued by cooverexpression of *PI4Kβ1* (Zhao et al., 2010), indicating that the balance between PtdIns4P and PtdIns(4,5)P<sub>2</sub> is essential for CME. AtPI4Kβs and/or PtdIns4P have previously been proposed to control CME, as inhibition of PI4Ks by phenylarsine oxide (PAO) (Vermeer et al., 2009) impairs the association of the cargo protein, cellulose synthase subunit A3 (CESA3) with clathrin foci at the PM and induces the aggregation of CESA3 (Fujimoto et al., 2014). However, pharmacological experiments may have uncertain side effects. Thus the role of PtdIns4P in endocytosis remains to be further investigated by genetic and more detailed cell biological approaches. In this thesis, molecular functions of PtdIns4P are addressed based on the cytokinesis defects described for the Arabidopsis *pi4kβ1 pi4kβ2* double mutant (Kang et al., 2011; Preuss et al., 2006). While this mutant has initially been characterized with a focus on polar tip growth of root hairs (Preuss et al., 2006), later prominent cytokinesis defects have been described (Fig. 1.4). However, so far these defects have not been rationalized and the molecular function of PtdIns4P in cytokinesis has remained unknown.

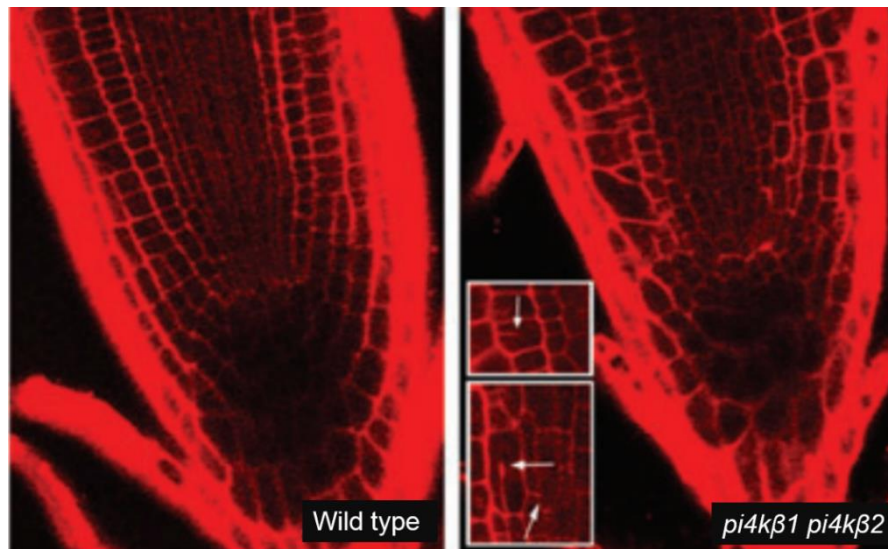


**Fig 1.4. The presence of cytokinetic defects in the *pi4kβ1 pi4kβ2* double mutants.** Wild type and double mutants were stained with propidium iodide. The *pi4kβ1 pi4kβ2* double mutants showed cell wall stubs (arrows), indicating failure of cytokinesis. The figure is modified from Kang et al., 2011.

### 1.3 Endocytosis in plants

Data presented in this thesis suggest a role for PtdIns4P in the control of endocytosis. Endocytosis refers to membrane trafficking events that internalize material from the PM or the apoplast. The EE is the first endomembrane compartment reached by endocytosed material. Then the material is sorted in the EE for distribution to various destined compartments, including recycling back to the PM or delivery to the lysosome or the vacuole for degradation (Bradford, 1976). Endocytosis is an important aspect in the control of abundance and type of PM proteins; for responses to external stimuli, such as changes of environment or nutrients; and for the recycling machinery for proteins after vesicle fusion (McMahon and Boucrot, 2011). Endocytosis is comprised of CME and clathrin-independent pathways, the latter involving the proteins caveolin and flotillin. In contrast to CME, which has been extensively studied and will be described in detail further down, much less is known about clathrin-independent endocytosis. In animals, flotillin and caveolin are both involved in clathrin-independent endocytosis. Flotillin and caveolin are topologically similar and are anchored into the membrane inner leaflet by acylation and hydrophobic hairpins (Otto and Nichols, 2011; Valencia et al.,

2016). In animal cells, the flotillin isoforms flotillin 1 and flotillin 2 co-assemble to form flotillin microdomains for the clathrin-independent endocytosis of specific cargoes, such as the GPI-anchored protein CD59 or the receptor for cholera toxin (Otto and Nichols, 2011). Plants possess flotillins, but no caveolins. *A. thaliana* flotillin 1 has been shown to form microdomains at the PM to function in seedling development via microdomain-dependent endocytosis cooperation with CME of cargoes such as respiratory burst oxidase homolog D (RbohD) (Hao et al., 2014; Li et al., 2012). Furthermore, flotillin-positive endocytic vesicles are around 100 nm in diameter, which is approximately three times larger than clathrin-coated vesicles (Li et al., 2012). Even though microdomain-dependent endocytosis is involved in regulating PM protein dynamics, the exact mechanisms remain largely unknown.

In contrast, the mechanisms of CME are well documented in both animals and plants. The discovery of CME dates back to the 1960s when the formation of 'bristle-coated' pits and vesicles was observed to mediate the uptake of yolk proteins in mosquito oocytes (Roth and Porter, 1964). Five years later, Kanaseki and Kadota (1969) further demonstrated that the 'bristle-coated' vesicles exhibited polygonal basket morphology, which was composed of pentagons and hexagons (Kanaseki and Kadota, 1969). Clathrin, the major component of the polygonal basket-coat of these vesicles, was first identified from pig brains (Pearse, 1975). Clathrin assembles into triskelia containing three legs which are comprised by one heavy chain and one light chain in each leg (Ungewickell and Branton, 1981). Clathrin-coated vesicles feature a three-layer structure, an outer layer represented by clathrin (clathrin lattice), an inner layer made up of membrane lipids and cargo proteins, and a layer of adaptor proteins-formed between the other two layers. The adaptor proteins have an important function in bridging between vesicle transport cargoes and the clathrin coat of the vesicle.

CME is composed of five steps, including i) nucleation, ii) cargo selection, iii) clathrin coat formation, iv) scission, and v) uncoating and recycling of coat components (Fig. 1.5) (McMahon and Boucrot, 2011). These stages are introduced in more detail in the following paragraphs.

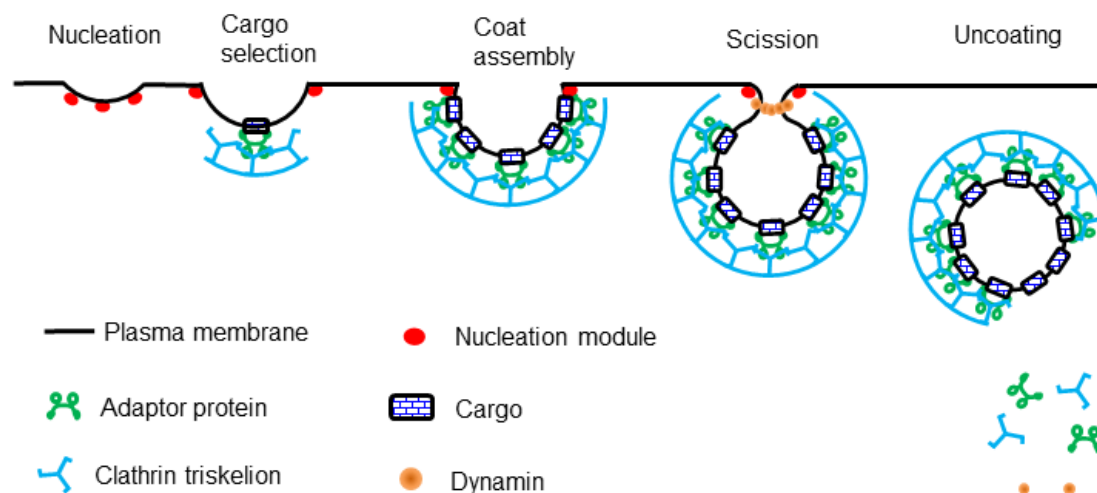


**Fig 1.5. The progression of CME.** CME is comprised of five steps including nucleation, cargo selection, coat assembly, scission, and uncoating. Nucleation induces membrane curvature and the recruitment of adaptor proteins. The recruited adaptor proteins subsequently bridge cargoes and clathrin coats together to assemble the clathrin coat. The clathrin coated vesicles are released by dynamin proteins constricting the neck of the vesicles. Clathrin coats and adaptor proteins are disassembled from released vesicles and recycled. The figure is recreated on the basis of the review article (McMahon and Boucrot, 2011).

i) **Nucleation:** Nucleation was initiated by recruitment of the adaptor protein 2 (AP-2) to the PM, triggering the formation of pits by membrane invagination in mammalian cells. This notion was challenged by the discovery of the nucleation module, which assembles prior to the recruitment of AP-2 and clathrin. The nucleation module of FES-CIP4 homology (FCH) domain ony (FCHO) proteins, epidermal growth factor receptor (EGFR) pathway substrate 15 (EPS15) and intersectins, is formed at the PM via binding to the PPI, PtdIns(4,5)P<sub>2</sub>, and functions as a “seed” to initiate the assembly of the CME machinery (McMahon and Boucrot, 2011).

ii) **Cargo selection:** After establishment of the nucleation module, AP-2 as well as cargo-specific accessory adaptor proteins are recruited to pits to select cargoes for endocytosis. Binding of AP-2 to cargoes occurs via cargo-sorting

motifs and involves the PM-localized PPI, PtdIns(4,5)P<sub>2</sub>. The AP-2 complex is a tetramer of two large subunits named  $\alpha$ - and  $\beta$ -adaptors, which directly bind to accessory adaptor proteins, a medium-subunit  $\mu$ -adaptor that selects cargo proteins by recognizing cargo sorting motifs, and the small-subunit  $\sigma$ -adaptor (Godlee and Kaksonen, 2013; McMahon and Boucrot, 2011; Traub, 2009). Two kinds of sorting motifs in the cytoplasmic tails of cargo proteins are recognized by the AP-2 complex, a YXX $\emptyset$ -type sorting signal (in which X is any amino acid and  $\emptyset$  a bulky hydrophobic amino acid), and a dileucine motif (McMahon and Boucrot, 2011; Traub, 2009). Phosphorylation of the  $\mu$ -adaptor by the adaptor-associated kinase 1 (AAK1) promotes binding of  $\mu$ -adaptor to cargo sorting motifs and to PtdIns(4,5)P<sub>2</sub>, effecting a switch from the “locked” conformation to the “open” conformation, in which the cargo sorting motif-YXX $\emptyset$ -binding domain is exposed (Traub, 2009). The YXX $\emptyset$  motif is now recognized by the  $\mu$ -subunit. This interaction can be inhibited by the drug, tyrphostin A23 (TyrA23), an inhibitor broadly used for the analysis of CME pathways in animals and plants (Banbury et al., 2003; Ortiz-Zapater et al., 2006). The [DE]XXXL[LIM] type acidic diLeu sequence differs from the YXX $\emptyset$ -type sorting signal as it is recognized by an  $\alpha$ - $\sigma$ -subunit hemicomplex of AP-2, and thus it does not compete with the YXX $\emptyset$  motif to bind to the AP-2 complex (Traub, 2009). In addition to the above cargo sorting motifs, there are also other sorting motifs, for example, an [FY]XNPX[YF] motif or an ubiquitin motif, which are recognized by cargo-specific accessory adaptor proteins rather than by the AP-2 complex itself. It should be noted that a cargo may have more than one sorting signal, as was shown for the mammalian low-density-lipoprotein (LDL) receptor-related protein 1 (LRP1) (Traub, 2009).

iii) Clathrin coat formation: In CME, clathrin does not bind to the cargo proteins directly, but rather binds to the adaptor proteins or the accessory adaptor proteins, as outlined above. After recruitment of the adaptor proteins (AP-2) or cargo-specific accessory adaptor proteins, the clathrin triskelia are

recruited from the cytosol to the PM by AP-2 or the accessory adaptor proteins to form the clathrin lattice representing the polymeric "coat" of clathrin-coated vesicles (CCVs). The formation of the clathrin lattice stabilizes the increased curvature of the PM of the forming vesicle to assist the membrane invagination and form the pit (McMahon and Boucrot, 2011).

iv) Scission: The deformation of the PM and the assembly of the clathrin lattice result in the formation of a CCV, which still remains connected to the PM by a narrow neck. Dynamins, large mechanochemical GTPases, are recruited to the neck by Bin–amphiphysin–Rvs (BAR) domain-containing proteins (McMahon and Boucrot, 2011). The hydrolysis of GTP favors the dynamin proteins to constrict the ongoing vesicle, pinching it off from the PM in the processes termed "scission" (McMahon and Boucrot, 2011; Young, 2007), and as a result, a CCV is released from the PM.

v) Uncoating and recycling of coat components: After a CCV has been separated from the PM, the clathrin coat is disassembled and the components are recycled back to the cytosol to allow the vesicle to fuse with the acceptor membrane. Disassembly of the coat involves the ATPase heat shock cognate 70 (HSC70) and its cofactor, auxilin. Subsequently, the intermediate layer holding the adaptor proteins is removed (McMahon and Boucrot, 2011; Young, 2007).

In mammalian cells, there are five adaptor protein complexes, AP-1 to AP-5. Except for AP-2, which is involved in CME, the other adaptor protein complexes mediate endomembrane budding. Like AP-2, the other complexes also each consist of four adaptin subunits, containing large  $\alpha/\gamma/\delta/\epsilon/\zeta$  and  $\beta$  subunits, a medium  $\mu$  subunit, and a small  $\sigma$  subunit (Fujimoto and Ueda, 2012; Hirst et al., 2011). The machinery for CME is thought to be well conserved across species and kingdoms, and components and functions of CME in plants can be deduced by analogy to the situation in animals. However, in plants many assumed details of mechanistic CME function remain to be experimentally

verified. So far, only AP-1 to AP-4 adaptor proteins have been described in plants (Park and Jürgens, 2012). AP-5 subunits, except for the  $\sigma$  subunit, have been identified only by sequence similarity to mammalian AP-5 (Hirst et al., 2011; Park and Jürgens, 2012). The current data indicate that *A. thaliana* AP-2 also functions in CME from the PM (Bashline et al., 2013; Fan et al., 2013; Yamaoka et al., 2013). While adaptor proteins and clathrin isoforms have, thus, been found in plants, the components of the nucleation module are still ambiguous. Recently, it has been proposed that the newly identified octameric TPLATE complex (TPC) from *A. thaliana* may exert a corresponding function, because components of the TPC, such as TPLATE, TWD40-1, TWD40-2, TPLATE-associated Src-homology 3 (SH3) domain containing protein (TASH3), Longin-like protein interacting with TPLATE adaptor (LOLITA), TPLATE complex muniscin-like (TML), Arabidopsis thaliana EPS15 homology (EH) domain containing protein 1 (AtEH1), and AtEH2, precede the recruitment of AP-2, clathrin, and dynamin proteins at the PM. Furthermore, TPC interacts with clathrins, AP-2, dynamin-related proteins (DRPs), and two AP180 N-terminal homology (ANTH) domain containing proteins including epsin-like clathrin adaptor 4 (AtECA4) and putative clathrin assembly protein 1 (CAP1) (Gadeyne et al., 2014). Moreover, some protein components resemble possibly mammalian counterparts, including AtEH1, and AtEH2, which contain conserved EH domains that are present in EPS15 Like-1 and intersectin1 in human; TASH3, which contains an SH3 domain; and TML, which possesses a  $\mu$  homology domain ( $\mu$ HD) involved in interacting with membrane, recognizing cargoes, recruiting accessory proteins (Gadeyne et al., 2014; Zhang et al., 2015). Nevertheless, to date FCHO-like proteins have not been identified in plants (Paez Valencia et al., 2016). Considering the trafficking function of CME, numerous proteins of plants have been demonstrated to be cargoes for CME, e.g., the auxin efflux transporters-PIN-FORMED (PIN) 1 and 2 required for the establishment of the tissue-transcending auxin gradient (Dhonukshe et al., 2007), the brassinosteroid receptor-BRASSINOSTEROID INSENSITIVE1

(BRI1), and cellulose synthase subunit A6 (CESA6), which is continuously endocytosed and recycled (Bashline et al., 2013; Di Rubbo et al., 2013; Miart et al., 2014). There are only few examples of membrane proteins, such as the Qa-SNARE Syntaxin of Plants132 (SYP132), which are stable at the PM and do not cycle (Reichardt et al., 2011). Upon budding from the PM, endocytosed proteins face two destinies, recycling back to the PM or delivery to the vacuole for degradation.

### 1.3.1 Common chemicals used for studying endocytosis

The lipophilic dye, (N-(3-triethylammoniumpropyl)-4-(6-(4-(diethylamino) phenyl) hexatrienyl) pyridinium dibromide) (FM 4-64), displays characteristic fluorescence only in a lipophilic environment, making it an ideal dye for cellular membrane systems. FM 4-64 is a common chemical used for tracking endocytic pathways, as it is incorporated first into the PM, undergoes endocytosis, and over time will label endomembrane compartments (Bolte et al., 2004).

Brefeldin A (BFA), a fungal toxin, is used to specifically disrupt membrane trafficking mediated by ARF-GEFs. All defined ARF-GEFs have a Sec7 domain, which is homologous to the yeast Sec7p and composed of around 200 amino acids, to exchange GDP for GTP. The Sec7 domain is the putative target of BFA, and BFA binding mediates ARF-GEF inhibition by stabilizing ARF-GDP-GEF intermediates, preventing the release of free ARF for further GTP exchange reaction and activation (Mansour et al., 1999; Peyroche et al., 1999). There are numerous ARF-GEFs in eukaryotic cells. For instance, the human genome encodes 15 ARF-GEFs, and 5 ARF-GEFs have been characterized in yeast. By contrast, the *A. thaliana* genome encodes eight ARF-GEFs (Anders and Jürgens, 2008). In plants BFA triggers an aggregation of endomembrane compartments surrounded by Golgi, which appears in the microscope as so called “BFA bodies” (Lam et al., 2009).

In *A. thaliana* only ARF-GEFs of the Golgi-specific brefeldin A-resistance guanine nucleotide exchange factor/Brefeldin A-inhibited guanine nucleotide-

exchange protein(GBF/BIG) family are found, comprising the GBF1-related GEFs GNOM (EMB30), GNOM-LIKE 1 (GNL1), GNL2 and BIG1-5 (Anders and Jürgens, 2008). Only GNL1 and BIG3 are BFA resistant, whereas others can be inhibited by BFA treatment (Richter et al., 2007; Richter et al., 2014). GNOM functions in recycling basal PM-localized proteins, such as PIN1. Originally, GNOM has been described to localize at the recycling endosome, mediating basal PM localization of PIN1 but not PIN2 (Geldner et al., 2003). However, in later studies using higher resolution microscopy, GNOM was found to reside at subdomains of the Golgi apparatus of (Naramoto et al., 2014). A minor portion of GNOM was also found at the PM, forming foci partially colocalizing with clathrin, likely to mediate endocytosis (Naramoto et al., 2010). GNL1 localizes to the Golgi and regulates ER-Golgi trafficking through coat protein 1 (COP1)-coated vesicle formation. Surprisingly, GNOM can rescue the *gnl1* phenotype, but not vice versa (Richter et al., 2007), suggesting partially functional redundancy of GNOM with GNL1. Based on genetic studies, GNL2 is critical for polar tip growth of root hairs and pollen tubes, but its subcellular localization remains unknown. Interestingly, GNL2 can partially or fully rescue polar recycling defects of *gnom* mutant (Jia et al., 2009; Richter et al., 2012), indicating partial functional overlap between GNL2 and GNOM. Among the BIG family, only BIG5 has been intensively investigated. BIG5, also known as BFA-visualized endocytic trafficking defective1, BEN1 or *A. thaliana* HopM interactors, AtMIN7, is localized to the TGN/EE and mediates pathogen responses and trafficking of endocytic cargoes at the TGN (Nomura et al., 2006; Tanaka et al., 2009; Tanaka et al., 2013). More recently, BIG1-4 were reported to function redundantly to regulate post-Golgi trafficking and the secretion of newly synthesized proteins from the TGN rather than recycling of endocytosed cargoes to the PM (Richter et al., 2014).

### **1.3.2 Endosomal compartments and their specific markers in plants**

Encytosed proteins are transported by membrane trafficking to their destinations via transit through endosomal compartments. Each endosomal compartment has its own specific identity, which can be distinguished by

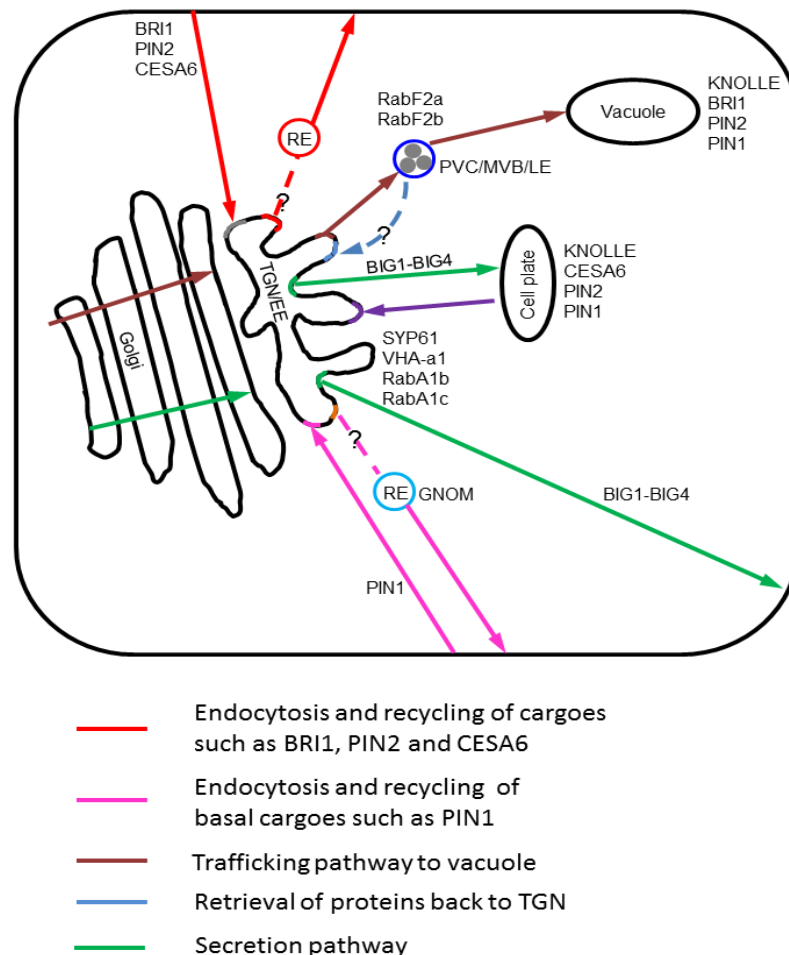


**Fig 1.6. Overview of membrane trafficking in plant cells.** Endocytosis and secretion both converge at the TGN/EE. Thus, the TGN has various subdomains to receive and secrete proteins. Cargo proteins such as BRI1, PIN2, CESA6 are endocytosed and recycled back to the PM via unidentified pathways, which are likely mediated by REs. Basal PIN1 protein is also endocytosed and recycled back to the PM via REs mediated by GNOM. De novo synthesized proteins are secreted to the PM mediated by BIG1 to BIG4 proteins through secretory vesicles labelled by some TGN-localized proteins such as SYP61, VHA-a1, RabA1b, RabA1c. The endocytosed proteins (e.g., KNOLLE, BRI1, PIN2, PIN1) can also be delivered to the vacuole for degradation through MVBs labelled by proteins such as RabF2a, and RabF2b. Some proteins (e.g., vacuolar sorting receptors, VSRs) are retrieved back to the TGN/EE from MVBs through unclear pathways. Protein targeting to the cell plate mainly depends on secretion pathways, and endocytosed proteins are also rerouted to secretory pathways. Cell plate-residing proteins are endocytosed back to the TGN, similar to proteins endocytosed from the PM. The figure is created based on the review from Park and Jürgens, 2012.

transmission electron microscopy and the labeling of unique markers residing

in the endosomal compartments, such as SNARE proteins, Rab GTPases, or others (Fig. 1.6).

### **1.3.2.1 TGN, an EE in plants**

The EE is the first compartment to receive proteins endocytosed from the PM. Other than in animals, where endocytosed proteins are passed to the EE for sorting, in plants the TGN, which derives from the maturation of trans-Golgi cisternae, directly functions as an EE. The TGN/EE is a separate compartment independent of Golgi in *A. thaliana* (Viotti et al., 2010). Thus, in plants both secretion and endocytosis converge at the TGN. This situation raises a question how cargoes are sorted in the TGN for further in-bound or out-bound trafficking. As several TGN markers do not completely overlap, it is currently believed that the plant TGN/EE contains distinct subdomains, which are involved in the sorting of different cargoes for trafficking (Chow et al., 2008; Qi and Zheng, 2013; Wattelet-Boyer et al., 2016). Commonly used TGN/EE markers include the vacuolar H<sup>+</sup>-ATPase subunit a1 (VHA-a1), the Qc-SNARE SYP61, RabA1b and RabA1c (Bassham et al., 2000; Dettmer et al., 2006; Qi and Zheng, 2013; Sanderfoot et al., 2001).

### **1.3.2.2 Multivesicular bodies (MVBs)/prevacuolar compartment (PVC)/late endosome (LE)**

MVB represents a prevacuolar compartment characterized by intraluminal vesicles, which is initiated by local endosomal sorting complex required for transport (ESCRT) mediating invagination of membrane away from the cytoplasm (Valencia et al., 2016). A main function of MVBs is to deliver cargo proteins for degradation to the lysosome or the vacuole (Park and Jürgens, 2012; Scheuring et al., 2011). In plants, fusion of MVBs with the tonoplast leads to the release of intraluminal cargoes into the vacuole. An example is the degradation of the Qa-SNARE (also known as syntaxin) KNOLLE, which is

degraded in the vacuole at the end of cytokinesis (Reichardt et al., 2007; Scheuring et al., 2011). The destiny of proteins going into MVBs is controlled by ubiquitination of cargoes, sorting of ubiquitinated cargoes to endosomes, and the formation and scission of intraluminal vesicles (Piper and Katzmann, 2007).

Commonly used markers for MVBs include ARA7/RabF2b, RHA1/RabF2a, or the Qa-SNARE SYP21 and SYP22 (Bottanelli et al., 2012; Lee et al., 2004; Shirakawa et al., 2010; Uemura et al., 2010).

### **1.3.2.3 Recycling endosome (RE)**

It is still debatable whether there is the RE in plants, as it has not been morphologically identified. However, several lines of evidence suggest that an RE may exist in plants. 1) In *A. thaliana* the BFA sensitive GEF, GNOM, is required for the recycling of PIN1 and PIN2 to the basal PM of the root (Geldner et al., 2003; Kleine-Vehn et al., 2008). Other proteins such as AUXIN-RESISTANT 1 (AUX1) are also recycled back to the PM independently of GNOM (Kleine-Vehn et al., 2006). 2) Recently it was proposed that endosomes labeled by RabA1E or RabA1G are REs due to their higher sensitivity to BFA compared to the TGN/EEs (Geldner et al., 2009). Together, these results imply distinct REs may exist in plants, but obviously the identification of the RE will require additional evidence. Overall, membrane trafficking in plants is as complex as in other eukaryotes. Importantly, plant membrane trafficking is coordinated with environmental or developmental cues. There is currently only limited information how signaling pathways transducing such cues are integrated with plant membrane trafficking. As this thesis is concerned with the interplay of protein kinase cascades and membrane trafficking, relevant protein kinases will be introduced in the following paragraphs.

## 1.4 Mitogen activated protein kinase (MAPK) cascades in plants

Some aspects described in this thesis are controlled by mitogen activated protein kinase (MAPK) cascades. MAPK cascades have been conserved in evolution among all eukaryotes. MAPK signaling decodes environmental and developmental cues, such as stress, pathogen invasion, differentiation, etc., to regulate intracellular responses. The activation of MAPK cascades can be triggered by stimuli from the inside or the outside of the cell. For instance, PM-localized receptors may trigger the phosphorylation of mitogen activated protein kinase kinase kinases (MAPKKKs, MAP3Ks, MEKKs); the activated MAP3Ks phosphorylate downstream mitogen activated protein kinase kinases (MAPKKs, MAP2Ks, MKKs, MEKs) through conserved serine and/or threonine residues in the S/T-X<sub>3-5</sub>-S/T motif located in the activation loop (T-loop) between kinase subdomains VII and VIII; then the terminal component of these cascades- mitogen activated protein kinases (MAPKs, MPKs) are dually phosphorylated on conserved serine and threonine residues in the T-X-Y motif in the T-loop by the upstream MAP2Ks (Cristina et al., 2010; Group et al., 2002; Meskiene and Hirt, 2000). The activated MAPKs then phosphorylate a variety of target proteins in the cell. These targets include channel proteins or transporters at the PM, various enzymes in the cytoplasm or transcription factors in the nucleus (Cristina et al., 2010; Yu et al., 2010).

In contrast to the yeast and mammals with only 6 and 13 MPKs, respectively (Meskiene and Hirt, 2000), plant MAPK cascades are more complex. There are 60 MAP3Ks, 10 MAP2Ks, 20 MPKs in *A. thaliana* (Group et al., 2002), which allow a wealth of combinations for each cascade. Plant MAPK cascades participate in a wide range of responses to different signals, such as pathogen invasion, salt and drought stress, hormone responses, mitosis and cytokinesis (Cristina et al., 2010). Each MAPK cascade is triggered by specific extra- or intra-cellular stimuli. Owing to the diversity of regulatory mechanisms for the activation of MAP3Ks (Meskiene and Hirt, 2000), and to

MAP2K being capable of phosphorylating 1-2 MAPKs, the MAPK cascades vary between responses (Meskiene and Hirt, 2000). In other words, some components may be shared by several MAPK cascades in response to different stimuli, and one MAPK cascade may be involved in several responses. For example, MPK3/6 are shared between a MEKK (MAP3K)-MAP2K4/5-MPK3/6-mediated ethylene synthesis pathway and a YODA (MAP3K)-MAP2K4/5-MPK3/6-controlled pathogen resistance pathway (Asai et al., 2002; Cristina et al., 2010; Djamei et al., 2007; Liu and Zhang, 2004). Moreover, YODA-MAP2K4/5-MPK3/6 is not only responsible for pathogen resistance, but also for the control of stomatal development (Cristina et al., 2010; Kanaoka et al., 2008; Lampard et al., 2008; Ohashi-Ito and Bergmann, 2006); MAP3K1-MKK2-MPK4 is involved in defense responses, SA synthesis, and ROS homeostasis (Andreasson et al., 2005; Cristina et al., 2010; Nakagami et al., 2006; Petersen et al., 2000; Qiu et al., 2008; Suarez-Rodriguez et al., 2007).

The diversity and flexibility of the plant MAPK network raises the questions how integrity and specificity of MAPK cascades are established and maintained, and how crosstalk of MAPK cascades is avoided. It has been demonstrated that intrinsic docking domains of MAPK cascades, scaffold proteins and phosphatases function together to confer specificity and integrity to MAPK cascades and avoid interference (Cristina et al., 2010). Most MAP2Ks have a docking domain which is a predominant determinant of the MAP2K-MAPK pathway in eukaryotes (Bardwell et al., 2001; Bardwell et al., 2009; Group et al., 2002) and preferentially bind to their cognate MAPKs instead of non-cognate MAPKs, e.g., the human c-Jun N-terminal kinase 1 (JNK1) binds to MKK4 and MKK7; AtMPK4 binds to MKK1 and MKK2 in *A.thaliana* (Bardwell et al., 2009; Cristina et al., 2010). How docking domains capture cognate MAPKs remains unknown. In comparison to docking domains, in other eukaryotic systems scaffold proteins are well investigated to control the specificity of MAPK cascades and also accelerate reaction rates. Many scaffold

proteins are found to regulate spatio-temporal assembly of MAPK cascades in yeast and mammals. However, only one scaffold protein for a MAPK cascade in *A. thaliana* has been identified so far, i.e., the receptor for activated C kinase 1 (RACK1) links G protein to MPK3/6 cascade to govern immunity system of *A. thaliana* through forming complexes with  $G_{\beta}$ , MEKK1, MKK4/5, and MPK3/6 (Cheng et al., 2015). MAPK phosphatases (MKPs) are also important regulators for the specificity and duration of MAP cascades. Protein tyrosine phosphatases (PTPs), dual-specificity (Tyr and Ser/Thr) phosphatases (DSPs) and PP2C phosphatases (a subfamily of serine/threonine phosphatases) are reported to dephosphorylate MAPKs in plants (Cristina et al., 2010; Kerk et al., 2002). There are only five MKPs encoded in the *A. thaliana* genome, namely AtMKP1, AtMKP2, DsPTP1, PROPYZAMIDE HYPERSENSITIVE 1 (PHS1) and indole-3-butyric acid response 5 (IBR5) (Lee et al., 2009).

### 1.5 Microtubules, MAPs and MAPKs

The cytoskeleton plays pivotal roles in membrane trafficking, but also in sensing environmental cues, in polarized growth, and in cell division in all eukaryotes (Bornens, 2008; Brandizzi and Wasteneys, 2013; Fletcher and Mullins, 2010; Gurel et al.; Šamaj et al., 2004; Yang, 2008). In contrast to animals, which possess microfilaments, microtubules and intermediate filaments, plants only have microfilaments and microtubules. Microtubules form tubular structures by polymerization of  $\alpha$ - and  $\beta$ -tubulins (Fig. 1.7). Microtubules have an inherent polarity conferred by head-to-tail assembly between the  $\beta$ -subunit of one tubulin dimer at one end connecting to the  $\alpha$ -subunit of the coming dimer, giving rise to plus ends (where only  $\beta$ -subunits are exposed) and minus ends (where only  $\alpha$ -subunits are exposed). Tubulin heterodimers are preferentially added to the plus ends of microtubules. The  $\alpha$ -tubulins of incoming tubulin dimers function as GTPase-activating proteins (GAPs) to hydrolyze GTP present on  $\beta$ -tubulins at the plus end. GTP-bound  $\beta$ -tubulins

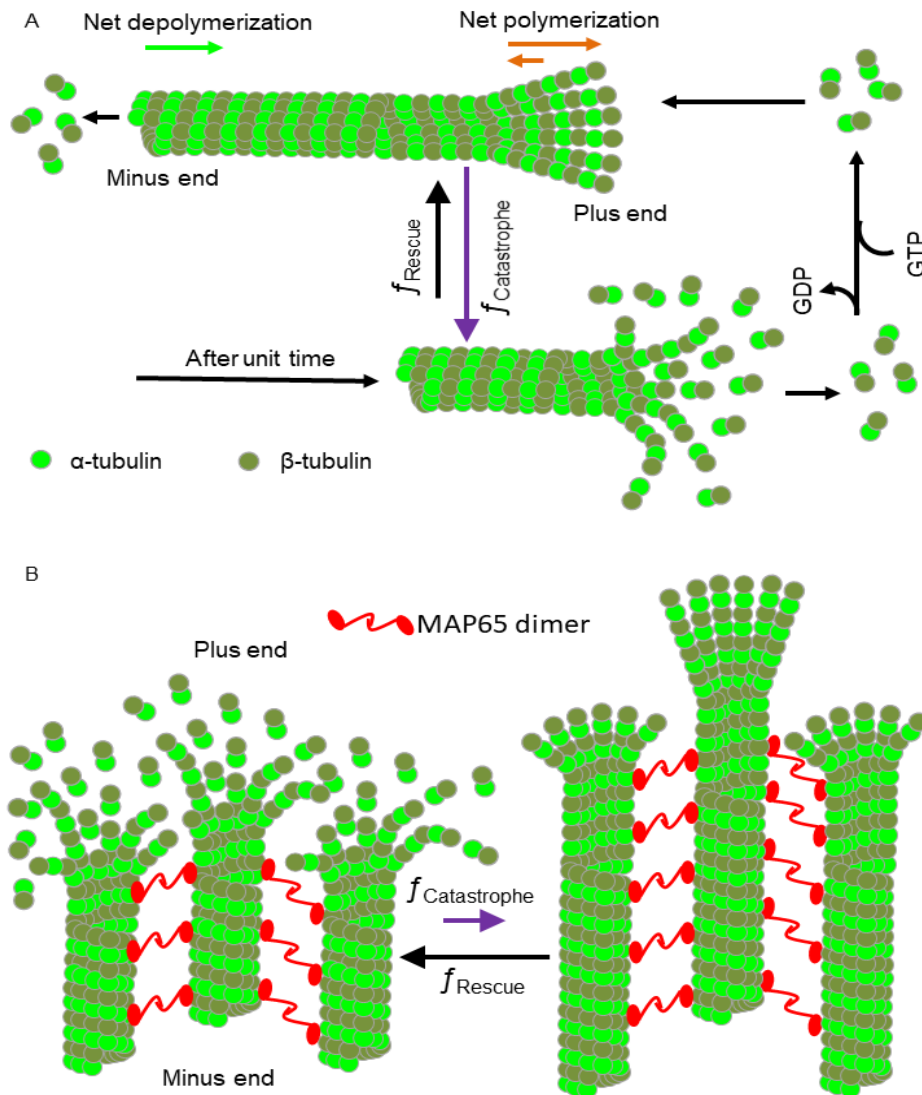


**Fig 1.7. Microtubule dynamic instability and bundling.** (A) Dynamic instability at the plus end and treadmilling. Tubulin dimers containing GTP-bound  $\beta$ -tubulin and  $\alpha$ -tubulin are polymerized at the plus end to give rise to microtubules consisting of 13 protofilaments. The  $\alpha$ -tubulin functions as a GAP to hydrolyze GTP present on  $\beta$ -tubulin of the plus end to form GDP-bound  $\beta$ -tubulin. Protofilaments containing GDP-bound  $\beta$ -tubulins are prone to spray out and depolymerize. GTP-bound  $\beta$ -tubulin at the plus end prevents protofilaments from being dissociated and depolymerized. Thus, GTP-bound  $\beta$ -tubulin function as a cap to promote growth of microtubules (also known as GTP-cap). Occasional loss of GTP-cap leads to depolymerization (i.e. catastrophe), whereas, accident gain of GTP-cap restores microtubule growth (i.e. rescue). GDP in free tubulin dimers is exchanged with GTP, and polymerized at the plus end. Polymerization happens at the plus end with addition of tubulin dimers, while depolymerization tends to happen at the minus end with release of tubulin dimers. When the depolymerization and polymerization are balanced, causing net addition at one end and net loss at the opposite end, which is termed as “treadmilling”. (B) Bundling of microtubules. Microtubules are bundled by proteins (MAP65 family proteins, etc.). The frequency of catastrophe and rescue may be decreased and increased by bundling, respectively (the case for MAP65-4). Thus the net length of microtubules is elongated. The figure is recreated based on the publications (Ehrhardt and Shaw, 2006; Fache et al., 2010; Hashimoto, 2003).

stabilize the plus end and promote its growth by forming GTP-cap. Occasional loss of GTP-cap results in rapid shortening at the plus end which is termed as catastrophe (transition from growth to shrinkage), while gain of GTP-cap restores microtubule growth at the plus end which is termed as rescue (transition from shrinkage to growth). Catastrophe and rescue are intrinsic parameters that confer dynamic instability to microtubules. In addition, microtubules also move through adding dimers to the plus end and concomitant removing at the minus end, a process called “treadmilling” (Ehrhardt and Shaw, 2006; Hashimoto, 2015). In addition to these, microtubule dynamics are also controlled by the action of microtubule-associated proteins (MAPs) (Fig. 1.7). These effects will be explained with a focus on microtubule arrays acting in plant cell division.

### **1.5.1 Control of microtubule dynamics by MAPs**

MAPs play important roles on controlling microtubule dynamics. For instance, MAP65/Anaphase spindle elongation 1 (Ase1)/PROTEIN REGULATING CYTOKINESIS 1 (PRC1) proteins mediate the crosslinking or bundling of adjacent microtubules; katanin proteins sever microtubules; and kinesin proteins may destabilize or stabilize microtubules. Among these MAPs, the MAP65 family has been extensively investigated. MAP65 proteins are conserved among all eukaryotes. Ase1 was the first MAP65 protein to be identified in yeast, where it localizes at the midzone of the anaphase spindle and is essential for spindle elongation during cytokinesis (Pellman et al., 1995). Subsequently, the Ase1 homologue from human, PRC1, was found to also localize to the midzone of the spindle and identified as a target for cyclin-dependent kinases (CDKs) (Jiang et al., 1998). The first MAP65 protein in plants was found in tobacco BY-2 cells and coassembles with and bundles microtubules, and it labels microtubules throughout the whole cell cycle (Chang-Jie and Sonobe, 1993). Smertenko and co-workers used MAP65

antisera to analyze a tobacco BY-2 cDNA library, identifying three MAP65 proteins, i.e., NtMAP65-1a, NtMAP65-1b, NtMAP65-1c which label both cortical and mitotic microtubules (Smertenko et al., 2000). Further MAP65 family members were uncovered upon completion of the genomic sequence of *A. thaliana*. Nine MAP65 proteins are encoded in the *A. thaliana* genome (Hussey et al., 2002), and their biological functions have been investigated *in vitro* and *in vivo*. AtMAP65-1 interacts with microtubules through its C-terminal two microtubule binding regions (MTBs) in which Ala409 and Ala 420 residues are key determinants for binding to microtubules. AtMAP65-1 is able to crosslink adjacent microtubules via dimerization mediated by its N-terminus (Mao et al., 2005; Smertenko et al., 2004; Smertenko et al., 2008). Although MAP65-1 has a capacity to bundle antiparallel microtubules, it remains debated whether MAP65-1 can promote microtubule polymerization (Mao et al., 2005; Smertenko et al., 2004; Tulin et al., 2012). MAP65-2, which is functionally redundant with MAP65-1 (Lucas et al., 2011), can also promote the bundling of microtubules, but its role in microtubule polymerization is also still controversial (Li et al., 2009; Smertenko et al., 2008). MAP65-3 crosslinks antiparallel microtubules at the midline of the phragmoplast (see also section 1.6) to form IMTs for cytokinesis, and it may promote microtubule polymerization (Ho et al., 2011; Smertenko et al., 2008). By contrast, MAP65-4 bundles both antiparallel and parallel microtubules to enable elongation of kinetochore microtubule bundles by lowering and increasing the frequency of catastrophe and rescue events, respectively. This function is somewhat in contradiction to Smertenko and colleagues' finding, where little signal of MAP65-4 decorated mitotic spindle microtubules in immunostaining experiments (Fache et al., 2010; Smertenko et al., 2008; Van Damme et al., 2004). MAP65-5 can induce microtubule bundling *in vivo*, conferring resistance to microtubule-depolymerizing drugs, and it also promotes microtubule polymerization (Smertenko et al., 2008; Van Damme et al., 2004). By contrast, the mitochondria-associated MAP65-6 appears in dot-like patterns in microscopic images and induces microtubules to form mesh-like

networks, apparently displaying neither bundling nor polymerizing activities (Mao et al., 2005). Little is currently known about MAP65-7, which only was shown to label cortical microtubules in tobacco cells. MAP65-8 and -9 do not decorate microtubule structures in dividing cells by immunostaining experiments reported so far, and their function remains unknown (Smertenko et al., 2008).

### 1.5.2 Phosphorylation mediated regulation on microtubule dynamics

It is well documented that phosphorylation on tubulin subunits or MAPs directly or indirectly affects microtubule dynamics and organization (Holmfeldt et al., 2009; Sasabe et al., 2006; Wloga and Gaertig, 2010). In mammals, phosphorylation of tyrosines at the C-terminus of  $\alpha$ -tubulins by insulin receptor kinase or of Ser172 residues of  $\beta$ -tubulins by cyclin-dependent kinase1 (CDK1) prevents tubulins from being incorporated into microtubule polymers (Fourest-Lieuvain et al., 2006; Wandosell et al., 1987). Similarly, both phosphorylation-dead and phosphorylation-mimic variants of the conserved Ser172 of  $\beta$ -tubulin alter microtubule dynamics and affect cell division in yeast (Caudron et al., 2010). The microtubule-associated proteins MAP4 from human and the *Xenopus* homologue (p220, also called XMAP4) can be phosphorylated by the corresponding protein kinases, cdc2 kinase and p34<sup>cdc2</sup> kinase, respectively. These phosphorylation events mediate a decrease in microtubule-binding affinity of MAP4 during mitosis (Ookata et al., 1997; Shiina and Tsukita, 1999). Cdc2 is furthermore able to phosphorylate PRC1 to inhibit its microtubule-bundling activity in metaphase, whereas during anaphase the dephosphorylation of PRC1 promotes bundling of interdigitating antiparallel microtubules in the midzone that is essential for cytokinesis (Mollinari et al., 2002; Zhu et al., 2006). Nevertheless, the yeast PRC1 homologue Ase1 differs from human PRC1 in its effects on microtubule organization, i.e., it regulates the integrity of spindle microtubules through cell cycle-specific degradation by Anaphase-promoting Complex (APC) (Juang et al., 1997). A mechanism similar

to PRC1-mediated control of cytokinesis in mammals was also found in plants. In tobacco BY-2 cells, the nucleus- and phragmoplast-localized protein kinase 1 (NPK1)-activating kinesin-like proteins (NACKs) directly bind to and activate the MAPKKK, NPK1 (Nishihama et al., 2002; Sasabe and Machida, 2012). The activated NPK1 triggers phosphorylation of downstream components of the cascade, such as the MAPKK, NQK1 (Soyano et al., 2003), and the MAPK, NRK1. The NRK1 then phosphorylates the NtMAP65-1a to decrease its capacity of bundling microtubules to facilitate turnover and expansion of the phragmoplast (Sasabe et al., 2006). This pathway is named the NACK-PQR pathway and is inactivated by CDKs phosphorylating NACK1 and NPK1 to prevent their interaction before metaphase, and activated by dephosphorylation of NACK1 and NPK1 via inactivation of CDKs and activation of unknown phosphatases after metaphase to allow the interaction between these two proteins that are critical for the progression of cytokinesis (Sasabe et al., 2011a). This aspect differs from direct actions of CDKs on MAP4 or PRC1 to control cytokinesis (Mollinari et al., 2002; Ookata et al., 1997; Shiina and Tsukita, 1999; Zhu et al., 2006). All counterparts for the tobacco pathway have been identified in *A. thaliana*, including sequential action of the proteins HINKEL/STUD (homologues of NACK1 and NACK2) activating a MAPK cascade consisting of ANP1-3 (MAPKKKs), MKK6/ANQ, MPK4, and finally MPK4 phosphorylates the targets MAP65-1, MAP65-2 and MAP65-3 that are supposed to promote phragmoplast expansion (Beck et al., 2010; Sasabe et al., 2011b; Strompen et al., 2002; Takahashi et al., 2010; Tanaka et al., 2004). Direct phosphorylation on tubulin subunits also exist in plants, but will not be discussed in detail here.

## **1.6 Cytokinesis requires membrane trafficking and cytoskeletal rearrangement**

Cytokinesis is the final step of cell division to separate a mother cell into two daughter cells, both in animals and plants. In contrast to inward constriction

of cytokinetic cells in animals, plant cells cytokinesis adopts a specialized strategy because of the presence of plant cell walls, and involves the formation of the cell plate as a plant-specific membrane compartment for cell division (Jürgens, 2005; McMichael and Bednarek, 2013). In early telophase, the cell plate initiates between the phragmoplast, which provides guidance to membrane trafficking events delivering and recycling membrane vesicles to and from the expanding cell plate. After its insertion in the cortical division site, the cell plate will mature and incorporate new PM and cell wall material. During this process, the phragmoplast expands radially outward around the growing cell plate, transiting from a solid to a ring-like structure. Although details of their cell division machineries differ, in both animals and plants membrane trafficking and cytoskeleton rearrangements are necessary and critical for successful cytokinesis (D'Avino et al., 2005; McMichael and Bednarek, 2013).

It is believed that during cytokinesis both newly synthesized and endocytosed proteins are delivered to the cell division plane (Dhonukshe et al., 2006; Miart et al., 2014; Reichardt et al., 2007). In general, secretion occurs by default to deliver Golgi-derived vesicles to the cell plate for fusion and, thus, secretion plays a critical role in cytokinesis in plants. For instance, KNOLLE is only newly synthesized and secreted to the cell plate (Reichardt et al., 2007). Whether endocytosis is essential for cell plate formation is still controversial. For instance, inhibition of ER-Golgi trafficking or trafficking at the TGN disrupted cytokinesis, whereas inhibition of endocytosis had no effect on cell plate formation (Reichardt et al., 2007). It is now clear that during cytokinesis the recycling of PM proteins is strongly reduced, so that most recycling proteins are routed via the secretory pathway to the cell plate mediated by BIG1-BIG4, with the exception that PIN1 can be polarly recycled back to the basal PM mediated by GNOM (Müller and Jürgens, 2016; Richter et al., 2014). Protein retrieval from the cell plate is another respect to regulate membrane remodeling during cell plate formation. CME is a key pathway to remove proteins from the cell

plate and is involved in cell plate expansion and maturation. Dynamins, clathrins and CCVs are all found at or in close proximity to the cell plate during late stages of cell plate formation (Ito et al., 2012; Seguí-Simarro et al., 2004). *A. thaliana* mutants with defects in dynamin-related protein1A (*drp1a* (also known as *rsw9*) show cytokinetic defects, such as incomplete cell walls, and curved cell plates (Collings et al., 2008). Correct restriction of KNOLLE at the plane of cell division depends on clathrin and DRP1A which are influenced by sterol-containing membrane areas (Boutté et al., 2010), and is endocytosed during late cytokinesis from the cell plate to the vacuole via MVB-mediated trafficking for degradation (Boutté et al., 2010; Reichardt et al., 2007). The recently identified protein complex TPLATE has been detected at the PM and the cell plate and functions in concert with the AP-2 complex to regulate endocytosis in *A. thaliana*. Knock down of *TPLATE* results in ectopic callose deposition and cell wall modifications and cytokinetic defects (Gadeyne et al., 2014; Van Damme et al., 2006). Together, these examples highlight the importance of membrane trafficking, exocytosis and endocytosis for cytokinesis.

Equally important for cytokinesis are dynamic cytoskeletal rearrangements specifically those of microtubule arrays. An early study reported that inhibition of microtubule depolymerization by taxol blocked the lateral expansion of the phragmoplast and the cell plate (Yasuhara et al., 1993). Subsequently, it was shown that cytokinetic defects, as obvious from cell wall stubs and multinucleated cells, arose in consequence of impaired lateral expansion of the phragmoplast (Nishihama et al., 2002; Sasabe et al., 2006; Strompen et al., 2002). Inactivation of components of the NACK-PQR pathway abolishes the progression of cytokinesis. Specifically, disrupting the recruitment of NPK1 to the cell plate by NACK1 upon expression of a dominant-negative truncated variant of NACK1, or the introduction of a kinase-negative variant of NPK1 both inhibited lateral expansion of the cell plate, resulting in incomplete

cell walls and the formation of multinucleated cells (Nishihama et al., 2001; Nishihama et al., 2002). The importance of MAPK-dependent control of microtubule arrays for cytokinesis is supported by numerous studies. The overexpression of kinase-negative NQK1 in tobacco cells impaired cytokinesis and resulted in cytokinetic defects (Soyano et al., 2003). Similarly, the overexpression of a variant of NtMAP65-1a that cannot be phosphorylated by NRK1 overstabilized microtubules and blocked lateral expansion of the phragmoplast, causing the appearance of cytokinetic defects (Sasabe et al., 2006). The impairment of the homologous proteins in *A. thaliana* disrupts cytokinesis as well. NACK1 counterparts- HINKEL and STEUD function redundantly to regulate gametogenetic cytokinesis (Nishihama et al., 2002; Strompen et al., 2002; Tanaka et al., 2004). While the Arabidopsis MAPKKs ANP1 - ANP3 are redundant and single mutants do not show cytokinetic defects, double mutants, such as *anp1 anp3* show defective cell growth in hypocotyls and *anp2 anp3* displays cytokinetic defects beside the phenotype observed for *anp1 anp3* (Krysan et al., 2002). Altered microtubule bundles resulted in broad cellular defects, including branching of root hairs and swelling of epidermal cells in *anp2 anp3* in *A. thaliana* (Beck et al., 2010). Mutations in the *A. thaliana* *MPK4* gene affect not only cortical microtubule organization but also mitotic microtubule transition, resulting in cytokinetic defects in addition to phenotypes which are similar to *anp2 anp3* (root hairs and epidermal cells). Phosphorylation of MAP65-1 is also diminished in the *A. thaliana* *mpk4-2* mutant and the abundance of the proteins MAP65-1 and MAP65-3 increased and decreased, respectively (Beck et al., 2010). Transcription of MPK11, which belongs to the same subgroup of MAPKs as MPK4, is elevated in *mpk4-2*, and *mpk4-2 mpk11* double mutants have more severe cytokinetic defects compared to single mutants (Beck et al., 2010; Beck et al., 2011; Kosetsu et al., 2010). Although the individual *map65-1* or *map65-2* mutants and the *map65-1 map65-2* double mutant do not display cytokinetic defects (Lucas and Shaw, 2012; Lucas and Shaw, 2012; Sasabe et al., 2011b), the expression of a

AtMAP65-1 variant that cannot be phosphorylated in tobacco cells delays the transition from metaphase to anaphase (Smertenko et al., 2006). Moreover, the *map65-1 map65-3* or *map65-2 map65-3* double mutants cause more severe cytokinetic defects than the *map65-3* single mutant (Sasabe et al., 2011b). As the swapping of an extended C-terminal microtubule binding region of MAP65-3 to MAP65-1 partially rescues cytokinetic defects in *map65-3 (dyc283)* mutant (Ho et al., 2011; Ho et al., 2012; Lucas and Shaw, 2012; Müller et al., 2004; Sasabe et al., 2011b; Smertenko et al., 2006), it appears that MAP65-1 and MAP65-2 function partially redundantly with MAP65-3 in mitosis and cytokinesis. Evidently, microtubular bundling by MAP65 isoforms and its control by MAPKs are important aspects of the regulation of plant cell division. Considering the assumed role of cytokinetic microtubule arrays in the direction of membrane trafficking, it is important to ask how MAPKs, microtubules and membrane trafficking are integrated.

In plant cells, the transition of the phragmoplast from a solid to a ring-like array drives vesicles delivered along phragmoplast microtubules from the center towards the leading edges of the cell plate, resulting in their fusion and leading to the cell plate growing outward. Membrane trafficking during formation, expansion and maturation of the cell plate is highly controlled and selective, and also coordinates well with phragmoplast expansion, yet little is known about how membrane trafficking functions in spatiotemporal concert with phragmoplast lateral expansion. The Sec/Munc18 KEULE, which binds to the open form of KNOLLE to enable it to form *trans*-SNARE complexes with three other SNAREs, mediating membrane fusion (Park et al., 2012), is required for phragmoplast reorganization during cytokinesis in *A. thaliana*. Mutation in the *KEULE* gene compromises phragmoplast reorganization to form solid phragmoplasts during late cytokinesis (Steiner et al., 2016a). MAP65-3 can interact with the tethering factors TRS120 and TRS130/CLUB of Transport Protein Particle II (TRAPP II) that tether and dock vesicles for membrane fusion

(Qi et al., 2011; Rybak et al., 2014) and link membrane trafficking and microtubule reorganization. However, this interaction does not affect the recruitment of either MAP65-3 or TRAPP II (Steiner et al., 2016b). Although membrane trafficking and phragmoplast reorganization are functionally connected, the exact mechanisms remain unknown.

Membrane trafficking in all eukaryotes is controlled by phosphoinositides, which have important functions in the regulation of endomembrane trafficking. As was outlined in section 1.2.2, PtdIns4P is such a lipid residing at the TGN and the cell plate. The *pi4kβ1 pi4kβ2* double mutant displays a dwarf phenotype accompanied by cytokinesis defects (Kang et al., 2011; Preuss et al., 2006). PtdIns4P also negatively regulates chloroplast division in a PLASTID DIVISION1 (PDV1)- and DYNAMIN-RELATED PROTEIN5B (DRP5B)-dependent manner (Okazaki et al., 2015). These examples indicate that PtdIns4P is involved in the regulation of cell or organelle division. However, so far the molecular mechanisms of this influence remain to be elucidated.

### **1.7 Aims and objectives**

This thesis is dedicated to elucidate how the minor membrane lipid PtdIns4P influences cytokinesis in *A. thaliana*. Different experimental approaches were combined to uncover the roles of PtdIns4P in cytokinesis, including genetic complementation, whole-mount immunostaining, genetic segregation analysis, Co-IP, BFA treatments, and imaging of fluorescence tagged proteins by laser scanning confocal microscopy and spinning disc microscopy. The main goals were:

- 1) to determine whether or not PtdIns4P was involved in cytokinesis and which kind of cytokinetic defects were caused by loss-of-function of *PI4Kβ1* and *PI4Kβ2*;
- 2) to identify potential molecular targets for the PtdIns4P pathway;
- 3) to test whether these potential targets take part in membrane trafficking

mediated by PtdIns4P;.

4) to uncover which mechanism is responsible for PtdIns4P controlling cytokinesis through affecting the potential target with the aid of whole-mount immunostaining.

## 2. Material and methods

### 2.1 Plant materials

All *A. thaliana* lines used in this thesis were in the Columbia-0 background and wild type (Columbia-0, Col-0) was used as a control. *pi4kβ1* (Preuss et al., 2006) (SALK\_040479), *pi4kβ2* (Preuss et al., 2006) (SALK\_098069), *pi4kβ1×β2* (Preuss et al., 2006) were used as described before. The lines GFP-*PLE/*MAP65-3 (Steiner et al., 2016a), MPK4-YFP (Berriri et al., 2012), mCherry-TUA5 (Endler et al., 2015), mRFP<sub>FAPP1-PH</sub> (Vermeer et al., 2009), CLC2-GFP (Konopka et al., 2008) in this study have been described previously. *mpk4-2* (SALK\_056245) was obtained from the Nottingham Arabidopsis thaliana Stock Centre (NASC, UK). GFP-MAP65-3, MPK4-YFP, mCherry-TUA5 and CLC2-GFP were crossed into *pi4kβ1 pi4kβ2*, respectively, and homozygous lines were used in the F3 generation.

### 2.2 Sterilization of seeds

Seeds were sterilized for 5 min in 6 % (v/v) sodium hypochlorite solution containing 0.1 % (v/v) Triton X-100. Then, seeds were rinsed with sterile double-distilled water (ddH<sub>2</sub>O) three times. Seeds were resuspended in ddH<sub>2</sub>O and sown on 1 % (w/v) agar plates consisting of ½ Murashige and Skoog (MS) medium (pH 5.7) and 1 % (w/v) sucrose.

### 2.3 Plant growth conditions

Sterilized *A. thaliana* seeds on plates were imbibed in the dark at 4 °C for two days before being transferred into growth chambers with 16-h-day, 22 °C, 7000 Lux / 8-h-night, 18 °C, 0 Lux cycles. In general, 5-6-day-old seedlings were used for the experiments, unless stated otherwise.

### 2.4 Genotyping

Genomic DNA was extracted following the cetyltrimethylammonium bromide (CTAB) method (Murray and Thompson, 1980). The polymerase chain

reaction (PCR) reaction was performed using OneTaq DNA Polymerase (NEB) according to the recommended protocol (see below section 2.6.1). Primers are given in Appendix Table 7.2.

## **2.5 DNA separation and purification**

### **2.5.1 Agarose DNA gel electrophoresis**

The gel was made of 1 % (w/v) agarose dissolved in 1 x TAE buffer (40 mM trisaminomethane (Tris), pH 7.6, 20 mM acetic acid, 1 mM ethylenediaminetetraacetic acid (EDTA)) and PCR products or DNA fragments digested by restriction enzymes were loaded into gels. DNA was separated under constant voltage at 130 V. Then gels were stained with ethidium bromide (EB) and observed with Gel iX Imager 20 (INTAS Science Imaging) featuring a 12-bit CCD camera or bands were cut off and subjected to the following extraction.

### **2.5.2 Extraction of DNA from gels**

The kit (GeneJET Gel Extraction Kit, K0692, Thermo Fisher Scientific) for extracting DNA from gels was used. Excised gel slices were dissolved in binding buffer at 1:1 (volume: weight) at 50-60 °C for about 10 min. Then DNA was absorbed to GeneJET purification column and washed twice with washing buffer. Then DNA was eluted with pre-warmed ddH<sub>2</sub>O.

## **2.6 PCR strategies**

### **2.6.1 Standard PCR**

All PCR components were purchased from New England Biolabs (NEB). PCR reactions were prepared according to the manual provided by NEB. In brief, the PCR reactions were performed in a volume of 25 µl and contained the

following components: 20 ng of template DNA, 0.4  $\mu$ M of each primer, 200  $\mu$ M of each dNTPs, 1 x reaction buffer and 1 U of *Taq* DNA polymerase or high-fidelity Phusion DNA polymerase (NEB), and mixed thoroughly. The reaction was performed using following settings: a pre-denaturation step (98 °C, 3 min) was performed followed by 35 cycles of denaturation (98 °C, 40 s), annealing (~ 60 °C, 30 s), extension (72 °C, 30 s/kb), and a final extension step (72 °C, 6 min).

### **2.6.2 Colony PCR**

Colony PCR reaction was prepared as same as standard PCR reaction, except template DNA was replaced by colony of bacteria. The reaction settings were as same as that of standard PCR.

### **2.6.3 Restriction free (RF) cloning**

RF cloning was done as previously described (Unger et al., 2010) with some modifications. In brief, RF cloning utilizes DNA fragments from PCR amplification as mega-primers for the linear amplification of circular vectors and inserts. After that, a methylation sensitive restriction enzyme DpnI was used to digest parent plasmids to leave recombinant plasmids. The following protocol was used: for the first PCR cycle, a pre-denaturation step (98 °C, 5 min) was performed followed by 35 cycles of denaturation (98 °C, 1 min), annealing (~ 60 °C, 30 s), extension (72 °C, 30 s/kb), and a final extension step (72 °C, 6 min). The PCR reactions were performed in a volume of 50  $\mu$ l and contained the following components: 20 ng of template DNA, 0.4  $\mu$ M of each primer, 200  $\mu$ M of each dNTPs, 1 x Phusion buffer and 1 U of high-fidelity Phusion DNA polymerase (NEB). PCR products were purified and used as the megaprimers for the following RF cloning. RF cloning was performed using a pre-denaturation step (98 °C, 5 min) followed by 20 cycles of: denaturation (98 °C, 40 s), annealing (~ 60 °C, 60 s), extension (72 °C, 60 s/kb), and a final extension

step (72 °C, 10 min). PCR reactions were performed in a volume of 50 µl including the following components: 5 ng of destination plasmid, 100 ng purified megaprimers, 400 µM of each dNTPs, 1 x Phusion buffer and 2 U of high-fidelity Phusion DNA polymerase (NEB). PCR products were digested with 40 U DpnI (20 U/µl, NEB) at 37 °C for 3 h or over night. Aliquots of 10 µl were transformed into *E. coli* DH5α cells (see below section 2.7.2). Colony PCR was performed (see section 2.6.2) using gene specific primers to verify successful insertion. Positive colonies were picked and cultivated for extracting plasmids which were then digested by BsrGI (NEB) to recheck correct insertion (see section 2.7.4). After transformation into *E. coli* and reisolation of the plasmid DNA (see section 2.7.2 and 2.7.3), the constructs were verified by restriction enzyme digestion (see section 2.7.4) and by sequencing (see section 2.7.5).

## 2.7 Manipulation of DNA constructs

### 2.7.1 Preparation of *E. coli* competent cells

A single colony of DH5α strain was inoculated into small volume lysogeny broth (LB) liquid media (1 % (w/v) peptone, 0.5 % (w/v) yeast extract, 1 % (w/v) sodium chloride (NaCl)) without antibiotics and incubated at 37 °C over night with continuous shaking. Then the preculture cells were inoculated into large volume LB medium (around 250 ml) to let OD<sub>600</sub> to be 0.2, and grown to OD<sub>600</sub> of 0.6-0.8. The cultures were chilled for 10 min on ice and then pelleted at 4 °C and 1000 x g for 10 min. The pellet was resuspended in 80 ml TFB-buffer (10 mM piperazine-N,N'-bis(2-ethanesulfonic acid) (PIPES), pH 6.7, 250 mM potassium chloride (KCl), 55 mM manganese chloride (MnCl<sub>2</sub>), 15 mM calcium chloride (CaCl<sub>2</sub>)) and chilled on ice for another 10 min, and centrifuged. The pellet was resuspended in 20 ml of TFB-buffer containing 7 % (v/v) dimethyl sulfoxide (DMSO) and incubated on ice for 10 min. Cells were aliquoted to 100-200 µl and immediately frozen in liquid nitrogen. Cells were stored at -80 °C for future use.

### **2.7.2 Transformation of plasmids into *E.coli***

The *E.coli* strain DH5 $\alpha$  is used for transformation. *E.coli* competent cells were mixed with 10  $\mu$ l DNA on ice for 30 min, followed by heat shock at 42 °C for 90 s. Then the cells were grown at 37 °C for 1 h in LB liquid media without antibiotics. Finally, positive clones were selected on LB solid plates containing corresponding antibiotics. The plasmids were extracted and verified by restriction enzyme digestion.

### **2.7.3 Extraction of plasmids from *E.coli***

Plasmids were extracted using the GeneJET Plasmid Miniprep Kit (K0503, Thermo Fisher Scientific) following standard protocol recommended by Thermo. Briefly, over night small scale cell cultures of *E.coli* grown at 37 °C were collected by centrifugation. Cells were resuspended, lysed and neutralized to release plasmids. Then solution was transferred to GeneJET spin column and the flow-through was discarded. The absorbed plasmids in column were washed twice with washing solution. Finally, plasmids were eluted with pre-warmed ddH<sub>2</sub>O.

### **2.7.4 Restriction enzyme digestion**

All restriction enzymes were purchased from NEB. Reactions were prepared in a volume of 10  $\mu$ l containing 1 U restriction enzyme, 1  $\mu$ g DNA, 1 x reaction buffer. The reaction was incubated at recommended temperature for at least 3 h or over night. The digested DNA was separated by DNA gel electrophoresis (see section 2.5.1) to check correct insertions.

### **2.7.5 DNA sequencing**

DNA samples were sequenced based on Sanger sequencing using ABI 3730xl DNA Analyzer systems (GATC Biotech, Germany).

## 2.8 Gateway LR reaction

LR reaction was performed according to the manufacturer's instructions. Generally, entry clone harboring attL sites was mixed with destination vector containing attR sites in the presence of 0.5  $\mu$ l LR clonase (Invitrogen) and 1 x TE buffer (10 mM Tris, pH 8.0, 1 mM EDTA). The reaction was incubated at room temperature over night and then stopped by adding 1  $\mu$ l proteinase K followed by another 30 min incubation at 37 °C. Subsequently, the reaction was transformed into *E.coli* for amplification and selection.

## 2.9 Electrophoretic separation of proteins by sodium dodecyl sulfate polyacrylamide gel electrophoresis (SDS-PAGE)

Resolving gels for SDS-PAGE contained 10 % (w/v) acrylamide, 0.38 M Tris-hydrogen chloride (HCl), pH 8.8, 0.1 % (w/v) SDS, 0.05 % (w/v) ammonium persulfate (APS), 0.1 % (v/v) tetramethylethylenediamine (TEMED), 10 % (v/v) acrylamide were used for resolving gels, except for immunocomplex kinase assays, where 12 % (w/v) acrylamide was used. Resolving gels were overlaid by stacking gels containing 5 % (w/w) acrylamide, 0.132 M Tris, pH 6.8, 0.1 % (w/v) SDS, 0.05 % (w/v) APS and 0.1 % (v/v) TEMED. Protein samples were incubated at 95 °C for 5 min in SDS loading buffer (50 mM Tris-HCl, pH 6.8, 2 % (w/v) SDS, 6 % (v/v) glycerol, 0.001 % (w/v) bromophenol blue, 1 % (v/v) mercaptoethanol) and loaded onto the gels via a micro syringe. Electrophoresis was performed in running buffer containing 25 mM Tris, 192 mM glycine, 0.1 % (w/v) SDS (do not adjust pH) at constant 25 mA for 1 h (for general protein analysis) or at constant 120 V for 3-4 h (for Co-IP analysis) until the bromophenol blue migrated out of the gels. Gels were subsequently stained with Coomassie brilliant blue solution (0.1 % (w/v) Coomassie brilliant blue R-250, 25 % (v/v) isopropanol, 10 % (v/v) acetic acid) and destained with a solution containing 40 % (v/v) methanol, 10 % (v/v) acetic acid or further processed for western blotting (see next section).

## 2.10 Immunodetection of specific proteins (Western blotting)

For immunodetection, proteins were transferred from SDS-PAGE gels to 0.45  $\mu\text{m}$  nitrocellulose membranes (GE Healthcare) using a wet tank electroblotting system (Bio-Rad). The blotting sandwich was assembled according to the manufacturer's instructions. The cassette was locked and placed in the transfer tank filled with transfer buffer containing 25 mM Tris, 192 mM glycine, 20 % (v/v) methanol (do not adjust pH). The transfer was performed at constant 60 V for 1.5 h or constant 20 V over night. After transfer, the blotting membranes were briefly washed with phosphate buffered saline (PBS, 137 mM NaCl, 2.7 mM KCl, 10 mM disodium hydrogen phosphate ( $\text{Na}_2\text{HPO}_4$ ), 2 mM potassium dihydrogen phosphate ( $\text{KH}_2\text{PO}_4$ )), followed by incubation with 5 % (w/v) nonfat dry milk (Bio-Rad) for 1 h to saturate the membrane surface ("blocking"). The blocked membrane was incubated with primary and corresponding secondary antibodies in correct dilutions (see Appendix Table 7.7) according to each experiment for 2-3 h, respectively, the signal was collected by Fusion Solo S chemiluminescence imaging system (VWR) featuring a 16-bit CCD camera. Exposure times were adjusted as required according to the intensities of the signals.

## 2.11 Molecular cloning and plant transformation

For cloning, all primer sequences are given in Appendix Table 7.3.

For genetic complementation of *pi4k $\beta$ 1 pi4k $\beta$ 2*, the coding sequences (CDSs) of *PI4K $\beta$ 1* and *PI4K $\beta$ 2* were amplified by PCR with the primers PI4K $\beta$ 1-F and PI4K $\beta$ 1-R; PI4K $\beta$ 2-F and PI4K $\beta$ 2-R. The fragments were subsequently digested and ligated into pEntry E vectors. Then, 1360bp and 1198bp genomic DNA sequences upstream of start codons of *PI4K $\beta$ 1* and *PI4K $\beta$ 2* were amplified, respectively, with the primers pPI4K $\beta$ 1-F and pPI4K $\beta$ 1-R; pPI4K $\beta$ 2-F and pPI4K $\beta$ 2-R. These fragments were digested and ligated into pEntry E vectors in front of CDSs of *PI4K $\beta$ 1* and *PI4K $\beta$ 2*, respectively, called *pPI4K $\beta$ 1-PI4K $\beta$ 1* and *pPI4K $\beta$ 2-PI4K $\beta$ 2*. The sequences for the *FLAG* tags were

introduced at the 5'-end of *PI4Kβ1* and *PI4Kβ2* by RF cloning, respectively. The *pPI4Kβ1-FLAG-PI4Kβ1* and *pPI4Kβ2-FLAG-PI4Kβ2* cassettes were moved into pMDC123 binary vectors via LR reaction (see section 2.8).

To generate the *pKNOLLE-driven FLAG-PI4Kβ1*, 3013 bp of the *KNOLLE* cis regulatory element upstream of the start codon was amplified using the primers pKNOLLE-F and pKNOLLE-R. The native promoter *pPI4Kβ1* of *pPI4Kβ1-FLAG-PI4Kβ1* was excised by SfiI, and *pKNOLLE* digested by SfiI was inserted in front of the *FLAG-PI4Kβ1* cassette to produce *pKNOLLE-FLAG-PI4Kβ1*. The sequence of *pKNOLLE-FLAG-PI4Kβ1* was verified by sequencing (see section 2.7.5) and transferred into the pMDC123 binary vector by LR reaction (see section 2.8).

To create the fusion of *mCherry* to the genomic sequence of *PI4Kβ1(mCherry-PI4Kβ1)*, as the genomic DNA of *PI4Kβ1* is quite large at around 11,000bp, the *PI4Kβ1* sequence was amplified as five individual fragments and assembled by RF cloning with the following sets of primers: RF-pi4kbeta1-F1, RF-pi4kbeta1-R1; RF-pi4kbeta1-F2, RF-pi4kbeta1-R2; RF-pi4kbeta1-F3, RF-pi4kbeta1-R3; RF-pi4kbeta1-F4, RF-pi4kbeta1-R4. After assembly of full genomic *PI4Kβ1* sequence in the pEntry E vector, *mCherry* including a short linker (*SGPSG* encoded by TCTGGTCCATCTGGT) was amplified using the primers mCherry-gPI4Kb1-F and mCherry-SGPSG-gPI4Kb1-R, and fused by RF cloning upstream of the start codon of *PI4Kβ1*. The construct was sequenced before transformation into *Agrobacterium* for further complementation analysis.

The verified vectors were transformed into *Agrobacterium tumefaciens* strain AGL0, and transformed into the *pi4kβ1 pi4kβ2* double mutant by floral dipping (Clough and Bent, 1998) to check genetic complementation. Positive T1 seedlings were selected with 2-amino-4-methylphosphinobutyric acid (Basta, Bayer) in soil or on ½ MS plates containing 10 µg/ml phosphinothricin (Duchefa). T2 or T3 lines were used for further analyses.

## 2.12 Staining of cell walls

Five-day-old seedlings were stained by 10 µg/ml propidium iodide (PI) in H<sub>2</sub>O for 2 min, then washed with water. After staining, the seedlings were directly mounted in ddH<sub>2</sub>O and immediately observed by confocal microscope.

## 2.13 Generation of the Rabbit anti-AtPI4Kβ1 antibody

A peptide (CTRQYDYYQRVLNGIL) representing the C-terminus of AtPI4Kβ1 was commercially synthesized (Eurogentec, Liège, Belgium) as an antigen and cross-linked to keyhole limpet hemocyanin (KLH) via an additional amino-terminal cysteine (underlined). This conjugate was used to immunize seven rabbits, as previously described (Preuss et al., 2006). IgG was purified from rabbit serum and affinity purified against the column-coupled antigen. (Eurogentec, Liège, Belgium). The antibody specificity was tested against proteins extracts from wild type, *pi4kβ1* and *pi4kβ1 pi4kβ2* mutant plants before application in downstream experiments (see Figure 3.4C). Peptide synthesis, immunization and affinity purification of the antisera were all performed by Eurogentec.

## 2.14 Whole-mount immunostaining

Immunostaining was carried out as described before (Sauer et al., 2006) with some modifications. In brief, seedlings were fixed with 4 % (w/v) paraformaldehyde in PEM buffer containing 50 mM PIPES, pH 6.9, 1 mM ethylene glycol-bis(β-aminoethyl ether)-N,N,N',N'-tetraacetic acid (EGTA), 0.5 mM magnesium chloride (MgCl<sub>2</sub>), 0.05 % (v/v) Triton X-100 for 1 h *in vacuo*, followed by three washing steps in PEM buffer without Triton X-100. The materials were partially digested using 2 % macerozyme R-10 (28302, Serva) in PEM buffer (no Triton X-100) with 0.4 M mannitol at room temperature for 30 min - 1 h, followed by three washing steps in PBS buffer. The samples were permeabilized by incubating with methanol at -20 °C for 20 min, subsequently rehydrated in PBS for 10 min, followed by another permeabilization in 2 % (v/v)

IGEPAL CA-630 and 10 % (v/v) DMSO in PBS buffer for 1 h. The seedlings were washed with PBS three times, and blocked with 5 % (w/v) BSA in PBS for 30 min. The samples were incubated with primary antibodies diluted in 3 % (w/v) BSA in PBS over night at 4 °C with successive washing. Samples were then labelled with secondary antibodies diluted in 3 % (w/v) BSA in PBS for 3 h at room temperature followed by another series of washing. Finally, samples were counterstained with 4',6-diamidino-2-phenylindole (DAPI) applied at a concentration of (1 µg/ml) for 30 min. The stained samples were mounted in PBS, and immediately observed. The appropriate concentrations for primary and second antibodies were used (see Appendix Table 7.8)

### **2.15 Determination of MAPK activity by immunocomplex kinase assays**

MAPK activity was determined by immunocomplex kinase assays in protein extracts as described previously (Kosetsu et al., 2010). In brief, 2-week-old seedlings were ground in liquid nitrogen and proteins were extracted with TG150 buffer containing 25 mM Tris-HCl, pH 7.5, 10 mM EDTA, 10 mM EGTA, 150mM NaCl, 10 % (v/v) glycerol, 0.01 % (v/v) Triton X-100, 1 mM dithiothreitol (DTT), 1 mM sodium orthovanadate (Na<sub>3</sub>VO<sub>4</sub>), 10 mM sodium fluoride (NaF), 50 mM β-glycerophosphate, 1 mM phenylmethane sulfonyl fluoride (PMSF), 1 x complete EDTA-free protease inhibitor cocktail (Roche) (Kosetsu et al., 2010). After brief centrifugation at 20,000 × g for 15 min, the protein concentration of the protein supernatant was determined according to Bradford assay (Bradford, 1976). 400 µg of the protein extracts were adjusted with TG150 buffer to a concentration of 1 mg/ml, and precleared with 20 µl of Protein A-Sepharose® 4B, Fast Flow (suspension in 20 % ethanol, Sigma) at 4 °C for 2 h. Then, the samples were briefly sedimented by centrifugation for 1 min at 4000 × g, and the resins were discarded. The precleared supernatants were incubated with 2 µg of anti-MPK4 antibody (A6979, Sigma) at 4 °C over night. Again, 20 µl of Protein A-Sepharose® 4B, Fast Flow was added to the solution and incubated for another 2 h at 4 °C. After short centrifugation at 4000 × g, the beads were

washed with 1 ml of TG150 buffer three times, and twice with kinase reaction buffer lacking substrate and ATP, which was composed of 50 mM HEPES-KOH, pH 7.5, 20 mM MgCl<sub>2</sub>, 5 mM EGTA, 1 mM DTT, 1 mM Na<sub>3</sub>VO<sub>4</sub>, 10 mM NaF, 50 mM β-glycerophosphate. The beads were incubated in 20 μl kinase reaction buffer containing 5 μg myelin basic protein (MBP, M1891, Sigma) as a phosphorylation substrate and 10 μCi γ-[<sup>33</sup>P]ATP (Hartmann Analytic GmbH, Germany) in 50 μM carrier ATP for 30 min at 30 °C. The reaction was stopped by adding 5 μl of 5 × SDS loading buffer, and the sample was denatured at 95 °C for 4 min. 10 μl of the reaction was loaded on an SDS-PAGE gel. After electrophoresis, staining and destaining (see section 2.9), the gels were dried over night by putting the gel in a solution containing 3 % (v/v) glycerol, 30 % (v/v) methanol and 10 % acetic acid between two cellphone sheets. A phosphor imager screen (BAS-MP 2040s, Fujifilm, Düsseldorf, Germany ) was exposed to the gel for 3 h – 24 h. and the signal was analyzed by using a phosphorimager (BAS-1500, Fujifilm, Düsseldorf, Germany).

### **2.16 Co-immunoprecipitation (Co-IP) from *A. thaliana***

For Co-IP, 14-day-old seedlings expressing functional MPK4-myc (Berriri et al., 2012) and wild-type controls were used. About 5 g of seedlings were harvested, ground with liquid nitrogen and extracted for 1 h on ice with extraction buffer containing 50 mM Tris-HCl, pH 7.5, 150 mM NaCl, 1 mM EDTA, 10 % (v/v) glycerol, 20 mM NaF, 10 mM Na<sub>3</sub>VO<sub>4</sub>, 1 × complete protease inhibitor cocktail (Roche), 1 × PhosSTOP phosphatase inhibitor cocktail (Roche), and 1 % (v/v) Triton X-100. Samples were centrifuged at 10,000 × g for 30 min. Supernatants were collected and diluted with one volume of extraction buffer. Then equal volume around 10 ml of supernatants were used as the starting volume for the Co-IP. Before Co-IP, equal volumes around 33 μl were taken from the starting volumes and used as input. Anti-myc antibodies (C3956, Sigma) were bound to magnetic protein G Dynabeads (10003D, Thermo Fisher) over night in PBS containing 0.05 % (v/v) Tween-20 and added

to the supernatant. The samples were incubated at 4 °C in a cold room for 2.5 h with mild agitation. Beads were washed two times with 1 ml extraction buffer lacking NaF and Na<sub>3</sub>VO<sub>4</sub> containing 0.1% (v/v) Triton X-100, and three times with extraction buffer without NaF, Na<sub>3</sub>VO<sub>4</sub> and Triton X-100. For final washing, beads were resuspended in the extraction buffer without NaF, Na<sub>3</sub>VO<sub>4</sub> and Triton X-100 and transferred into new 1.5-ml reaction tubes in order to avoid contamination from proteins bound to the tube walls. Immunocomplexes were eluted with 65 µl of 2 × SDS loading buffer at 70 °C for 10 min. The proteins were subjected to SDS-PAGE and analyzed by western blotting. The signal was collected as described in section 2.10. Usage and dilutions for antibodies were summarized in Appendix Table 7.7.

## **2.17 Protein interaction analysis based on yeast two-hybrid (Y2H)**

### **2.17.1 Yeast competent cells preparation**

In brief, several yeast colonies of the strain Y2H Gold (Clontech) were picked and inoculated into 10-15 ml fresh YPD media (1 % (w/v) yeast extract, 2 % (w/v) peptone, 2 % (w/v) glucose) supplemented with adenine (Ade, A, 0.004 % (w/v)) for over night growth at 30 °C. The preculture of yeast was then diluted into 50 ml YPD media to let OD<sub>600</sub> be 0.15 and incubated at 30 °C for about 5 h until the OD<sub>600</sub> was 0.6. Cells were collected by centrifugation at 2500 x g for 5 min at room temperature and resuspended in 20 ml TE buffer containing 100 mM Tris-HCl, pH 7.5, 50 mM EDTA followed by centrifugation at 2500 x g for another 5 min at room temperature. The pellet was washed with 1 ml of LiAc/TE buffer and sedimented at 2500 x g for 3 min at room temperature. The pellet was resuspended in 0.7 ml LiAc/TE buffer and these competent cells were stored at room temperature until use within 2 h after preparation.

### 2.17.2 Yeast transformation

Lithium acetate (LiAc) was used to mediate yeast transformation. Various combinations of plasmid constructions were prepared as following: 3  $\mu$ l each bait and prey vector, 100  $\mu$ l competent cells, 700  $\mu$ l PEG/LiAc. The mixtures were mixed briefly and incubated at 30 °C for 30 min with constant shaking. Then, 80  $\mu$ l DMSO was added and immediately mixed accompanied by heating at 42 °C for 15 min. The cells were centrifuged at 700 x g for 5 min and washed with 500  $\mu$ l 0.9 % (w/v) NaCl. The cells were sedimented, resuspended in 100  $\mu$ l 0.9 % (w/v) NaCl, and spread on selective synthetic dropout (SD) media supplemented with 5 % (w/v) glucose and adenine but lacking the respective amino acids for selection. The plates were allowed to grow at 30 °C for 3 days. Then at least of five colonies from each combination were re-streaked onto new plates for protein interaction tests.

### 2.17.3 Yeast two-hybrid tests

cDNA fragments encoding truncated variants of PI4K $\beta$ 1 (PI4K $\beta$ 1<sub>422-1121</sub>, PI4K $\beta$ 1<sub>1-566</sub>) were amplified using the primer combinations PI4K $\beta$ 1<sub>422-1121</sub>-F, PI4K $\beta$ 1<sub>422-1121</sub>-R and PI4K $\beta$ 1<sub>1-566</sub>-F, PI4K $\beta$ 1<sub>1-566</sub>-R, respectively (see Appendix Table 7.3 ). The cDNA fragments were purified (see section 2.5.2), digested with corresponding restriction enzymes (see Appendix Table 7.3) and inserted into the prey vector pGADT7. The cDNA sequence of *MPK4* was amplified using the primer combination MPK4-F and MPK4-R, purified (see section 2.5.2), digested with corresponding restriction enzymes (see Appendix Table 7.3) and moved into the bait vector pGBKT7. All constructs were verified by sequencing (see section 2.7.5). The respective combinations of prey and bait vectors (see Figure 3.4B) were co-transformed into the yeast strain Y2H Gold using the LiAc mediated transformation protocol described above. Positive transformants were identified on selective media lacking the corresponding amino acids, as indicated (see Figure 3.4B). To test for auto-activation, MPK4 in the bait vector

pGBKT7 was individually transformed into Y2H Gold and selected on media lacking only tryptophane (Trp, W). Positive colonies were picked, resuspended in 500  $\mu$ l TE buffer and diluted to OD<sub>600</sub> of 0.5, of which 5  $\mu$ l drops were spotted onto media lacking Trp only or Trp and Leucine (Leu, L) or Trp, Leu and Histine (His, H) to check protein interaction and auto-activation. The yeast were allowed to grow for 3 days at 30 °C.

### 2.18 Chemical treatments

All treatment experiments were performed on seedlings grown on half-strength liquid MS medium containing 1 % (w/v) sucrose, pH 5.6. BFA and cycloheximide (CHX) were dissolved in DMSO in 50 mM stocks, respectively. FM 4-64 was dissolved in ddH<sub>2</sub>O as a 2 mM stock. For MPK4-YFP co-localization with FM 4-64, seedlings were incubated with 10  $\mu$ M FM 4-64 for 10 min, and rinsed with water twice. For BFA treatments, seedlings expressing MPK4-YFP were stained with 10  $\mu$ M FM 4-64 for 5 min, washed twice, and then treated with 50  $\mu$ M BFA or DMSO for 30 min. Seedlings expressing MPK4-YFP and mCherry-TUA5 were also incubated with 50  $\mu$ M BFA or DMSO for 30 min. For CHX plus BFA treatment, MPK4-YFP seedlings were pretreated 50  $\mu$ M CHX for 30 min, then pulsed with 10  $\mu$ M FM 4-64 together with 50  $\mu$ M CHX for 5 min, followed by 2 min washing in 50  $\mu$ M CHX, then incubated with 50  $\mu$ M BFA plus 50  $\mu$ M CHX or 50  $\mu$ M CHX alone at the indicated time points. For CME inhibitor treatments, five-day-old plants expressing MPK4-YFP and RFP<sub>FAPP1-PH</sub> were pretreated with the respective inhibitors without BFA for 1 h, then seedlings were treated with BFA plus inhibitors for 30 min.

### 2.19 Analysis of PtdIns4P levels by thin layer and gas chromatography

Lipid extraction was performed using an acidic lipid extraction method to allow quantification of anionic lipids (König et al., 2008). About 0.2 g two-week-old seedlings were harvested and ground in liquid nitrogen completely. The samples were dissolved in the acidic extraction solvent containing 5 - 10 ml chloroform – methanol (1 : 2), 250  $\mu$ l EDTA solution, 500  $\mu$ l HCl-solution, and

500 µl chloroform with incubated on ice for 2 h with occasionally shaking. Then samples were centrifuged at 600 x g for 2 min to separate phases. The organic phases containing lipids were transferred to new glass tubes by Pasteur pipette. The aqueous phase were reextracted with the extraction solvent twice, and organic phases were combined together. The combined organic phases were washed two times using 1.5 ml of 0.5 N HCl in 50 % (v/v) methanol backwashing solvent with discard of the upper aqueous phases for each washing step. The organic phases were transferred to new glass tubes and evaporated under N<sub>2</sub> flow. The dried PtdIns monophosphates were dissolved in chloroform and spotted onto silica S60 (Merck) preactivated with developing solvent I, as described before (Heilmann and Heilmann, 2013). Lysophosphatidylcholines (LysoPC) was added as a control. The separation of lipids were performed by putting plates in 20 × 20 × 10-cm vertical glass chambers preequilibrated with 100 mL of developing solvent I and containing one sheet (20 × 20 cm) of filter paper to maintain a constant solvent atmosphere. The corrected PtdIns monophosphates indicated by phosphoinositide standards used (Avanti) were scraped and collected in new glass tubes. Tripentadecanoin (15:0) was added to the glass tubes as an internal standard for quantification, lipids were trans-methylated as described previously (Heilmann and Heilmann, 2013), and dissolved in acetonitrile. The samples were analyzed using a 30 m x 250 µm DB-23 capillary column (Agilent) and a GC-2010 plus GC/FID-system (Shimadzu). The lipid amount was quantified by using the internal control and normalized against the sample fresh weight.

## **2.20 Phosphorylation assay**

### **2.20.1 Protein expression and purification**

The CDSs of MPK4, MKK6 and PI4Kβ1 were amplified and ligated into pGEX4T-1 to produce GST tagged fusion proteins, respectively. Subsequently, the Ser (S221) and Thr (T227) residues in the activation loop in MKK6 were

replaced with acidic residues to create a constitutively active kinase MKK6<sup>DE</sup> (S221D, T227E). The GST-MPK4 and GST-MKK6<sup>DE</sup> were expressed in *E. coli* BL21 (DE3). Briefly, the preculture of cells were diluted into 200 ml LB liquid medium in 1 : 50 and allowed to grow till OD<sub>600</sub> reached 0.6-0.8 at 37 °C. Then 1 mM IPTG was added to the cell culture for protein expression for 6 - 8 h at 30 °C. For GST-PI4Kβ1 expression, the cells were grown till OD<sub>600</sub> reached ~ 1.0 at 37 °C. Then five milliliters of the cells was transferred into 200 ml of LB medium filled in a 1 - liter flask containing 0.1 mM IPTG and incubated overnight at 25 °C.

Cells were harvested and lysed by sonication in PBS buffer containing 2 mg/ml lysozyme, 5 mM DTT and 0.1 mM PMSF. The GST fusion proteins were purified with glutathione-Sepharose 4B beads (Thermo), following the manufacturer's instructions.

### **2.20.2 In vitro phosphorylation assay**

Recombinant GST-tagged MPK4 (0.3 µg) were activated by incubation with recombinant MKK6<sup>DE</sup> (0.2 µg) in the reaction buffer (30 mM Tris-HCl pH 7.5, 10 mM MgCl<sub>2</sub>, 50 µM ATP and 1 mM DTT) at 30 °C for 40 min. Activated MPK4 was then used to phosphorylate recombinant GST-PI4Kβ1 proteins (3 µg, 1:10 enzyme substrate ratio) in the same reaction buffer (30 mM Tris-HCl pH 7.5, 10 mM MgCl<sub>2</sub>, 50 µM ATP, and 1 mM DTT) at 30 °C for 30 min in the presence of 10 µCi γ-[<sup>32</sup>P]ATP (Hartmann Analytic GmbH, Germany). Then proteins were subject to SDS-PAGE and staining described in section 2.9 and 2.15, and phosphorylation was scanned as described in section 2.15.

### **2.20.3 In vitro catalytic activity of PI4Kβ1 assay**

Phosphorylation of GST-PI4Kβ1 was performed as described in section 2.21. The catalytic activity of PI4Kβ1 was performed as described before (Cho and Boss, 1995). The prephosphorylated GST-PI4Kβ1 (30 µl reactions) was

added to 30  $\mu$ l reaction buffer to give rise to final concentrations of 30 mM Tris-HCl (pH 7.5), 1 mM cold ATP, 1 mM  $\text{Na}_2\text{MoO}_4$ , 15 mM  $\text{MgCl}_2$ , 10  $\mu\text{Ci}$   $\gamma$ - $^{32}\text{P}$ ATP in the presence of 6  $\mu\text{g}$  PtdInsP substrate presolubilized in 2% Triton X-100. Reactions were incubated at RT for 1h. Then the reaction was stopped by adding 1.5 ml of CHCl<sub>3</sub>: MeOH (1 : 2, v/v). The lipids were extracted and analyzed as described in section 2.19. The TLC plates were scanned as described in section 2.15 and the intensity of phospho-labeled PtdIns4P was determined by using Fiji software (<https://fiji.sc/>).

## 2.21 Microscopy usage and data analysis

### 2.21.1 Confocal laser scanning microscopy (CLSM) and data analysis

Five-day-old seedlings were used for all experiments, if not stated otherwise. Images were acquired with LSM780 or LSM880 confocal microscopes, the latter featuring a highly sensitive Airyscan detector (Carl Zeiss GmbH, Jena, Germany). 20x or 63x oil immersion objectives were used. All images were processed with Fiji software (<https://fiji.sc/>), except images of whole-mount immunostaining, which were assembled using Adobe Photoshop.

For time lapse imaging of the MPK4-YFP and RFP<sub>FAPP1-PH</sub> dual markers, images were taken using the LSM880. As the MPK4-YFP signal is very weak, the highly sensitive Airyscan detector was used in sensitivity mode to acquire images. In this case, laser intensity was reduced to 1% to enable long-term imaging and avoid bleaching. YFP and RFP was excited with argon (514 nm) and DPSS (561 nm) laser lines, respectively, at 0.5 % laser power. The interval was set to 90 s and resolution vs. sensitivity (R-S) mode of Airyscan was used. YFP emission was collected with BP 420-480 + BP 495-550 filter sets; while BP 570-620 + LP 645 filter set was used to collect RFP emission. Movies were recorded using the macro Correct\_3D\_Drift\_Plus (<https://github.com/tischi/fiji-correct-3d-drift>).

For comparison of MPK4 localization between wild type and *pi4kβ1 pi4kβ2* mutants, the Airyscan was used in R-S mode. YFP and mCherry were excited with 1 % laser intensities at 514 nm and 561 nm, respectively. The band pass filter BP 420-480 + BP 495-550 was used to record YFP emission while BP 570-620 + LP 645 was used to collect mCherry emission.

For the internalization of PIN2-GFP, the five-day-old seedlings were preincubated with 50 μM CHX for 30 min, followed by 2 μM FM 4-64 staining for 3 minutes. The seedlings were briefly washed in ½ MS, and mounted in 80 - 100 μl ½ MS containing 50 μM and 50 μM BFA using agrose pads in growth chamber. The definite focus equipped in LSM880 was used to prevent z focus drifting, and images were recorded every 2 min. GFP was excited at 488 nm with 5 % laser power, and emission was collected between 517 - 535 nm. FM 4-64 was excited at 514 nm with 15 % laser power, and emission was collected between 636 - 689 nm.

For CLC2-GFP costained with FM 4-64, a Gallium Arsenide phosphide (GaAsP) detector of the LSM880 was used to record CLC2-GFP. GFP was excited at 488 nm with 5 % laser power, and emission was collected between 517 - 535 nm. FM 4-64 was excited at 514 nm with 15 % laser power, and emission was collected between 636 - 689 nm. 1 μm interval of z stacks containing 5-7 slices covering median sections of cells was used and images were taken every 3 min. Then the slice which is close to the median section was selected and reconstructed. For quantification of delayed events in the mutants, the time point when the cell plate had just attached with the plasma membrane was set to time "0". In this case, any recruitment of CLC2-GFP earlier before the cell plate fusion with plasma membrane would give minus values. By contrast, plus values mean later recruitment of CLC2-GFP to the cell plate after the cell plate fusion with plasma membrane.

For BFA treatment of seedlings expressing MPK4-YFP and mCherry-TUA5, YFP was excited at 514 nm with 50 % laser power, and emission was collected

between 517 - 553 nm; 2 % laser power was set to excite RFP and emission was collected between 586 - 696 nm.

For the mCherry-PI4K $\beta$ 1 marker line, 1 % laser power at 561 nm was used to excite mCherry, and a BP 570-620 + LP 645 filter was applied to collect the mCherry emission. The virtual pinhole (VP) mode of the Airyscan detector was used and the pinhole for image output was set to 2.

### **2.21.2 Spinning disc microscopy and data analysis**

Spinning disc images were acquired with a Zeiss Cell observer microscope equipped with a Yokogawa CSU-X1 spinning disc head. A 100x oil immersion objective and a Photometrics Evolve 512 Delta EM-CCD camera were used for image acquisition. YFP and mCherry was excited at 488 nm and 561 nm, respectively, and a DBP 527/54+645/60 band pass filter (Chroma Technology) was used to collect the emissions. For dynamic microtubule analysis, images were recorded at 5 s intervals. Images were contrast enhanced, background subtracted, registered, and subjected to a walking average calculation. Then a Fiji macro (Endler et al., 2015) was used to separate growing and shrinking ends by time phase to phase subtraction. The Fiji plugin MultiKymograph ([https://www.embl.de/eamnet/html/body\\_kymograph.html](https://www.embl.de/eamnet/html/body_kymograph.html)) was used to generate kymographs. For quantification of microtubular density and bundling, the method described before was used (Higaki et al., 2010). For MPK4 budding and fusion events analysis, MPK4-YFP was excited at 488 nm, and images were recorded at 2 s intervals. The exposure time was set to 1 s. For the movies, individual frames were enhanced for contrast and background noise was subtracted. Then movies were registered using the plugin "Stackreg", followed by using "WalkingAverage" plugin to reduce noise. Finally, movies were deconvolved using the plugin "DeconvolutionLab" (<http://bigwww.epfl.ch/deconvolution/>).

### **2.21.3 Structured illumination super-resolution microscopy (3D-SIM)**

To analyse immunostains and chromatin beyond the classical Abbe/Raleigh limit at a lateral resolution of ~120 nm (super-resolution, achieved with a 488 nm laser), a spatial 3D-structured illumination microscopy (3D-SIM) was applied using a 63× 1.4 NA Oil Plan-Apochromat objective of an Elyra PS.1 microscope system. The software ZEN black was used to capture images (Carl Zeiss GmbH) (Weisshart et al., 2016) . Images were captured separately for each fluorochrome using the 561, 488, and 405 nm laser lines for excitation and appropriate emission filters. 3D rendering based on SIM image stacks was done using the Imaris 8.0 (Bitplane) software.

### **2.22 Quantification of BFA bodies and dynamic microtubule parameters**

The homogeneity of variance was evaluated using Predictive Analytics Software (PASW) version 18. Confidence intervals for statistical differences ("significances") were then determined by independent-samples two-tailed Student's t-tests. Excel software (Microsoft) was used to create bar charts. For all experiments, the corresponding numbers of repeats and sample sizes are given in the text describing the respective results.

### 3. Results

At the onset of this study, it was known that the *Arabidopsis pi4kβ1 pi4kβ2* double mutant displays defective cytokinesis (Kang et al., 2011; Preuss et al., 2006). However, there was no information about the molecular mechanism by which PtdIns4P influences cytokinesis. Experiments presented in this thesis were performed to elucidate these mechanisms.

#### 3.1 PI4Kβ1 is involved in cytokinesis and localizes to the cell plate

As a basis to explore the cytokinesis defects of the *A. thaliana pi4kβ1 pi4kβ2* double mutant (Kang et al., 2011; Preuss et al., 2006), the coding sequences of *PI4Kβ1* and *PI4Kβ2* were expressed under their endogenous promoters in the *pi4kβ1 pi4kβ2* background. As a result, the dwarf phenotype of the double mutant was fully rescued by the ectopic expression of either gene (Fig. 3.1A), indicating that the phenotypes were indeed a result of mutations in

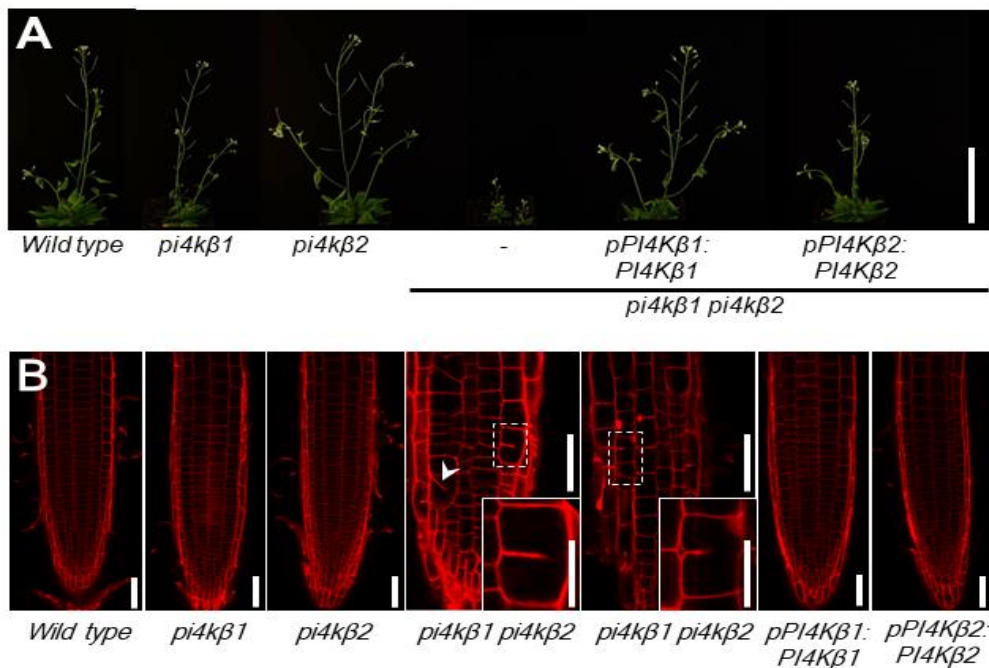


**Figure 3.1. Genetic complementation of the *A. thaliana pi4kβ1 pi4kβ2* double mutant.** (A) The growth phenotype of the *pi4kβ1 pi4kβ2* double mutant can be complemented by ectopic expression of *PI4Kβ1* or *PI4Kβ2*. Plants shown are one-month-old. Bar, 10 cm. (B) The root tissue patterning defect of the *pi4kβ1 pi4kβ2* double mutant is also complemented by ectopic expression of *PI4Kβ* variants, as shown by PI staining of five-day-old roots. The number of seedlings used for experiments was more than 10 seedlings for each genotype, and the experiments were repeated four times. Arrowhead, oblique cell wall. Insets, magnifications of areas showing cell wall stubs. Bars, 50  $\mu$ m.

*PI4Kβ1* and *PI4Kβ2*. Cytokinetic defects were further analyzed by PI staining in the single mutants, the double mutant and the complemented lines. Cell wall stubs or oblique cell walls reported previously for the *pi4kβ1 pi4kβ2* double mutant (Kang et al., 2011) were not found in the complemented lines (Fig. 3.1B), indicating all complementation constructs were functional.

As no functional fluorescence tagged variant of PI4Kβ1 or PI4Kβ2 has been reported so far, the *in vivo* localization of PI4Kβ isoforms in *A. thaliana* has remained unclear. Therefore, a functional complementation construct was created by fusing the CDS of an N-terminal mCherry tag upstream of an 11-kb genomic fragment of the *PI4Kβ1* gene including introns, 5' UTR, 3' UTR and parts of sequences of the upstream and downstream neighboring genes (Fig. 3.2A). PI4Kβ1 was focused on for this experiment, as it has 83 % identity to PI4Kβ2 and the enzymes are functionally redundant (Preuss et al., 2006). The expressed mCherry-tagged PI4Kβ1 fully complemented the phenotype of the *pi4kβ1 pi4kβ2* double mutant (Fig. 3.2B), and the mCherry-PI4Kβ1 fluorescence decorated the cell plate of cytokinetic root cells *in vivo* (Fig. 3.2C). As *in vivo* fluorescence was weak, additional whole-mount immunostaining was performed. The immunostaining against mCherry-PI4Kβ1 expressed in the *pi4kβ1 pi4kβ2* double mutant clearly showed mCherry-PI4Kβ1 at the cell plate from early to late cytokinesis and concentrated at the leading edges of the cell plate (Fig. 3.2D, [III] and [IV]). Under its intrinsic promoter, the mCherry-PI4Kβ1 fusion was also expressed in preprophase and metaphase, but the marker fluorescence showed diffuse localization patterns (Fig. 3.2 [I] and [II]), suggesting PI4Kβ1 may have functions throughout mitotic phases. No fluorescence label was detected at the cell plate when using wild type plants as a negative control (Fig. 3.2E), indicating the mCherry detection was specific.

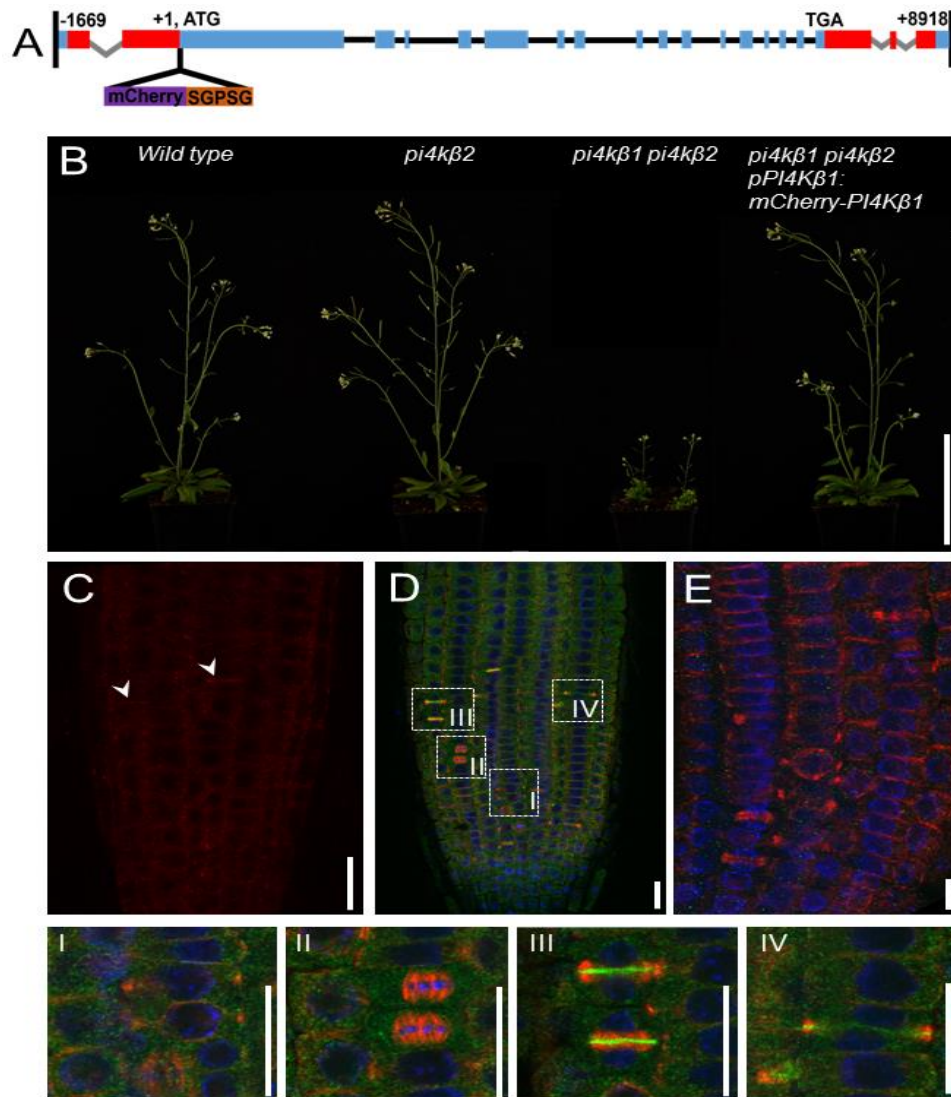


**Figure 3.2. PI4K $\beta$ 1 is involved in cytokinesis and localizes to the cell plate.** (A) Schematic of genomic construct for expression of mCherry-PI4K $\beta$ 1 in the *pi4k $\beta$ 1 pi4k $\beta$ 2* double mutant. A whole genomic DNA of the *PI4K $\beta$ 1* including the *PI4K $\beta$ 1* cis-regulatory elements and partial sequences of upstream and downstream genes. A DNA fragment of *mCherry* containing a short linker encoding *SGPSG* was fused in frame with the start codon of the *PI4K $\beta$ 1* that is represented as +1, ATG. Blue, exons; black, introns; red and grey, untranslated regions (UTRs). (B) Genetic complementation of the *pi4k $\beta$ 1 pi4k $\beta$ 2* double mutant by the *mCherry-PI4K $\beta$ 1* construct. Plants shown are one-month-old. Bar is 10 cm. (C) *In vivo* localization of mCherry-PI4K $\beta$ 1 expressed from the *pPI4K $\beta$ 1* promoter in root tips of five-day-old *pi4k $\beta$ 1 pi4k $\beta$ 2* plants ( $n \geq 9$ ). The mCherry-PI4K $\beta$ 1 distribution was imaged using Airyscan Virtual Pinhole (VP) mode with pinhole set to 2. Arrowheads, nascent cell plates. Bar, 20  $\mu$ m. (D) Whole-mount immunostaining of five-day-old seedlings expressing *pPI4K $\beta$ 1:mCherry-PI4K $\beta$ 1* in the *pi4k $\beta$ 1 pi4k $\beta$ 2* double mutant background using anti-tubulin (red), anti-mCherry (green) antibodies and DAPI (blue). The image is representative for 8 roots and experiments were repeated twice. (E) Whole-mount immunostaining of five-day-old *wild type* seedlings (negative control). Antibodies used were as same as (D) use. The image is representative for 5 roots. Bar is 10  $\mu$ m. (I) to (IV), magnifications of regions marked in (D), representing early mitotic to late cytokinetic stages. Bars are 20  $\mu$ m.

### 3.2 *pKNOLLE*-driven expression of PI4K $\beta$ 1 rescues the *pi4k $\beta$ 1 pi4k $\beta$ 2* double mutant phenotype

To determine to which extent PI4K $\beta$ 1 contributed to the control of cytokinesis, a functional *FLAG-PI4K $\beta$ 1* construct (Fig. 3.3A) was expressed in *pi4k $\beta$ 1 pi4k $\beta$ 2* double mutants under the control of KNOLLE cis-regulatory elements (*pKNOLLE:FLAG-PI4K $\beta$ 1*), confining *FLAG-PI4K $\beta$ 1* expression to cells in the G2/M phase of the cell cycle (Müller et al., 2003). Interestingly, the *pKNOLLE*-driven expression of *FLAG-PI4K $\beta$ 1* rescued the double mutant phenotype (Fig. 3.3A and Appendix Fig. 7.2), even though this promoter is only active in a narrow spatio-temporal expression pattern. Complementation was further confirmed by PI staining, showing no cytokinetic defects in *pKNOLLE:FLAG-PI4K $\beta$ 1* lines (Fig. 3.3B). While the expression of the *pKNOLLE:FLAG-PI4K $\beta$ 1* marker was initiated in the G2/M, the stability and persistence of the expressed FLAG-PI4K $\beta$ 1 protein in post-cytokinetic cells is unclear. To this end, immunostaining of the FLAG-PI4K $\beta$ 1 protein in *pKNOLLE:FLAG-PI4K $\beta$ 1* lines and *pPI4K $\beta$ 1:FLAG-PI4K $\beta$ 1* lines was performed using several anti-FLAG antibodies. Unfortunately, the antibodies tested did not recognize FLAG tag at all (data not shown). Subsequently, detection of the FLAG-PI4K $\beta$ 1 fusion was also attempted with custom-raised anti-PI4K $\beta$ 1 antisera, but failed. Therefore, no statement about protein abundance can be made. To verify correct expression of FLAG-PI4K $\beta$ 1 in these lines, we used the anti-PI4K $\beta$ 1 antibody on the *pPI4K $\beta$ 1:FLAG-PI4K $\beta$ 1* line, and FLAG-PI4K $\beta$ 1 was detected successfully in the membrane fraction (Fig. 3.3C), consistent with previous results (Preuss et al., 2006), but not by immunostaining. The data suggest that the expression of PI4K $\beta$ 1 in G2/M phase unexpectedly produces sufficient protein to rescue the cytokinetic defects of the *pi4k $\beta$ 1 pi4k $\beta$ 2* double mutant. The full recovery of the dwarf phenotype of the double mutant is possibly due to stability of FLAG-PI4K $\beta$ 1 during cytokinesis but also in post-cytokinetic cells.

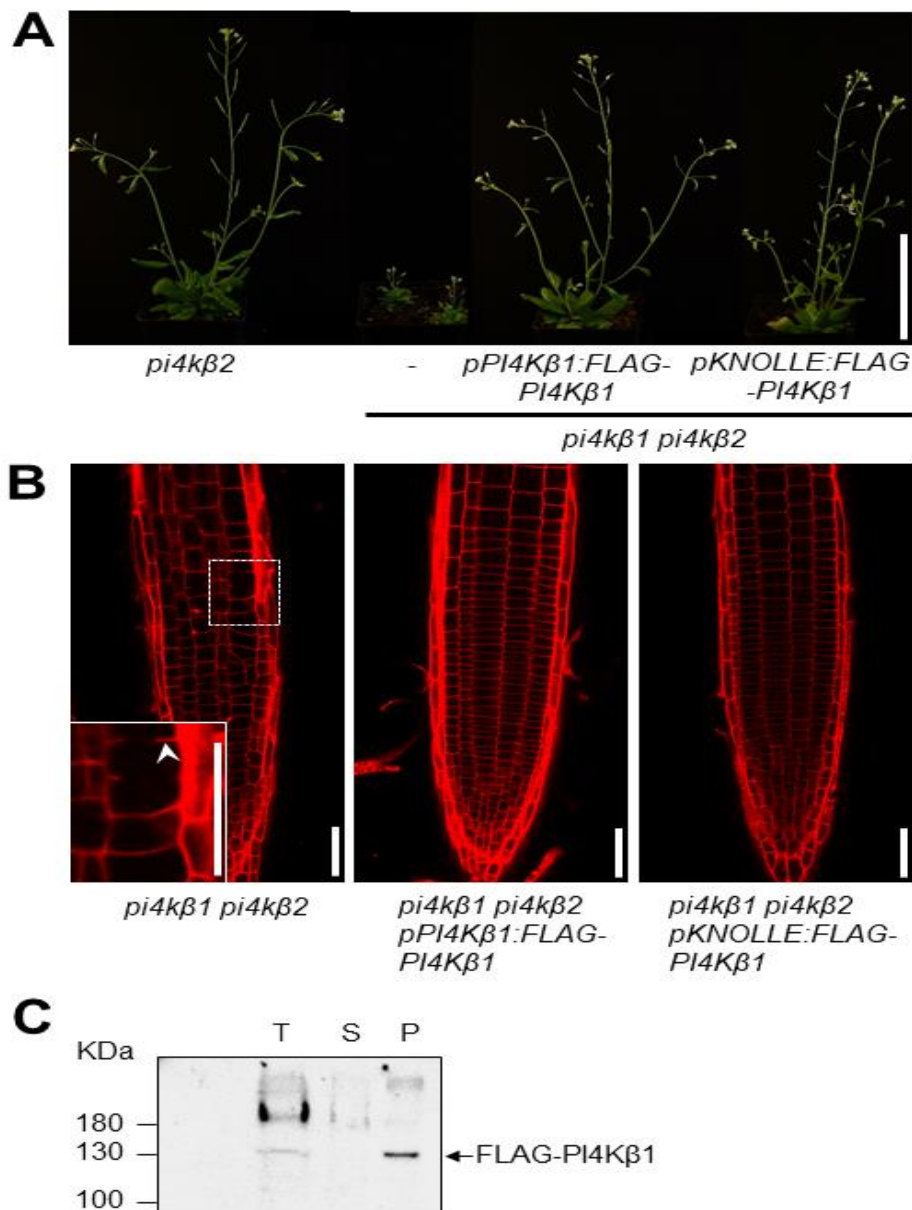


**Fig 3.3. The contribution of PI4Kβ1 to cytokinesis.** (A) Complementation of the *pi4kβ1 pi4kβ2* phenotype by functional *FLAG-PI4Kβ1* expressed from the intrinsic *pPI4Kβ1* or by the *pKNOLLE* promoters, as indicated. One-month-old plants are shown. Bar, 10 cm. Complementation with the *pKNOLLE* driven construct indicates functionality of PI4Kβ1 during cell plate formation in G2/M phase. (B) PI staining of *pKNOLLE:FLAG-PI4Kβ1* expressed in the *pi4kβ1 pi4kβ2* double mutant background showed full rescue of the cytokinetic defects of the *pi4kβ1 pi4kβ2* double mutant. The images are representative for at least 8 roots for each genotype and experiments were repeated three times. Inset, magnification marked in dashed area. Arrowhead, cell wall stub in the *pi4kβ1 pi4kβ2* double mutant. Bars, 50 μm. (C) Protein extracts were prepared from *A. thaliana pi4kβ1 pi4kβ2* double mutants expressing *FLAG-PI4Kβ1* driven by the intrinsic *pPI4Kβ1* promoter. The total protein extracts (T) were subjected to centrifugation at 100,000 x g to obtain soluble (S) and a particulate membrane fraction (P). FLAG-PI4Kβ1 was detected in the membrane fraction. The experiment was repeated twice showing consistent results. Arrowhead, FLAG-PI4Kβ1.

### 3.3 Endocytosis is impaired in the *pi4kβ1 pi4kβ2* double mutant

The results so far indicated a role for PI4K $\beta$  isoforms in cell plate formation. We next addressed the question why the *pi4kβ1 pi4kβ2* double mutant might fail to form proper cell plates. From previous reports it is only known that PI4K $\beta$ s contribute to the control of secretion which is essential for root hair development (Preuss et al., 2006), and it is proposed that PI4K $\beta$ s are critically important to the formation of the cell plate by controlling secretion (Kang et al., 2011). As phosphoinositides have mainly been associated with the control of endocytosis in plants (Ischebeck et al., 2008; Sousa et al., 2008; Zhao et al., 2010), we tested whether endocytosis was impaired in the *pi4kβ1 pi4kβ2* double mutant. Two well characterized endocytosis cargoes were tested for their subcellular distribution, the syntaxin KNOLLE (Fig. 3.4A) and the auxin export protein, PINFORMED 2 (PIN2, Fig. 3.4C). Both proteins are normally endocytosed from the plasma membrane and the cell plate, giving rise to their specific localization patterns at the cell plate and at the polarized apical plasma membrane domain, respectively. It is known that impaired endocytosis retains KNOLLE at the lateral plasma membrane upon the cell plate fusion with the parent plasma membrane at the end of cytokinesis (Boutté et al., 2010). In the *pi4kβ1 pi4kβ2* double mutant, the KNOLLE marker displayed lateral plasma membrane localization at the end of cytokinesis (Fig. 3.4A and B), suggesting a defect in endocytosis. The internalization of PIN2 upon BFA treatment was tracked overtime and the number of PIN2-associated endosomes was significantly decreased in the *pi4kβ1 pi4kβ2* (Fig. 3.4C and D), also supporting that endocytosis was impaired in the *pi4kβ1 pi4kβ2* double mutant. Given that CME in plants is well documented and in yeast the knock down of the PI4K, Pik1p, inhibits the recruitment of clathrin to the Golgi (Gloor et al., 2010), we hypothesized that clathrin dynamics may be affected also in the *A. thaliana pi4kβ1 pi4kβ2* double mutant. To test this hypothesis, a CLC2-GFP marker (Konopka et al., 2008) was introgressed into the *pi4kβ1 pi4kβ2* double mutant

and its association with the cell plate was analyzed over time in

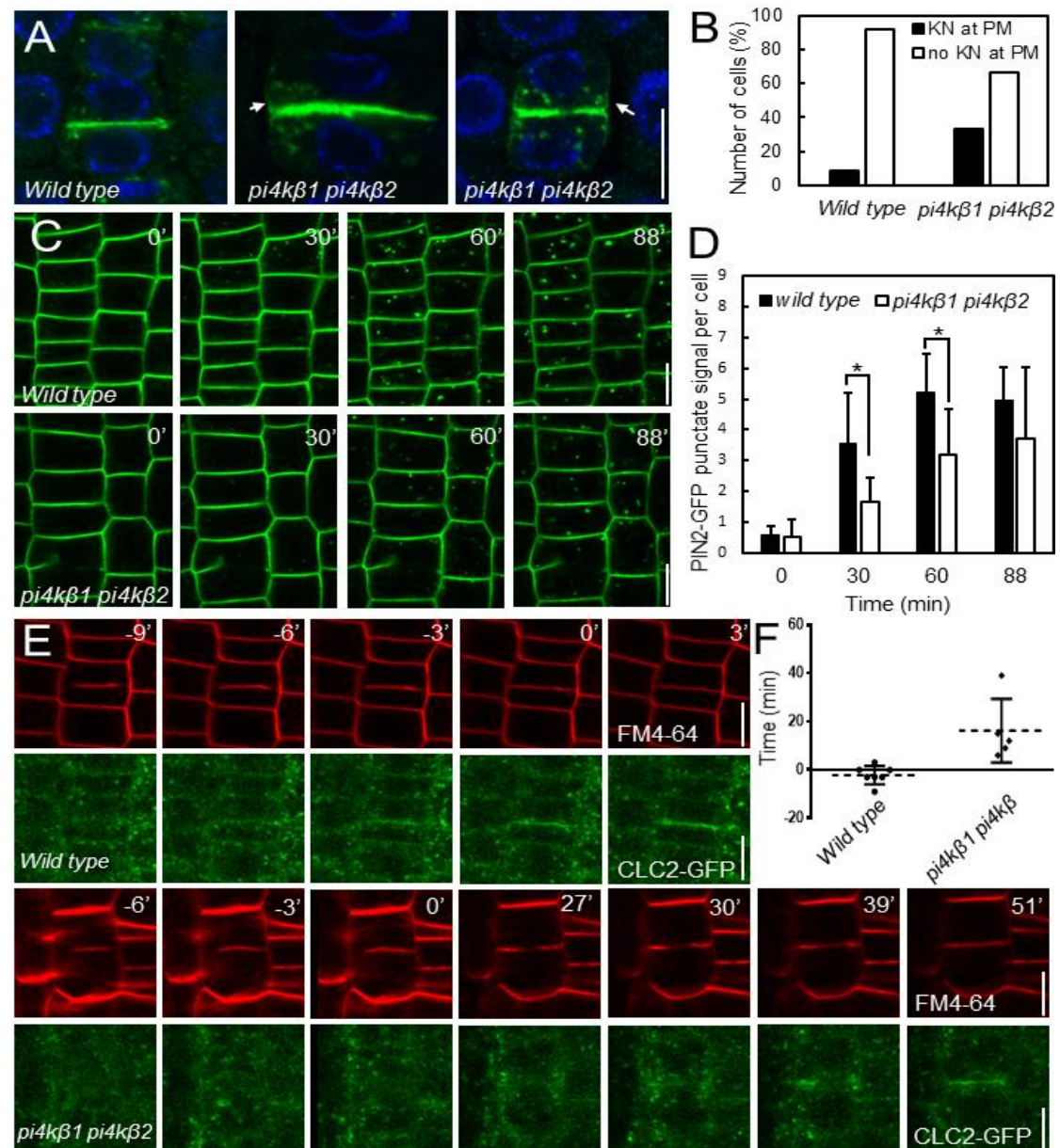


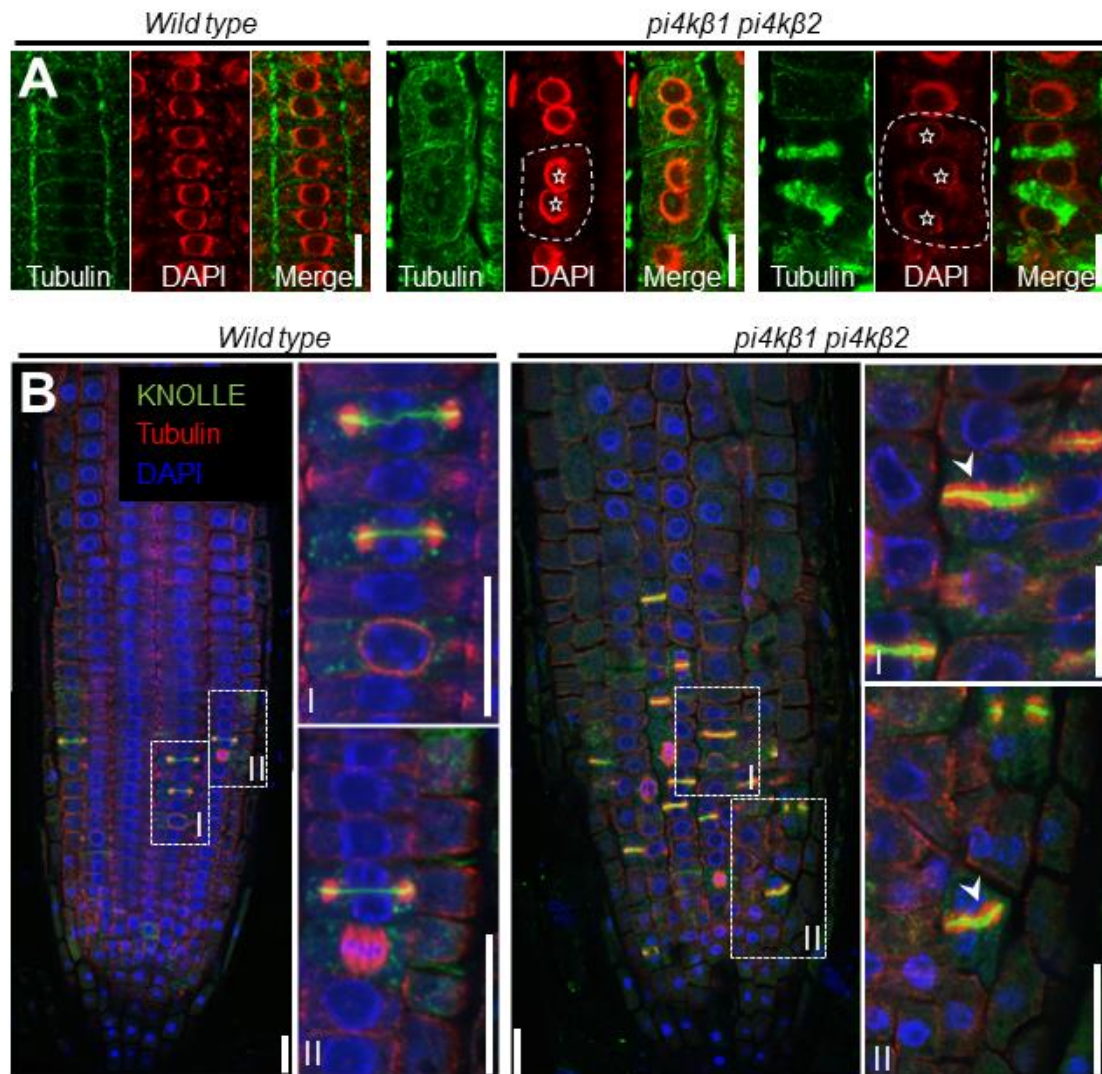
**Figure 3.4. Endocytosis is impaired in *pi4kβ1 pi4kβ2* double mutants.** (A) Five-day-old seedlings were immunostained with anti-KNOLLE (green) and counterstained with DAPI (blue). Later diffusion of KNOLLE upon fusion of the cell plate with lateral plasma membrane occurred in the *pi4kβ1 pi4kβ2* double mutant (arrows) (wild type, 47 cells, 21 roots; *pi4kβ1 pi4kβ2*, 114 cells, 52 roots). Bar is 10 μm. (B) Quantitative analysis of lateral diffusion of KNOLLE (KN) at the plasma membrane (PM). (C) Internalization of PIN2-GFP was tracked overtime in live roots pretreated with 50 μM CHX for 30 min, then washed and incubated with 50 μM CHX and 25 μM BFA. Bars are 10 μm. (D) Quantification of punctate signals from (C) induced by BFA in *wild type* (116 cells, 6 roots) and *pi4kβ1 pi4kβ2* double mutants (110 cells, 7 roots). Asterisks, significance at  $p=0.05$ . (E) Time lapse of CLC2-GFP recruitment to the cell plate in live roots of five-day-old seedlings costained with FM4-64. The recruitment of CLC2-GFP to the cell plate was delayed in the *pi4kβ1 pi4kβ2* double mutant. Bars are 10 μm. (F) Quantification of time required for CLC2-GFP recruitment to the cell plate in *wild type* (7 cells, 6 roots) and the *pi4kβ1*

*pi4kβ2* double mutant (5 cells, 5 roots). The time point when the cell plate had just fused with the parent plasma membrane was defined as time “0”.

root cells undergoing cytokinesis. In wild type controls, CLC2-GFP was recruited to the cell plate before the cell plate was attaching to the lateral plasma membrane or the cell plate just attached the lateral plasma membrane (Fig. 3.4E), consistent with previous findings (Ito et al., 2012). In the *pi4kβ1 pi4kβ2* double mutant the recruitment of CLC2-GFP to the cell plate occurred later after the cell plate attached the lateral plasma membrane (Fig. 3.4E). Quantification of those delay events in the *pi4kβ1 pi4kβ2* double mutant by defining the time point when the cell plate had just fused with the lateral plasma membrane as time “0” showed that the average time required for clathrin recruitment to the cell plate in wild type was  $-2.14 \pm 3.76$  min compared to  $16.20 \pm 13.18$  min in the *pi4kβ1 pi4kβ2* double mutant (Fig. 3.4F). Overall, the data indicate that endocytosis is impaired in the *pi4kβ1 pi4kβ2* double mutant, possibly accounting for reduced cell plate formation.

### **3.4 The *A. thaliana pi4kβ1 pi4kβ2* double mutant displays multinucleated cells and aberrant phragmoplasts**

To characterize the cytokinetic defects of the *pi4kβ1 pi4kβ2* double mutant in more detail, further immunostaining experiments were performed using anti-KNOLLE and tubulin antibodies. Multiple nuclei and phragmoplasts were found in root cells of the *pi4kβ1 pi4kβ2* double mutant compared to wild type controls (Fig. 3.5A), consistent with the notion that key aspects of cell division are impaired and/or retarded in the *pi4kβ1 pi4kβ2* double mutant. Here we characterized cytoskeletal structures with importance for cell plate formation. In wild type cells, KNOLLE marked the leading edges of the expanding cell plates and phragmoplasts formed ring-like structures during late cytokinesis, consistent with the model where central phragmoplast microtubules depolymerize and peripheral microtubules polymerize (Murata et al., 2013). In contrast, in the *pi4kβ1 pi4kβ2* double mutant the central areas of



cell plates and

**Figure 3.5. The *A. thaliana pi4kβ1 pi4kβ2* double mutant displays multinucleated cells and aberrant phragmoplasts.** (A) Immunostaining of meristem cells of five-day-old wild type or *pi4kβ1 pi4kβ2* double mutant plants, as indicated, using an anti-tubulin (green) antibody and DAPI staining (red). The images are representative for 5 cells of 5 seedlings. Asterisks indicate nuclei in multinucleated cells. Bars, 10 μm. (B) Whole-mount immunostaining of five-day-old seedlings of wild type or *pi4kβ1 pi4kβ2* double mutants, using anti-KNOLLE (green) and anti-tubulin (red) antibodies, and DAPI staining (blue). (I), (II), magnifications of areas highlighted in the overview images, as indicated. The images are representative for >15 independently grown plants. Arrowheads, solid phragmoplasts with immature cell plates in the *pi4kβ1 pi4kβ2* double mutant. Bars, 20 μm.

phragmoplasts were still solid even in late cytokinesis (Fig. 3.5B.), indicating that both KNOLLE and microtubules were ectopically stabilized. Furthermore, immature cell plates retaining KNOLLE protein were found in the *pi4kβ1 pi4kβ2* double mutant (Fig. 3.5B), possibly because of altered phragmoplast

organization or - possibly related to the role of PtdIns4P in membrane trafficking  
- indicating abolished or misrouted trafficking events.

### **3.5 The microtubule-associated protein MAP65-3 mislocalizes in *pi4kβ1 pi4kβ2* double mutants, concomitant with phragmoplast stabilization**

To better understand the altered microtubule patterns observed in the *pi4kβ1 pi4kβ2* double mutants, factors controlling phragmoplast expansion were further analyzed. The stabilization of phragmoplast microtubules is controlled by three MAP65 family members (MAP65-1, MAP65-2 and MAP65-3), which are targets for MAPKs in the NACK-PQR pathway for microtubule control (Kosetsu et al., 2010; Sasabe et al., 2011b; Sasabe and Machida, 2012). While mutations in MAP65-1 or/and MAP65-2 do not influence cytokinesis (Lucas and Shaw, 2012; Sasabe et al., 2011b), loss-of-function of MAP65-3 has been shown to result in severe cytokinetic defects (Müller et al., 2004). Furthermore, as MAP65-3 is concentrated at the midline of the phragmoplast during cytokinesis in a distribution pattern similar to that of PI4Kβ1, we hypothesized that MAP65-3 function and/or localization might be altered in the *pi4kβ1 pi4kβ2* double mutant. To test this hypothesis, a functional GFP-MAP65-3 fusion (Steiner et al., 2016a) was introgressed into the *pi4kβ1 pi4kβ2* background, and the fluorescence distribution was analyzed in root cells by confocal microscopy. While in wild type controls, GFP-MAP65-3 decorated the leading edges of the phragmoplast (100 %, n = 20 cells), the fluorescence distribution pattern in the *pi4kβ1 pi4kβ2* double mutant was clearly different and GFP-MAP65-3 solidly labeled the entire cell plate even during late stages of cytokinesis (66.2 %, n = 71 cells) (Fig. 3.6A). The *in vivo* findings were further supported by immunofluorescence, and in contrast to wild type cells, where GFP-MAP65-3 formed ring-like structures during late cytokinesis (100 %, n = 43 cells), in the *pi4kβ1 pi4kβ2* double mutant GFP-MAP65-3 still persisted at the center of the midline (69.4 %, n = 121 cells) (Fig. 3.6B). Analysis of this

pattern by 3D-SIM further detailed the differences in GFP-MAP65-3 distribution in 3-D reconstructions (Fig. 3.6C). The fluorescence patterns indicate that the turnover of MAP65-3 was altered. As MAP65-3 is a known target of Arabidopsis MPK4 (Kosetsu et al., 2010; Sasabe et al., 2011b), we further tested the distribution of GFP-MAP65-3 in an Arabidopsis *mpk4-2* mutant background. These experiments showed that in the *mpk4-2* mutant the confinement of GFP-MAP65-3 to the cell plate was inhibited in late cytokinesis (n = 38 cells)

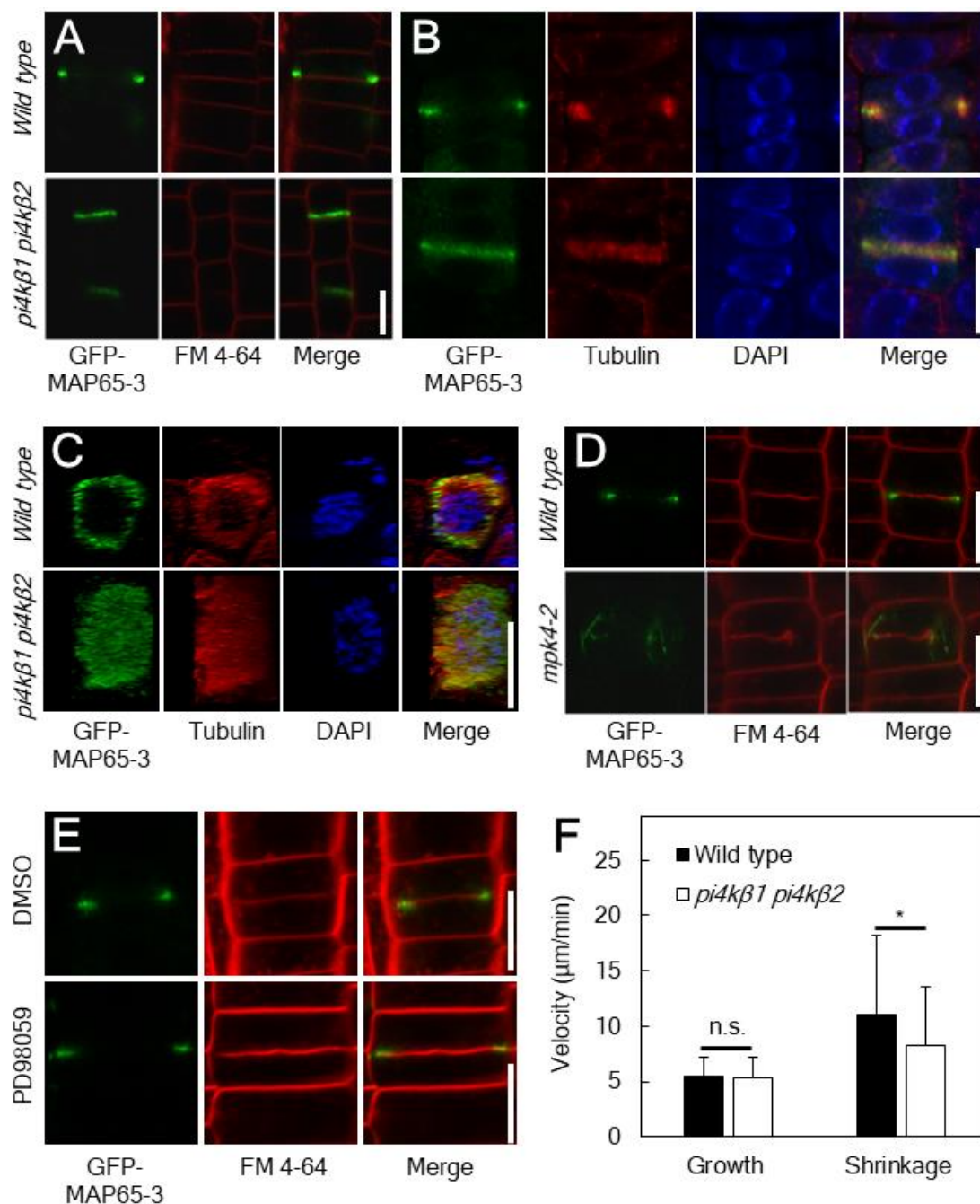


**Figure 3.6.** The MPK4 target, MAP65-3, mislocalizes in *pi4kβ1 pi4kβ2* double mutants, concomitant with reduced microtubule shrinkage. For detailed legend, see next page.

**Figure 3.6. The MPK4 target, MAP65-3, mislocalizes in *pi4kβ1 pi4kβ2* double mutants, concomitant with reduced microtubule shrinkage.** (A) Five-day-old seedlings of wild type (upper panels) or *pi4kβ1 pi4kβ2* double mutants (lower panels) expressing GFP-MAP65-3 were stained for 5 min with 2 μM FM 4-64, and the fluorescence distribution was recorded by confocal microscopy. Note the solid cell plate association of GFP-MAP65-3 in the *pi4kβ1 pi4kβ2* double mutant. The patterns are representative for ≥ 20 cells for each genotype. Bar, 10 μm. (B) Immunofluorescence of GFP-MAP65-3 (green) and microtubules (red), costained with DAPI (blue). MAP65-3 labeled the entire cell plate at late cytokinetic stages in the *pi4kβ1 pi4kβ2* double mutant. The patterns are representative for > 40 cells for each genotype. Bar, 10 μm. (C) Images from 3-D reconstruction of GFP-MAP65-3 and microtubules based on super resolution structured illumination microscopy (SIM). Upper panels, wild type; lower panels, *pi4kβ1 pi4kβ2* double mutants. Bar, 10 μm. (D) MPK4 is required to restrict GFP-MAP65-3 to the cell plate in late cytokinesis. The cell plate association of GFP-MAP65-3 was analyzed in wild type controls (upper panels, n = 63) and in *mpk4-2* mutants (lower panels, n=38). Bar, 10 μm. (E) Five-day-old seedlings expression GFP-MAP65-3 were incubated with 20 μM PD98059, a MAPKK inhibitor, for 2 h, and then were pulsed with 5 μM FM 4-64 for 5min. The patterns are representative for 37 cells for controls and 61 cells for inhibitor treatments from three independent experiments. Bar, 10 μm. (F) Velocities of microtubule polymerization (growth, n = 84 for wild type, n = 79 for *pi4kβ1 pi4kβ2*) and depolymerization (shrinkage; n = 68 for wild type, n = 53 for *pi4kβ1 pi4kβ2*) were determined *in vivo* in cells of the root elongation zone in wild type controls and *pi4kβ1 pi4kβ2* double mutants expressing the microtubule marker, mCherry-TUA5. Velocities are given in the panel (black bars, wild type; white bars, *pi4kβ1 pi4kβ2* double mutants). Data represent means ± SD. The experiment was repeated twice showing consistent results. The asterisk indicates a significant change from the wild type control according to a Student's *t*-test (\* p < 0.05). n.s., not significant.

compared to wild type where GFP-MAP65-3 was concentrated at the cell plate (n = 63 cells). Instead, in the *mpk4-2* mutant GFP-MAP65-3 was diffusely distributed around the cell plate, indicating that MPK4 is involved in the targeting of MAP65-3 to the cell plate (Fig. 3.6D). Since knock out of MPK4 resulted in the loss of both MPK4 protein and activity, in order to dissect whether occurrence of solid MAP65-3 was due to loss of MPK4 protein rather than activity, a universal MAPKK inhibitor PD98059 was used. After treatment for 2 h, which is sufficient to inhibit MPK4 activity (Beck et al., 2011), MAP65-3 was still localized to the cell plate without displaying fan-like patterns (n = 61 cells), suggesting that MPK4 localization instead of activity may be involved in MAP65-3 targeting to the cell plate during late cytokinesis (Fig. 3.6E).

An accumulation of MAP65-3 found at the midline, such as observed in

the *pi4kβ1 pi4kβ2* double mutant, would overstabilize nIMTs of phragmoplasts to form IMTs, which are thought to be more stable than nIMTs (Ho et al., 2011), and prevent phragmoplast transition. Therefore, we next asked whether the dynamics of microtubules were altered in the *pi4kβ1 pi4kβ2* double mutant. To this end, the microtubule marker mCherry-TUA5 (Endler et al., 2015) was introgressed into the *pi4kβ1 pi4kβ2* background to enable the recording of real-time microtubule dynamics *in vivo*. Because of robust microtubule bundles in the phragmoplast, it is often difficult to measure the dynamics of phragmoplast microtubules. Therefore, we alternatively determined dynamic parameters for cortical microtubules from cells of the root elongation zone. Most parameters of microtubule dynamics were globally unchanged in the *pi4kβ1 pi4kβ2* double mutant, including density, bundling and growth rate (Fig. 3.6F; Appendix Fig. 7.3 and 7.4), indicating there were no gross defects in microtubule arrays in these plants. However, the microtubular rate of shrinkage in the *pi4kβ1 pi4kβ2* double mutant was significantly lower than in wild type controls ( $P < 0.05$ ) (Fig. 3.6F), indicating that the occurrence of stabilized phragmoplast arrays in mitotic cells of the *pi4kβ1 pi4kβ2* double mutant was likely a consequence of reduced shrinkage rates in addition to overbundling of microtubules by MAP65-3 at the midline (Fig. 3.6A-C; cf. Fig. 3.5). Both the MAP65-3 distribution and the *in vivo* dynamics of microtubules are, thus, consistent with the microtubular patterns observed in the mitotic cells of the *pi4kβ1 pi4kβ2* double mutant. However, it must be stated that the data on *in vivo* microtubule dynamics were not obtained for phragmoplast microtubules,

### 3.6 PI4Kβ1 and MPK4 interact genetically and physically in *A. thaliana*

Besides an altered localization pattern of the MPK4 target, MAP65-3, the data so far indicated that the phenotypes of the *pi4kβ1 pi4kβ2* double mutant were reminiscent of those reported for the *mpk4* mutant, including cytokinetic defects (Beck et al., 2011; Kosetsu et al., 2010), stabilized microtubules (Beck et al., 2010), constitutive salicylic acid accumulation (Šašek et al., 2014), and

systemic acquired resistance (Petersen et al., 2000). Therefore, we investigated a possible link between PI4K $\beta$ s and the MAPK, MPK4, which both regulate cell plate formation.

First, it was investigated whether PI4K $\beta$  genetically interacted with MPK4. For this purpose, the *mpk4-2* mutant was crossed with the *pi4k $\beta$ 1 pi4k $\beta$ 2* double mutant, and the offspring of self-pollinated *pi4k $\beta$ 1<sup>(-/-)</sup> pi4k $\beta$ 2<sup>(+/-)</sup> mpk4-2<sup>(+/-)</sup>* plants was analyzed. The overall segregation pattern obtained from these crosses (see Appendix Table 7.1) diverged significantly from Mendelian law ( $P < 0.0001$ ). Among 181 progenies no triple homozygote plant could be isolated, suggesting that fertilization, the survival of gametes, or the viability of triple homozygotes might have been affected. It is interesting to note that the *mpk4-2* allele significantly repressed the distribution of the *pi4k $\beta$ 2* allele, or vice versa. A *pi4k $\beta$ 1<sup>(-/-)</sup> pi4k $\beta$ 2<sup>(+/-)</sup> mpk4-2<sup>(-/-)</sup>* mutant was much smaller than either the *mpk4-2* or *pi4k $\beta$ 1 pi4k $\beta$ 2* mutants (Fig. 3.7A). Taken together, the results suggest that the PI4K $\beta$  pathway interacted genetically with MPK4; however, epistasis effects were not clear from the phenotypes observed. We next examined whether PI4K $\beta$ 1 physically interacted with MPK4. For yeast two-hybrid analysis, the PI4K $\beta$ 1 sequence was divided in two fragments, PI4K $\beta$ 1<sub>1-566</sub>, PI4K $\beta$ 1<sub>422-1121</sub>, as reported previously (Preuss et al., 2006). This was done, because the full-length PI4K $\beta$ 1 has previously been shown to not interact with its partner protein, RabA4b, whereas the truncations showed positive interactions (Preuss et al., 2006). In these experiments, MPK4 used as a bait did not show autoactivation, and thus PI4K $\beta$ 1<sub>1-566</sub> clearly interacted with MPK4 (Fig. 3.7B). A positive test observed for PI4K $\beta$ 1<sub>422-1121</sub> cannot be interpreted, as the negative control for this fusion also gave a positive signal (Fig. 3.7B), possibly resulting from non-specific protein binding. The interaction of PI4K $\beta$ 1 and MPK4 was further corroborated by Co-IP *in vivo*. For this experiment, an antibody against the C-terminal fifteen amino acids of PI4K $\beta$ 1 (TRQYDYYQRVLNGIL) was re-raised, according to the protocol reported previously (Preuss et al., 2006). When the

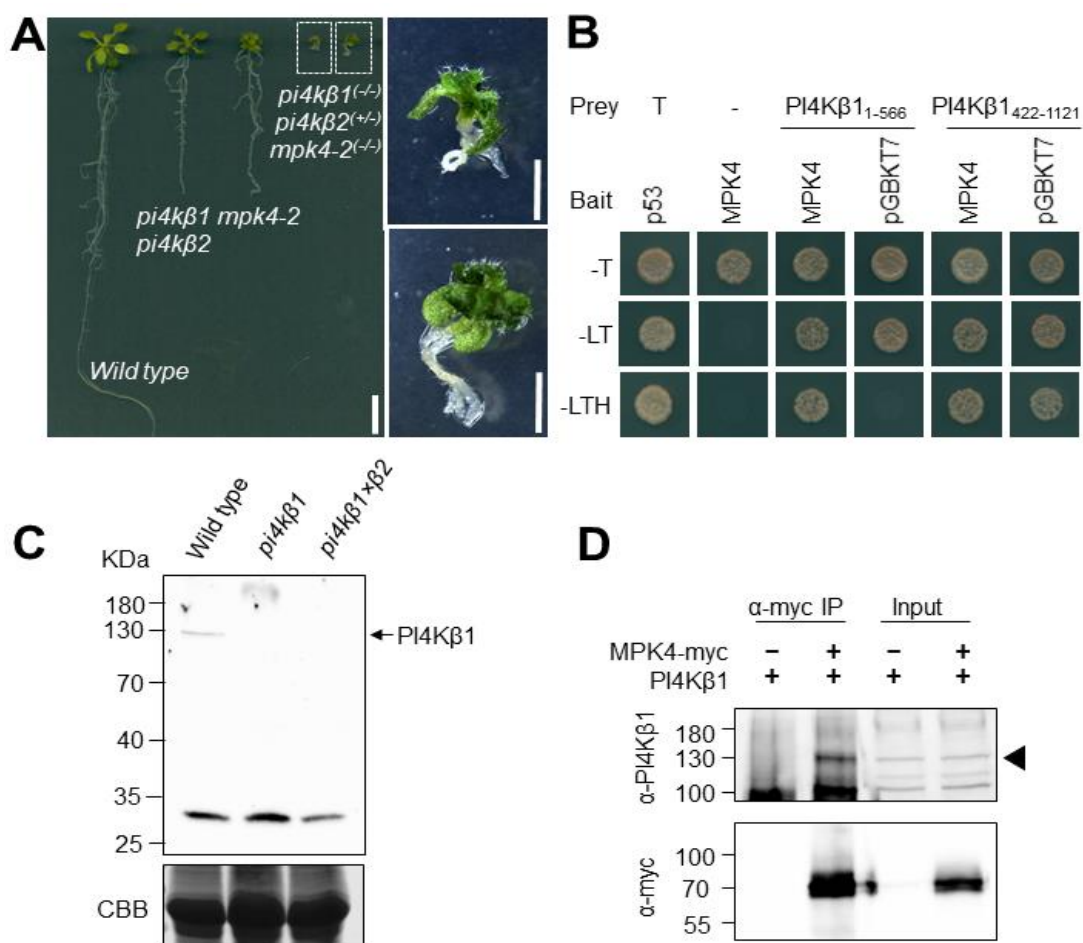


**Figure 3.7. Genetic and physical interaction of PI4Kβ1 and MPK4.** (A) Synergistic genetic interaction of the PI4Kβ and MPK4 pathways was analyzed by crossing the *mpk4-2* allele into the *pi4kβ1 pi4kβ2* background. 14-day-old seedlings are shown. Right panels, *pi4kβ1<sup>(-/-)</sup> pi4kβ2<sup>(+/-)</sup> mpk4-2<sup>(-/-)</sup>* mutants magnified from the marked areas in left panel. Bar in left panel is 1 cm; bars in right panels are 5 cm. A genetic interaction between *pi4kβ1 pi4kβ2* and *mpk4-2* is inferred from the segregation of genotypes (see Appendix Table 7.1). (B) Test for physical interaction of PI4Kβ1 and MPK4 by yeast two hybrid analysis. MPK4 was used as a bait. PI4Kβ1 was divided into two fragments, PI4Kβ1<sub>1-566</sub> and PI4Kβ1<sub>422-1121</sub>, which were separately analyzed as prey proteins. A no prey control was used to test for autoactivation by MPK4. The experiment was repeated thrice with consistent results. T and p53, positive controls; pGBKT7, negative control for interactions. (C) Protein extracts (100 μg protein per lane) of wild type controls, of the *pi4kβ1* mutants and of the *pi4kβ1 pi4kβ2* double mutant were electrophoresed by SDS-PAGE, blotted and probed with the custom antibody against the C-terminal PI4Kβ1 peptide sequence, TRQYDYYQRVLNGIL. An identically loaded gel, stained by Coomassie Brilliant Blue, was used as a loading control. The experiment was repeated twice showing similar results. CBB: Coomassie Brilliant Blue. Arrow, full length PI4Kβ1. Note, the unspecific band at around 30 kDa. (D) Test for physical interaction of PI4Kβ1 and MPK4 by *in vivo* Co-IP from 14-day-old *A. thaliana* plants. PI4Kβ1 was specifically co-precipitated with MPK4-myc using anti-myc antibodies. The experiment was repeated thrice with similar results. Arrowhead, PI4Kβ1. Proteins were detected using anti-PI4Kβ1 and anti-myc antisera, as indicated.

specificity of the antibody against the PI4K $\beta$ 1 peptide was verified by analyzing crude extracts from wild type *A. thaliana*, the *pi4k $\beta$ 1* single mutant, and the *pi4k $\beta$ 1 pi4k $\beta$ 2* double mutant, the antibody recognized a band at 130 kDa corresponding to the size of the PI4K $\beta$ 1 or PI4K $\beta$ 2 proteins in wild type material, but not in *pi4k $\beta$ 1* or *pi4k $\beta$ 1 pi4k $\beta$ 2* mutants (Fig. 3.7C), indicating the antibody was specific for PI4K $\beta$ 1. It is worth noting that the antibody also recognized an unspecific band at around 30 kDa (Fig. 3.7C). Using the new antibody, PI4K $\beta$ 1 was detected in protein complexes immunoprecipitated from *A. thaliana* seedlings expressing MPK4-myc when MPK4-myc was pulled down using an anti-myc antibody (Fig. 3.7D). Importantly, no PI4K $\beta$ 1 signal was detected upon immunoprecipitation from wild type seedlings used as a negative control (Fig. 3.7D), demonstrating that the observed *in planta* interaction of PI4K $\beta$ 1 and MPK4 was specific. Together, these experiments demonstrate a physical interaction of PI4K $\beta$ 1 and MPK4, suggesting that both players act in a common pathway to regulate cell plate formation.

### **3.7 MPK4 colocalizes with PI4K $\beta$ 1 at the cell plate but may precede PtdIns4P formation during somatic cytokinesis**

As PI4K $\beta$ 1 and MPK4 interacted, next their spatio-temporal coordination at the cell plate was investigated. In *A. thaliana* root cells, functional MPK4-YFP (Berriri et al., 2012) co-localized with mCherry-PI4K $\beta$ 1 from early to late cytokinesis and both signals concentrated at the periphery of the cell plates (Fig. 3.8A). The interaction and colocalization of PI4K $\beta$ 1 and MPK4 at the cell plate suggest a function of PI4K $\beta$ 1 in the control of somatic cytokinesis. Then the product PtdIns4P was recorded together with MPK4 at the cell plate. To this end, an Arabidopsis line expressing the PtdIns4P reporter, RFP<sub>FAPP1-PH</sub> (Vermeer et al., 2009), was crossed with plants expressing MPK4-YFP, and the association of MPK4-YFP with the cell plate was analyzed over time in relation to the distribution of the PtdIns4P reporter. Interestingly, MPK4-YFP

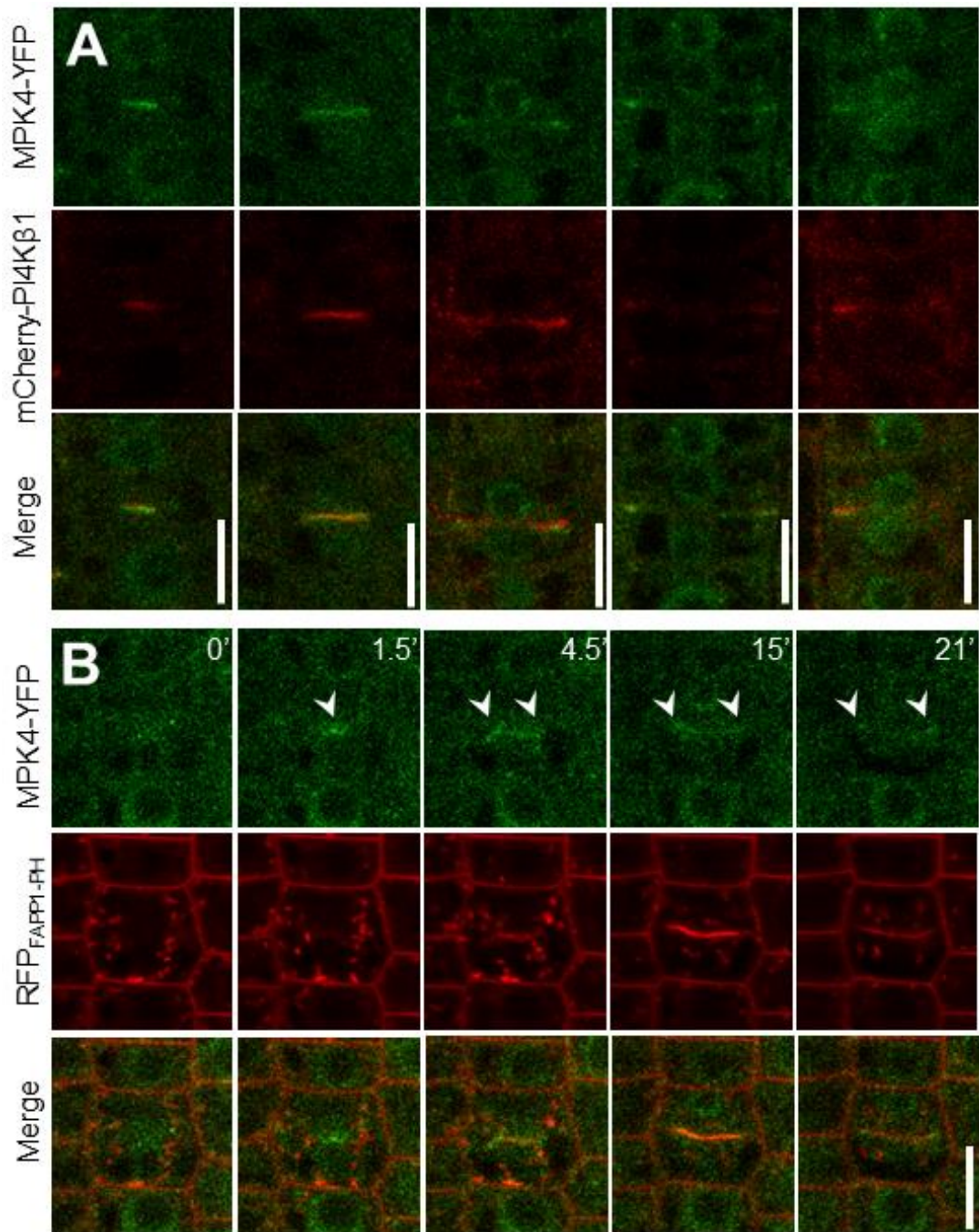


**Figure 3.8. Coordination of MPK4-YFP with mCherry-PI4K $\beta$ 1 and PtdIns4P in cytokinesis from five-day-old root meristem cells.** (A) The distribution of the interacting MPK4-YFP and mCherry-PI4K $\beta$ 1 was recorded *in vivo* during cytokinesis of root meristem cells in five-day-old seedlings using an LSM880 in Airyscan super-resolution (SR) mode. MPK4-YFP colocalized with PI4K $\beta$ 1 from early to late cytokinesis and gradually concentrated at the leading edges of cell plates. Bar, 10  $\mu$ m. (B) The distribution of MPK4-YFP and RFP<sub>FAPP1-PH</sub> was monitored during cytokinesis using an LSM880 in Airyscan R-S mode. MPK4-YFP labeled the entire cell plate during early cytokinesis and gradually concentrated at the leading edges of the expanding cell plate during late cytokinesis. In contrast, RFP<sub>FAPP1-PH</sub> was observed at the cell plate later than MPK4-YFP, labeling the entire cell plate throughout cytokinesis (n = 6 cells of 5 seedlings). Bar, 10  $\mu$ m; numbers indicate the recording time in min.

fluorescence occurred earlier at the nascent cell plate than the PtdIns4P reporter (Fig. 3.8B, n = 6 cells). This pattern suggests that PtdIns4P was not required for the recruitment of MPK4 to the cell plate. The colocalization of the interacting proteins at the cell plate and the delayed appearance of the PtdIns4P reporter suggest instead that the formation of PtdIns4P might be activated by MPK4.

### 3.8 Possible control of PI4K $\beta$ 1 by MPK4

The data so far suggested a physical and spatial interaction of PI4K $\beta$ s and MPK4. However, the functional consequences of the interaction remained obscure. It was recently reported that enzymes of plant phosphoinositide metabolism can be regulated by MAPKs (Hempel et al., 2017). As additionally PI4K $\beta$ 1 was recently reported as a phosphorylation target of MPK4 upon flagellin 22 (flag22) treatment (supplement to Latrasse et al., 2017), we next tested whether phosphorylation by MPK4 influenced the catalytic activity of PI4K $\beta$ 1. First, an influence of activated recombinant MPK4 on the PtdIns 4-kinase activity of recombinant PI4K $\beta$ 1 was tested *in vitro* (Fig. 3.9). While phosphorylation of PI4K $\beta$ 1 could be verified in our experiments (Fig. 3.9A), the phosphorylation did not affect catalytic activity of the enzyme (Fig. 3.9B). While phosphorylation of PI4K $\beta$ 1 by MPK4 suggests that MPK4 is an upstream regulator of PI4K $\beta$ 1, our experimental data do not support (nor refute) an effect of MPK4 on the activity of PI4K $\beta$ 1. Thus, the *in vitro* data do not provide evidence for an activation of PI4K $\beta$ 1 and/or PI4K $\beta$ 2 by MPK4, as might be concluded from the the delayed appearance of the PtdIns4P reported at the cell plate (Figure. 3.8 B).

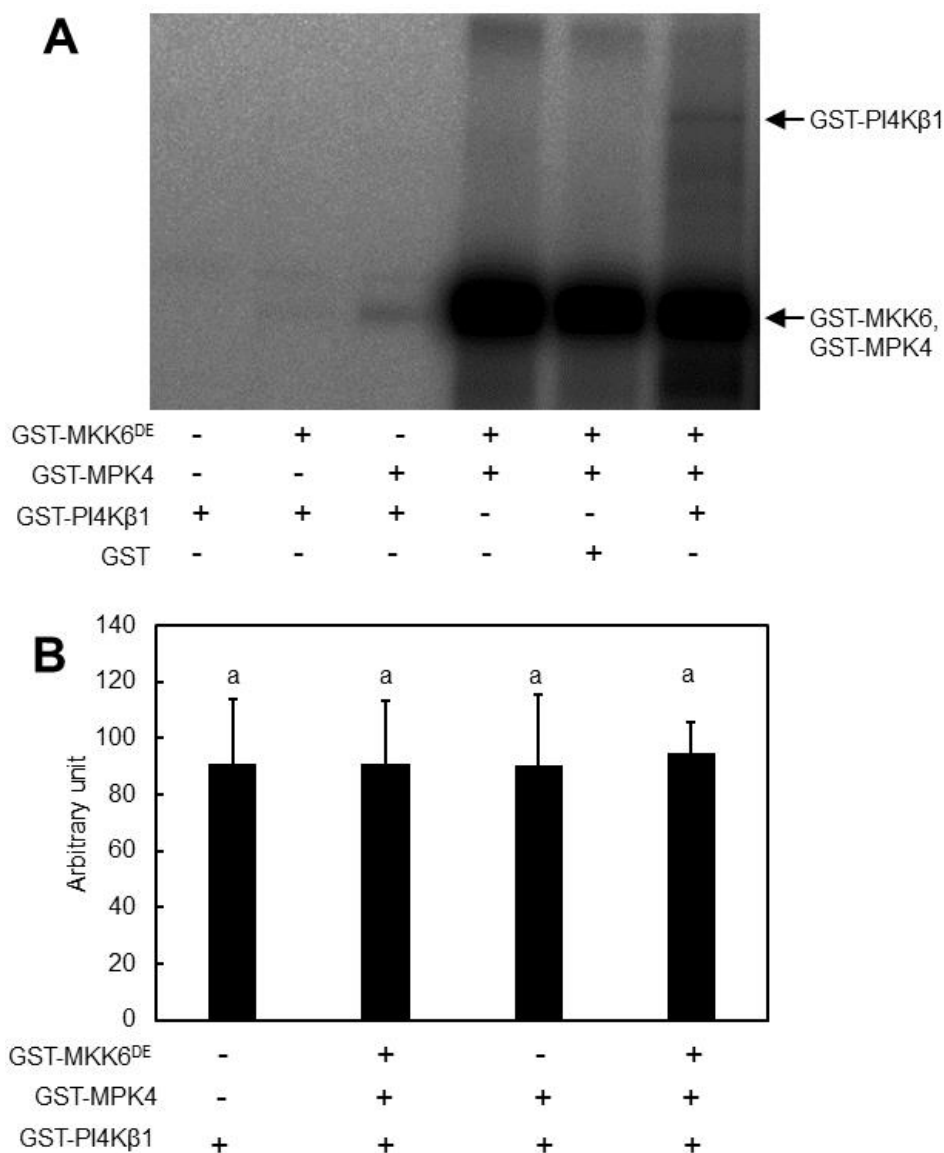


**Figure 3.9. Phosphorylation by MPK4 does not regulate PI4Kβ1 activity in vitro.** (A) In vitro phosphorylation assay of PI4Kβ1 by MPK4. Purified recombinant MPK4 were preactivated in the presence of MKK6<sup>DE</sup>, then activated MPK4 was incubated with purified GST-PI4Kβ1 in the presence of  $\gamma$ -[<sup>32</sup>P]ATP, proteins were separated by SDS-PAGE, and the incorporation of the radiolabel was analyzed by phosphor imaging. About 0.2  $\mu$ g MPK4, 0.3  $\mu$ g MKK6<sup>DE</sup>, 3  $\mu$ g GST-PI4Kβ1 and 3  $\mu$ g GST were used, respectively. The experiment was performed once showing consistent results with the published paper. (B) Phosphorylation of PI4Kβ1 has no effect on its activity. Recombinant PI4Kβ1 protein was preincubated with preactivated MPK4 by MKK6<sup>DE</sup>, and subsequently analyzed for catalytic activity against the lipid substrate, PtdInsP. The catalytic activity was calculated relative to the activity of GST-PI4Kβ1 alone. The data represent the mean  $\pm$  SD from three experiments, and performed twice.

Phosphorylation of PI4Kβ1 by MPK4 may alternatively influence PI4Kβ1 localization. Therefore, a functional mCherry-PI4Kβ1 fusion was introduced into

the *mpk4-2* mutant background and the fluorescence distribution compared to that in wild type (Appendix Fig 7.5) in preliminary experiments. As fluorescence was weak (cf. Figure 3.2 C), our analyses were limited to observation with a light-sensitive spinning disc system. These analyses were done by Dr. Praveen Krishnamoorthy (MLU). Despite of the low imaging resolution, we observed differences in the localization of mCherry-PI4K $\beta$ 1. Whereas in wild type mCherry-PI4K $\beta$ 1 labeled diffuse cytoplasmic structures (possibly Golgi) and brighter dot-like structures at their periphery (possibly TGN), in the *mpk4-2* mutant the bright TGN-like structures were reduced (Appendix Fig 7.5). Importantly, the reported subcellular location for PI4K $\beta$ 1 is the TGN (Kang et al., 2011; Preuss et al., 2006). Our preliminary data suggest that PI4K $\beta$ 1 may require MPK4 to correctly associate with the TGN and exert its function in PtdIns4P formation,

### 3.9 Possible control of MPK4 by PI4K $\beta$ 1

Based on the physical and genetic interactions between PI4K $\beta$  and MPK4 (cf. Fig. 3.7A-D), and the proposed role for PI4K $\beta$ 1 in cytokinesis, it was also explored whether the interaction of PI4K $\beta$ 1 with MPK4 affected MPK4 activity, which is known to be required for cytokinesis (Beck et al., 2011), or whether PI4K $\beta$ 1 and its product PtdIns4P may regulate MPK4 localization at the cell plate to control cytokinesis. As ineffective transition of phragmoplasts in late cytokinesis might be due to decreased activity of MPK4 in the *pi4k $\beta$ 1 pi4k $\beta$ 2* double mutant, the MPK4 activity in wild type and *pi4k $\beta$ 1 pi4k $\beta$ 2* double mutants was compared by conducting immunocomplex kinase activity assays using specific anti-MPK4 antibodies (Fig. 3.10A). In these experiments, MPK4 activity was not changed in the *pi4k $\beta$ 1 pi4k $\beta$ 2* double mutant (Fig. 3.10B). It shall be noted that MPK4 was not immunoprecipitated from dividing cells. In an alternative experiment, expression of constitutively active MPK4 in the *pi4k $\beta$ 1 pi4k $\beta$ 2* double mutants could not rescue the phenotype (Fig. 3.10C),

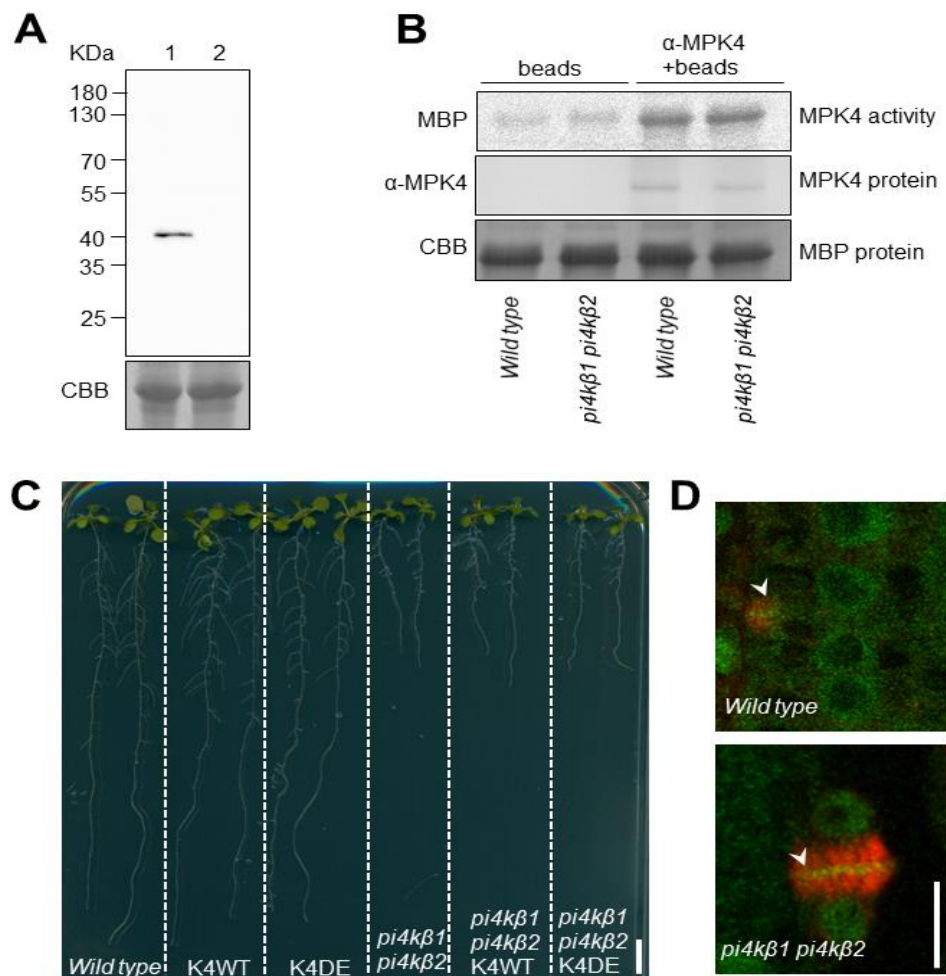


**Figure 3.10. Localization of MPK4 but not activity is changed in the *pi4kβ1 pi4kβ2* double mutant.** (A) The specificity of the anti-MPK4 antibodies against crude extracts from 7-day-old seedlings of *wild type* (1) and *mpk4-2* mutants (2) was verified by gel blotting. An identically loaded gel, stained by Coomassie Brilliant Blue, was used as a loading control. CBB: Coomassie Brilliant Blue. The experiment was performed with two replicates for each genotype. (B) Endogenous MPK4 was immunoprecipitated with the anti-MPK4 antibody, and incubated with myelin basic protein (MBP) as an *in vitro* phosphorylation substrate in the presence of  $\gamma$ - $^{33}\text{P}$ ATP. Phosphorylated MBP was visualized by autoradiography after SDS-PAGE. MPK4 proteins were detected with MPK4-specific antibodies via western blotting showing that equal amount of protein were precipitated from wild type controls and the *pi4kβ1 pi4kβ2* double mutants. MBP protein loading was assessed by CBB staining. The experiment was repeated trice with consistent results. (C) Constitutively activated MPK4 (K4DE) and *wild type* of MPK4 (K4WT) could not rescue the phenotype of the *pi4kβ1 pi4kβ2* double mutant. 11-day-old seedlings were shown. Bar is 1 cm. (D) Retention of MPK4-YFP (green) at the cell plate of cytokinetic root meristem cells of *pi4kβ1 pi4kβ2* double mutants. During late cytokinetic stages, as judged by the reappearance of nuclei, MPK4-YFP localized at leading edges of cell plates in wild type cells, whereas MPK4-YFP labeled the entire cell plate in the *pi4kβ1 pi4kβ2* double mutant. 6-day-old seedlings were imaged by LSM880 in Airyscan resolution vs sensitivity (R-S) mode. Arrowheads, forming cell plates. Note the solid phragmoplasts (red) at late cytokinetic stages in the *pi4kβ1 pi4kβ2* double mutants. Bars, 10  $\mu\text{m}$ .

suggesting that the function of MPK4 may be influenced in the *pi4kβ1 pi4kβ2* double mutant possibly by an effect on its localization.

To further test an influence of PtdIns4P on the localization of MPK4, MPK4-YFP and mCherry-TUA5 (Endler et al., 2015) fusions were introgressed into the *pi4kβ1 pi4kβ2* background and their subcellular distribution was analyzed by confocal microscopy. In wild type plants, MPK4-YFP concentrated at the leading edges of cell plates, radially expanding in ring-like structures of the phragmoplasts at late cytokinesis stages (94.9 %, n = 39 cells) (Fig. 3.10D), consistent with previous reports (Kosetsu et al., 2010). In contrast, in the *pi4kβ1 pi4kβ2* double mutant MPK4-YFP was not restricted to the leading edges of the phragmoplast and labelled the entire cell plate during late cytokinesis (60.0 %, n = 35 cells) (Fig. 3.10D), indicating that the turnover of MPK4-YFP at the cell plate was impaired, and thus depended on PI4Kβs. This result was surprising, as the ectopic stabilization of MPK4-YFP at the cell plate coincided with the stabilization of phragmoplast arrays, which contrasts with a previously reported destabilizing effect of MPK4 on microtubules (Kosetsu et al., 2010; Sasabe et al., 2006). To better understand this unexpected localization behavior of MPK4 in the *pi4kβ1 pi4kβ2* double mutant, we next investigated the effects of PI4Kβs on the dynamics of MPK4 at the cell plate.

### 3.9.1 MPK4 associates with BFA-sensitive membrane compartments

The cell plate-associated dynamics of MPK4 are currently not well defined. Therefore, MPK4 dynamics was tracked by spinning disc microscopy. Surprisingly, in root cells MPK4-YFP formed dot-like structures (Fig. 3.11A). To analyze whether these punctate structures were transitory compartments of membrane trafficking (e.g., vesicles), the root cells of *A. thaliana* plants expressing MPK4-YFP were labeled with the membrane dye, FM 4-64. MPK4-YFP partially colocalized with FM 4-64 in punctate structures (Fig. 3.11B, left panels), suggesting that MPK4-YFP associated with endosomes. To further test

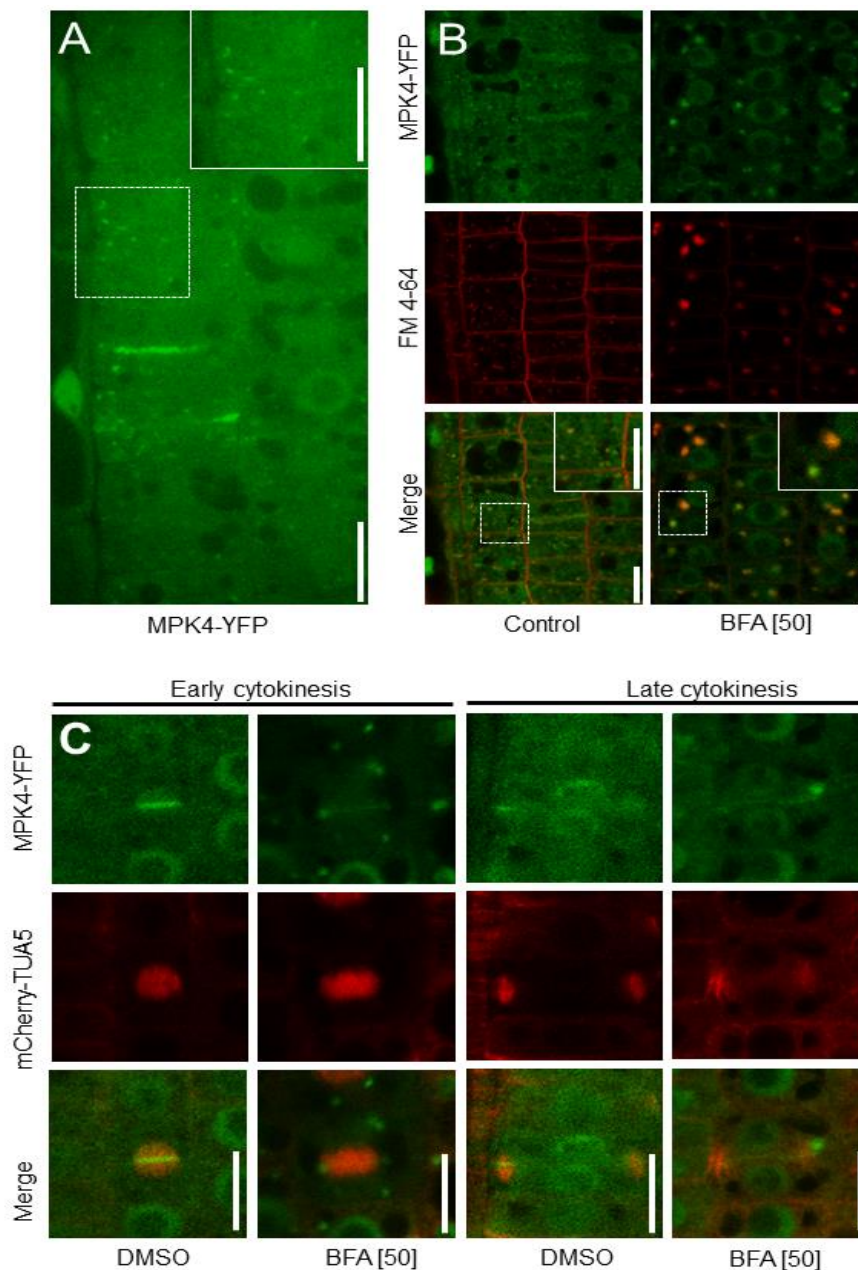


**Figure 3.11. MPK4 targeting to the cell plate is defined by a BFA-sensitive membrane trafficking pathway.** (A) An overview of five-day-old roots expressing MPK4-YFP by spinning disc microscopy. Inset, magnification from the dashed rectangle. The image is representative for at least 20 independent seedlings. Bars, 10  $\mu$ m. (B) MPK4-YFP partially co-localized with the membrane dye FM 4-64. Left panels, five-day-old seedlings were pulsed with 10  $\mu$ M FM 4-64 for 10 min, washed and images were recorded. Right panels, five-day-old seedlings were pulsed with 10  $\mu$ M FM 4-64 for 5 min, washed and then incubated with 50  $\mu$ M BFA (BFA [50]) for 30 min. Insets, magnifications of areas marked by dashed rectangles. The images are representative for 9 independent seedlings from two independent experiments for controls, and 21 independent seedlings from three independent experiments for BFA treatments, respectively. Bars, 10  $\mu$ m. (C) MPK4-YFP decorated cell plate-associated BFA bodies during early (left panels) and late stages (right panels) of cytokinesis. Five-day-old seedlings were treated with 50  $\mu$ M BFA or DMSO for 30 min. The patterns are representative for > 10 cells. Bars, 10  $\mu$ m.

for membrane-associated trafficking of MPK4-YFP, BFA was used to specifically block secretion and recycling (Fig. 3.11B). In these experiments, MPK4-YFP was observed in BFA bodies co-labeled with FM 4-64 (Fig. 3.11B, right panels). To further test MPK4 trafficking during cytokinesis, BFA was used alone, because extended CHX application prevented the progression of the cells to telophase (data not shown). When roots of *A. thaliana* plants expressing mCherry-TUA5 and MPK4-YFP were treated for 30 min with 50  $\mu$ M BFA, MPK4-YFP was found in BFA bodies during both early (73.9 %, n = 23 cells ) and late cytokinesis (66 %, n = 50 cells) (Fig. 3.11C ). No BFA bodies were observed in controls treated with DMSO alone. As MPK4-YFP-labeled BFA bodies were found to sometimes connect to cell plates (Fig. 3.11C), it was concluded that in the vicinity of the cell plate, MPK4-YFP associated with BFA-sensitive membrane compartments, possibly the TGN. An association of MPK4 with the TGN is consistent with the observed interaction of MPK4 with PI4K $\beta$ 1, because PI4K $\beta$ 1 has previously been shown to reside at the TGN (Kang et al., 2011; Preuss et al., 2006). It appears plausible that the interaction of MPK4 and PI4K $\beta$ 1 might mediate the association of MPK4 with TGN vesicles, and that the lack of PI4K $\beta$ s in the *pi4k $\beta$ 1 pi4k $\beta$ 2* double mutant prevents this recruitment and is a reason for MPK4 failing to exit from the cell plate.

## 4. Discussion

The new findings reported in this study indicate that PtdIns4P positively regulates somatic cytokinesis in *A. thaliana* by acting in a common pathway with MPK4 and MAP65-3 at the cell plate and consequently affecting phragmoplast expansion. While it had previously been demonstrated that PtdIns4P resides at the cell plate of plant cells, no focused study on the functional contribution of PtdIns4P to cell plate formation has been reported to date. This thesis sheds new light on how PtdIns4P contributes to the control of cytokinesis in *A. thaliana*.

### 4.1 Functional complementation of the *pi4kβ1 pi4kβ2* double mutant aids the analysis of PI4Kβs

In this thesis the cytokinesis defects of an *A. thaliana pi4kβ1 pi4kβ2* double T-DNA insertion mutant were analyzed, which was published more than a decade ago (Preuss et al., 2006). As approx. 50 % of mutants induced by T-DNA insertions in *A. thaliana* are accompanied by additional insertion sites in the genome ([http://signal.salk.edu/tdna\\_FAQs.html](http://signal.salk.edu/tdna_FAQs.html)), the first step was to assure that the phenotypes of the *pi4kβ1 pi4kβ2* double mutant are truly due to the insertions in the *PI4Kβ1* and *PI4Kβ2* genes and not a consequence of unrelated background mutations. Several complementation constructs were introgressed into the *pi4kβ1 pi4kβ2* double mutant to check for genetic complementation. The observation that all of these constructs rescued the phenotype of the double mutant (Fig. 3.1) indicates that the phenotype was indeed caused by knockout of the *PI4Kβ1* and *PI4Kβ2* genes. This information provided an important basis for all further experiments presented in this thesis.

### 4.2 PI4Kβ1/PtdIns4P at the growing cell plate is required for somatic cytokinesis in *A. thaliana*

It was previously reported that AtPI4Kβ1 localized to compartments labelled by RabA4b and subsequently the enzyme was shown to localize at the TGN by

electron microscopy/tomography (Kang et al., 2011; Preuss et al., 2006). While a PtdIns4P reporter has been shown to decorate the cell plate of dividing plant cells (Vermeer et al., 2009), an association of a PtdIns 4-kinase with the cell plate has not been reported. The AtPI4K $\beta$ 1 counterpart from *Schizosaccharomyces pombe*, Pik1p, is recruited to the medial cell plane during cytokinesis (Park et al., 2009). In contrast, the phosphatidylinositol 4-kinase III  $\beta$ , Four wheel drive (Fwd) of *Drosophila melanogaster* does not localize at the midzone during cytokinesis, even though PtdIns4P is present at the midzone (Polevoy et al., 2009). These distinct localizations suggest that PI4K $\beta$  proteins in different species may exert different functions during cytokinesis. At the beginning of this work, there was no information on the localization of PI4K $\beta$ 1 during cytokinesis in *A. thaliana* largely due to the fact that no functional fluorescence tagged PI4K $\beta$ 1 was available, as direct fusions of fluorophores with CDS of PI4K $\beta$ 1 were found to be non-functional (personal communication by Dr. Erik Nielsen, University of Michigan at Ann Arbor, MI, USA). To this end, we designed an mCherry-tagged variant of PI4K $\beta$ 1 encoded by a 11 kb genomic DNA fragment, which fully rescued the dwarf phenotype of the *pi4k $\beta$ 1 pi4k $\beta$ 2* double mutant (Fig. 3.2A and 3.2B). The successful complementation of the *pi4k $\beta$ 1 pi4k $\beta$ 2* double mutant by the genomic fusion, but not by previous and also presently tested cDNA constructs, suggests that some regulatory elements of the genomic sequence aid the processing of the functional mCherry-PI4K $\beta$ 1 chimaeric protein. As the signal for the expressed mCherry-PI4K $\beta$ 1 was weak, the Airyscan detector was used to capture mCherry-PI4K $\beta$ 1 distribution in mitotic cells and showed for the first time that mCherry-PI4K $\beta$ 1 localized to nascent cell plates *in vivo* (Fig. 3.2C). Further immunostaining clearly showed that mCherry-PI4K $\beta$ 1 was localized to the cell plate from the beginning till the end of cytokinesis (Fig. 3.2D; [III] and [IV]). Additionally, mCherry-PI4K $\beta$ 1 was also shown to be present in preprophase and metaphase but it was diffuse in these mitotic phases (Fig. 3.2; [I] and [II]). Taken together, these observations upon functional complementation with the

genomic fusion indicate that mCherry-PI4K $\beta$ 1 functions throughout mitotic and cytokinetic phases. Subsequently, the functional construct *pKNOLLE:FLAG-PI4K $\beta$ 1* was also created in order to determine to which extent PI4K $\beta$ 1 contributed to cytokinesis. Surprisingly, the *pKNOLLE*-driven construct also fully rescued the phenotype of the *pi4k $\beta$ 1 pi4k $\beta$ 2* double mutant (Fig. 3.3A and 3.3B; Appendix Fig. 7.2), suggesting that triggering expression of *FLAG-PI4K $\beta$ 1* in G2/M driven by *pKNOLLE* was enough to overcome cytokinetic defects. However, beside cytokinetic defects was rescued by this construct, the dwarf phenotype was also rescued, implying that FLAG-PI4K $\beta$ 1 may persist beyond cytokinetic cells. Such phenotype was reported for *cyclopropylsterol isomerase1 (CPI1)* expression driven by *pKNOLLE* and after cytokinesis, CPI1 still existed in interphase cells (Men et al., 2008). Bearing this in mind, immunostaining was performed to test whether FLAG-PI4K $\beta$ 1 could also be found in interphase cells. Unfortunately, several anti-FLAG antibodies were tested, and none of them worked for western blotting and immunostaining, demonstrating FLAG epitope was not accessible by these antibodies, possibly due to break between FLAG and PI4K $\beta$ 1 or FLAG epitope was masked by some modifications in planta such as sulfation which is reported to modify tyrosine (Y) of FLAG to prevent recognition of FLAG epitope by anti-FLAG antibodies. Together with the previous report that a kinase inactive variant of PI4K $\beta$ 1 failed to rescue the phenotype of the *pi4k $\beta$ 1 pi4k $\beta$ 2* double mutant (Antignani et al., 2015), we conclude that PI4K $\beta$ 1 present in mitotic and cytokinetic cells produced PtdIns4P required for mitosis and cytokinesis. As the persistence of the PI4K $\beta$ 1 protein expressed from the KNOLLE promoter could not successfully be analyzed by our methods, we have no information on the PI4K $\beta$ 1 abundance in these complemented lines. However, the biochemical analysis of global levels of PtdIns4P (Appendix Fig. 7.1) did not yield any differences between wild type controls, the *pi4k $\beta$ 1 pi4k $\beta$ 2* double mutants or the complemented lines tested, suggesting that the contribution of PI4K $\beta$ 1 to the global mass of cellular PtdIns4P might be small, and that the abundance of

PI4K $\beta$ 1 protein might overall be low. If the action of PI4K $\beta$ 1 and PI4K $\beta$ 2 is restricted to few mitotic cells in a tissue undergoing certain phases of cell division, this may amount to too small a pool of PtdIns4P to be detected by mass measurements against the larger contribution of PtdIns4P formed by other PI4K isoforms. Nonetheless, even a small pool of PtdIns4P formed by PI4K $\beta$ 1 and PI4K $\beta$ 2 might of great importance for plant cell division. Based on these experiments, it was attempted to delineate the regulatory effects of PI4K $\beta$  isoforms on plant somatic cytokinesis.

### **4.3 Characterization of cytokinetic defects of the *pi4k $\beta$ 1 pi4k $\beta$ 2* double mutant**

At the onset of this work, it was already known that the *pi4k $\beta$ 1 pi4k $\beta$ 2* double mutant shows defective root hair growth and that abolishing the interaction of PI4K $\beta$ s with RabA4b disrupts polarized secretion (Preuss et al., 2006). It had also been reported that the *pi4k $\beta$ 1 pi4k $\beta$ 2* double mutant has cytokinetic defects, signified by the appearance of cell wall stubs (Kang et al., 2011). However, no further study focused on the molecular mechanisms underlying the cytokinetic defects. In the present work the cytokinetic defects were examined in more detail, initially with the aid of PI staining and immunostaining. Cell wall stubs were found in the double mutant, but not in single mutants and complement lines (Fig. 3.1B). Furthermore, multinucleated cells and aberrant solid phragmoplasts were identified in the double mutant (Fig. 3.3), suggesting that cytokinesis was impaired in the *pi4k $\beta$ 1 pi4k $\beta$ 2* double mutant, possibly because of disrupted transition of phragmoplasts. These new observations served as the basis for further experiments, indicating a role of cell plate-associated PtdIns4P in the control of phragmoplast microtubule during somatic cytokinesis.

### **4.4 Regulatory interplay of MPK4 and PI4K $\beta$ 1**

Since in the *pi4k $\beta$ 1 pi4k $\beta$ 2* double mutant solid phragmoplasts occurred in late cytokinesis, it was concluded that phragmoplasts were more stable in the

double mutant, possibly due to altered dynamics of microtubules. Consistent with this notion, knockout of the kinesin *HINKEL* also results in solid phragmoplasts in *A. thaliana* (Strompen et al., 2002). Moreover, mutations causing defects in the terminal component of NACK-PQR, the MAPK MPK4, disrupt cortical and mitotic microtubule dynamics. In consequence, the *A. thaliana mpk4* mutant is characterized by a failure of cytokinetic progression and substantial stabilization of microtubules (Beck et al., 2010; Beck et al., 2011). Besides *mpk4*-like cytokinetic defects, phenotypes of the *pi4kβ1 pi4kβ2* double mutant also include other aspects resembling *mpk4*, including constitutive salicylic acid accumulation (Šašek et al., 2014), and systemic acquired resistance (Petersen et al., 2000). Together, these data suggest MPK4 may be a potential target for regulation by PI4Kβ1/PtdIns4P at the cell plate. Several lines of evidence presented in this thesis support this notion: First, *mpk4-2* genetically interacted with the *pi4kβ1 pi4kβ2* double mutant (Fig. 3.7A). The overall segregation analysis showed *mpk4* and *pi4kβ2* alleles interinhibited each other in the genotypic distribution of the offspring population. No homozygote triple mutant was isolated (see Appendix Table. 7.1), possibly owing to defective fertilization or reduced survival of gametes or the viability of triple homozygotes. The *A. thaliana mpk4* mutant is known to have defects in the male but not the female reproductive organs (Zeng et al., 2011). However, the *mpk4* mutation also affects the viability of female gametes when it is crossed into an *mkk6* mutant background (Kosetsu et al., 2010), suggesting that *mpk4* affects the function of gametes of both sexes. Further reciprocal crosses between *pi4kβ1<sup>(-/-)</sup> pi4kβ2<sup>(+/-)</sup> mpk4-2<sup>(+/-)</sup>* and wild type will be necessary to reveal whether *mpk4* influences the viability of all gametes or not, thereby affecting the generation of triple homozygous plants. As gametophytic survival was not a focus of this work, such additional experiments were not performed in this thesis. Instead, to further elucidate physiological roles of the proposed interaction of PI4Kβs with MPK4, physical interaction of the partners was tested by a combination of Y2H and Co-IP experiments. Here, MPK4 was shown to

physically interact with PI4K $\beta$ 1 (Fig. 3.7B and 3.7D). Specifically, MPK4 interacted with the N-terminus of PI4K $\beta$ 1 which contains the LKU domain and the repetitive domain. Interestingly, this N-terminal part of PI4K $\beta$ 1 also interacted with the Ca<sup>2+</sup> sensor protein, AtCBL1, to regulate tip growth of root hairs. As *mpk4* mutants also have defective root hair development (Kong et al., 2012; Kosetsu et al., 2010), it appears possible that PI4K $\beta$ 1 and AtCBL1 may function in concert with MPK4 during root hair development, a concept to further explore in the future.

Based on the physical interaction of PI4K $\beta$ 1 with MPK4, we next analyzed whether this interaction influenced localization or activity of the partners. In mammals PI4KIII $\beta$  can be phosphorylated by serine/threonine-specific protein kinases, protein kinase D1 (PKD1) and PKD2 at the Ser 294 residue, and 14-3-3 proteins bind to PI4KIII $\beta$  to protect this site-specific phosphorylation from being dephosphorylated to maintain its lipid kinase activity (Hausser et al., 2006; Hausser et al., 2005). In yeast, phosphorylation of Pik1p is involved in regulating its nucleocytoplasmic shuttling rather than altering its activity (Demmel et al., 2008a). These examples highlight that phosphorylation of PI4K $\beta$  proteins may change their activities or localizations. It has recently been reported in the supplemental data of a global screen for novel MAPK targets that PI4K $\beta$ 1 can be phosphorylated by MAPKs, including MPK4 (Latrasse et al., 2017). Furthermore, other enzymes of PI metabolism, such as PI4P 5-kinases, have been shown to be MAPK targets in pollen tubes, which are regulated in their activity by MAPK-mediated phosphorylation (Hempel et al., 2017). We found that PI4K $\beta$ 1 activity was not affected by MPK4, suggesting that localization may be affected by MPK4. In the future, it is tempting to examine whether and how phosphorylation of PI4K $\beta$ 1 by MPK4 might influence its localization. Our preliminary data (Appendix Fig. 7.5) suggest that MPK4 might be important for correct association of PI4K $\beta$ 1 with the TGN, its site of action. As PI4K $\beta$ 1/PtdIns4P appeared in a coordinated pattern with MPK4 at

the cell plate (Fig. 3.8), this thesis also addressed the hypothesis that PI4K $\beta$ 1 reciprocally controls MPK4. PI4K $\beta$ 1 colocalized with MPK4 at the cell plate from early to late cytokinesis, and both enzymes concentrated at the leading edges of cell plates. By contrast, PtdIns4P occurred later than MPK4 in the initiation stage of cytokinesis, and even though both colocalized at the leading edges of the cell plate, PtdIns4P also labeled the cell plate evenly. Based on these observations, it was hypothesized that PI4K $\beta$ 1/PtdIns4P may also control the function of MPK4 during cytokinesis.

#### **4.5 MPK4 activity is not a determinant for phenotypes of the *pi4k $\beta$ 1 pi4k $\beta$ 2* double mutant**

MPK4 activity is proposed to control somatic cytokinesis in plants by phosphorylating downstream MAP65 family members to promote lateral expansion of the phragmoplast (Beck et al., 2010; Beck et al., 2011; Kosetsu et al., 2010; Sasabe et al., 2011b; Sasabe et al., 2006). In the *pi4k $\beta$ 1 pi4k $\beta$ 2* double mutant, the delay of phragmoplast transition in late cytokinesis was reminiscent of that observed in the *hinkel* mutant (Strompen et al., 2002), suggesting that MPK4 function may be altered in the *pi4k $\beta$ 1 pi4k $\beta$ 2* double mutant. However, immunocomplex activity assay showed that MPK4 activity was not altered (Fig. 3.10B), and constitutively active MPK4 activity failed to reverse phenotype of the *pi4k $\beta$ 1 pi4k $\beta$ 2* double mutant (Fig.3.10C), suggesting that MPK4 function was impaired by other means than the regulation of enzyme activity. When thus the localization of MPK4 was examined in the *pi4k $\beta$ 1 pi4k $\beta$ 2* double mutant, during late cytokinesis MPK4 was found to occupy a massively enlarged domain at the cell plate (Fig. 3.10D), demonstrating that altered localization and not activity of MPK4 might be a defining factor for the cytokinetic defects in the *pi4k $\beta$ 1 pi4k $\beta$ 2* double mutant. To better understand a possible role of PtdIns4P in regulating cell plate association of MPK4, it is important to consider how MPK4 enters and leaves the cell plate.

#### 4.6 MPK4 recycling from the cell plate associates with a BFA sensitive membrane trafficking pathway

MPK4 is considered a soluble enzyme, which modifies target proteins in the cytoplasm as well as the nucleus (Cristina et al., 2010). However, our spinning disc microscopy analysis of dynamic MPK4-YFP localization unexpectedly showed punctate structures in root cells (Fig. 3.11A). This may indicate MPK4 also binds to membranes. Further experiments demonstrated that MPK4 was actually partially colocalized with endosomes labelled by FM 4-64 (Fig. 3.11B) and that BFA treatment induced MPK4 association with BFA bodies, overlapping with FM 4-64. These observations suggest that a subset of MPK4 may follow a BFA-sensitive membrane trafficking pathway in addition to soluble distribution patterns. As far as reported, only one member of the *A. thaliana* MAPK family, MPK6, localizes to the PM and the TGN/EE, and BFA treatment triggers MPK6 release from the membrane (Müller et al., 2010). Likewise, the *Medicago sativa* MAPK SIMK (the orthologue of *A. thaliana* MPK6) forms dot-like structures in growing root hair tips (Šamaj et al., 2002). In our experiments, MPK4 behaved differently from MPK6, which may have been due to MPK4 and MPK6 belonging to distinct MAPK subgroups (Group et al., 2002). In animals, MAPKs can bind to membranes through scaffolding proteins, such as MP1-p14, and KSR1, mediating the assembly of MAPK complexes (Dhanasekaran et al., 2007; Wunderlich et al., 2001). Further studies on scaffolding proteins may provide insights on whether MAPKs associating with membranes is also mediated by scaffolding proteins in plants. Since MPK4 associates with membranes that are subject to trafficking, it will be interesting to determine whether and how a subset of MPK4 proteins is targeted to the cell plate. While MPK4 has been demonstrated several years ago to localize at the cell plate during cytokinesis (Kosetsu et al., 2010), it remains largely unknown how MPK4 association with the cell plate is regulated. Currently, for the NACK-PQR pathway only the cell plate localization of the

MAPKKK NPK1 is known to be determined by NACK1 directly interacting via its stalk region (Nishihama et al., 2002).

#### 4.7 Loss-of-function of *PI4Kβ1* and *PI4Kβ2* affects endocytosis

While it has been known that *A. thaliana* PI4Kβ1 functions as an effector of RabA4b to regulate polarized secretion of tip-growth root hair cells (Kang et al., 2011; Preuss et al., 2006), there is currently no evidence that PI4Kβs are also involved in the regulation of endocytosis. This thesis uncovers that *A. thaliana* PI4Kβ1 does affect endocytosis and clathrin recruitment to the cell plate (Fig. 3.4). This notion is relevant with regard to cell plate formation, as CME is critically required for retrieving cargoes and recycling vesicles from cell plates during cell plate expansion and maturation. A critical marker used in this study, CLC2, is only recruited to the cell plate during late stages of cytokinesis and not during early stages (Ito et al., 2012). It was found the recruitment of CLC2 to the cell plate was delayed the *pi4kβ1 pi4kβ2* double mutant, and may cause an ineffective of endocytotic recycling of the cargo proteins from the cell plate. Reduced endocytosis and thus impaired membrane trafficking is consistent with the defects in cell plate formation observed in the *pi4kβ1 pi4kβ2* double mutant. Further analysis of endocytosis of KNOLLE and PIN2 revealed that PI4Kβs/PtdIns4P are also involved in endocytosis in interphase cells (Fig 3.4A and C), demonstrating PI4Kβs/PtdIns4P not only affect endocytosis in cytokinetic cells but also in interphase cells. Dual membrane trafficking roles of PI4Kβs are also the case for animals (Burke et al., 2014; de Graaf et al., 2004; Kapp-Barnea et al., 2006) and yeast (Audhya et al., 2000), suggesting that during the evolution of organismic kingdoms PI4Kβ proteins have retained functions in the regulation of secretion and endocytosis. Nevertheless, how does PI4Kβ/PtdIns4P affect CLC2 recruitment in plants? In eukaryotes, key components of the CME machinery include adaptor proteins mediating the recognition of endocytic cargoes and the recruitment of the clathrin coat (McMahon and Boucrot, 2011). In mammalian cells, the activated small

GTPase, ARF1, an initiating factor of vesicle budding, recruits the clathrin adaptor protein AP-1 (Zhu et al., 1998) and PI4KIII $\beta$  to the Golgi (Godi et al., 1999). PtdIns4P can bind to mammalian AP-1 and recruits the AP-1 complex to the Golgi to mediate secretion (Wang et al., 2003). In yeast, the ARF1-GEF, Sec7p associates with Pik1p and collaboratively they determine the recruitment of the clathrin to the Golgi (Gloor et al., 2010), and PtdIns4P binds to the adaptor protein Gga2p, and recruits Gga2p to the TGN for Golgi-to-endosome trafficking (Demmel et al., 2008b). These instances highlight a role for PI4K $\beta$ /PtdIns4P in regulating membrane trafficking through the recruitment of adaptor proteins. Assuming i) that the CME machinery is highly conserved in eukaryotes, ii) that clathrin is recruited by adaptor proteins, and iii) that clathrin recruitment to cell plates was delayed in the *pi4k $\beta$ 1 pi4k $\beta$ 2* double mutant (cf. Fig. 3.10D), our data imply that the recruitment or function of adaptor complexes reported to mediate CME might be changed at the plane of cell division or elsewhere in the *pi4k $\beta$ 1 pi4k $\beta$ 2* double mutant. Examples for *A. thaliana* adaptor proteins inviting more detailed future studies along these lines include the CME-specific factors, TPLATE or AP-2 (Di Rubbo et al., 2013; Gadeyne et al., 2014; Yamaoka et al., 2013). Besides reduced recruitment of clathrin to the cell plate in the *pi4k $\beta$ 1 pi4k $\beta$ 2* double mutant, it thus remains to be investigated whether recruitment of clathrin to the plasma membrane is also changed

#### **4.8 Unsuccessful transition of MAP65-3 in the *pi4k $\beta$ 1 pi4k $\beta$ 2* double mutant**

The combined data indicate that defects in CME and in microtubule patterns are key aspects underlying the cytokinetic defects of the *A. thaliana pi4k $\beta$ 1 pi4k $\beta$ 2* double mutant. Our experiments show that the downstream target of MPK4, MAP65-3, was also mislocalized in the *pi4k $\beta$ 1 pi4k $\beta$ 2* double mutant, forming a solid rather than a ring-like structure in late cytokinesis *thaliana* (Fig. 3.6A to 3.6C). As MAP65-3 is known to mediate the cross-linking

of antiparallel microtubules of phragmoplasts to form more stable IMTs, the overstabilization of phragmoplasts at late stages of cytokinesis is consistent with compromised regulation and/or localization of MAP65-3. The mislocalization of MAP65-3 may be a consequence of compromised localization of MPK4, because in the *mpk4-2* mutant MAP65-3 was not restricted to the cell plate, forming fan-like patterns around the cell plate in late cytokinesis (Fig. 3.6D), and MAP65-3 was still localized to the cell plate upon inhibition of activity of MAP kinases by PD98059 (Fig 3.6E). While *A. thaliana* MPK4 phosphorylates MAP65-3 *in vitro*, suggesting a physical interaction between MPK4 and MAP65-3 (Kosetsu et al., 2010), it remains unknown how MAP65-3 is localized to the cell plate. In animal cells the MAP65-3 homologue, PRC1, concentrating at the midline is dependent on a kinesin protein-KIF4. KIF4 directly binds to PRC1, and restricts PRC1 to the midline during cytokinesis (Kurasawa et al., 2004; Zhu and Jiang, 2005). In this thesis, MPK4 was demonstrated to play a role on targeting MAP65-3 to the cell plate in late cytokinesis, mostly likely independent of MPK4 activity (Fig 3.6E).

## 5. Summary

Plant somatic cytokinesis requires the coordination of membrane trafficking and cytoskeletal rearrangements. Despite their importance, the exact mechanisms coordinating these aspects remain ambiguous. PtdIns4P, a minor membrane lipid, is synthesized by PI4Ks and localizes to the PM, the TGN, and the cell plate in plants. The aim of this thesis was to identify how cell plate-associated PtdIns4P controls somatic cytokinesis in *A. thaliana*. The expansion of the cell plate requires directed membrane trafficking and the formation of coordinated cytoskeletal structures called phragmoplasts. In this study, PI4K $\beta$  isoforms and PtdIns4P are found to be important new factors controlling clathrin-mediated endocytosis at the cell plate. Furthermore, PI4K $\beta$  and PtdIns4P also influence phragmoplast expansion, which is controlled by MPK4-mediated phosphorylation of members of the MAP65 family. It has recently been shown that PI4K $\beta$  is a target of MPK4. While the regulatory effect of this modification remain largely obscure, the similar cytokinetic defects of *A. thaliana pi4k $\beta$ 1 pi4k $\beta$ 2* double mutants and *mpk4* mutants as well as genetic and physical interaction of PI4K $\beta$ 1 and MPK4 suggest that PI4K $\beta$  and MPK4 may act in a common pathway to control cytokinesis.

At a larger scale, this dissertation demonstrates the interplay of two ancient signaling pathways, the NACK-PQR pathway and the phosphoinositide system of *A. thaliana* in the context of somatic cytokinesis. Although MPK4 has previously been demonstrated to reside at the cell plate during cytokinesis, it has remained unclear how MPK4 is targeted to and removed from the cell plate. The finding that membrane association of MPK4 and its internalization from the cell plate is influenced by PI4K $\beta$ 1 expands our understanding of intertwined membrane trafficking and microtubule rearrangements during somatic cytokinesis in plants, which, possibly, may have relevance also in other species.

## 6. References

- Akhter, S., M.N. Uddin, I.S. Jeong, D.W. Kim, X.-M. Liu, and J.D. Bahk. 2016. Role of Arabidopsis AtPI4Ky3, a type II phosphoinositide 4-kinase, in abiotic stress responses and floral transition. *Plant Biotechnology Journal*. 14:215-230.
- Anders, N., and G. Jürgens. 2008. Large ARF guanine nucleotide exchange factors in membrane trafficking. *Cellular and Molecular Life Sciences*. 65:3433-3445.
- Andreasson, E., T. Jenkins, P. Brodersen, S. Thorgrimsen, N.H. Petersen, S. Zhu, J.L. Qiu, P. Micheelsen, A. Rocher, and M. Petersen. 2005. The MAP kinase substrate MKS1 is a regulator of plant defense responses. *The EMBO journal*. 24:2579-2589.
- Antignani, V., A.L. Klocko, G. Bak, S.D. Chandrasekaran, T. Dunivin, and E. Nielsen. 2015. Recruitment of PLANT U-BOX13 and the PI4K $\beta$ 1/ $\beta$ 2 Phosphatidylinositol-4 Kinases by the Small GTPase RabA4B Plays Important Roles during Salicylic Acid-Mediated Plant Defense Signaling in Arabidopsis. *The Plant Cell*. 27:243-261.
- Asai, T., G. Tena, J. Plotnikova, M.R. Willmann, W.-L. Chiu, L. Gomez-Gomez, T. Boller, F.M. Ausubel, and J. Sheen. 2002. MAP kinase signalling cascade in Arabidopsis innate immunity. *Nature*. 415:977-983.
- Audhya, A., M. Foti, and S.D. Emr. 2000. Distinct Roles for the Yeast Phosphatidylinositol 4-Kinases, Stt4p and Pik1p, in Secretion, Cell Growth, and Organelle Membrane Dynamics. *Molecular Biology of the Cell*. 11:2673-2689.
- Balla, A., and T. Balla. 2006. Phosphatidylinositol 4-kinases: old enzymes with emerging functions. *Trends in Cell Biology*. 16:351-361.
- Banbury, D.N., J.D. Oakley, R.B. Sessions, and G. Banting. 2003. Tyrphostin A23 Inhibits Internalization of the Transferrin Receptor by Perturbing the Interaction between Tyrosine Motifs and the Medium Chain Subunit of the AP-2 Adaptor Complex. *Journal of Biological Chemistry*. 278:12022-12028.
- Bannigan, A., M. Lizotte-Waniewski, M. Riley, and T.I. Baskin. 2008. Emerging molecular mechanisms that power and regulate the anastral mitotic spindle of flowering plants. *Cell Motility and the Cytoskeleton*. 65:1-11.
- Bardwell, A.J., L.J. Flatauer, K. Matsukuma, J. Thorner, and L. Bardwell. 2001. A conserved docking site in MEKs mediates high-affinity binding to MAP kinases and cooperates with a scaffold protein to enhance signal transmission. *Journal of Biological Chemistry*. 276:10374-10386.
- Bardwell, A.J., E. Frankson, and L. Bardwell. 2009. Selectivity of docking sites in MAPK kinases. *Journal of Biological Chemistry*. 284:13165-13173.
- Bashline, L., S. Li, C.T. Anderson, L. Lei, and Y. Gu. 2013. The Endocytosis of Cellulose Synthase in Arabidopsis Is Dependent on  $\mu$ 2, a Clathrin-Mediated Endocytosis Adaptor. *Plant Physiology*. 163:150-160.

- Bassham, D.C., A.A. Sanderfoot, V. Kovaleva, H. Zheng, and N.V. Raikhel. 2000. AtVPS45 Complex Formation at the trans-Golgi Network. *Molecular Biology of the Cell*. 11:2251-2265.
- Beck, M., G. Komis, J. Müller, D. Menzel, and J. Šamaj. 2010. Arabidopsis Homologs of Nucleus- and Phragmoplast-Localized Kinase 2 and 3 and Mitogen-Activated Protein Kinase 4 Are Essential for Microtubule Organization. *The Plant Cell*. 22:755-771.
- Beck, M., G. Komis, A. Ziemann, D. Menzel, and J. Šamaj. 2011. Mitogen-activated protein kinase 4 is involved in the regulation of mitotic and cytokinetic microtubule transitions in *Arabidopsis thaliana*. *New Phytologist*. 189:1069-1083.
- Berriri, S., A.V. Garcia, N.F. dit Frey, W. Rozhon, S. Pateyron, N. Leonhardt, J.-L. Montillet, J. Leung, H. Hirt, and J. Colcombet. 2012. Constitutively Active Mitogen-Activated Protein Kinase Versions Reveal Functions of Arabidopsis MPK4 in Pathogen Defense Signaling. *The Plant Cell*. 24:4281-4293.
- Bolte, S., C. Talbot, Y. Boutte, O. Catrice, N.D. Read, and B. Satiat-Jeunemaitre. 2004. FM-dyes as experimental probes for dissecting vesicle trafficking in living plant cells. *Journal of Microscopy*. 214:159-173.
- Bornens, M. 2008. Organelle positioning and cell polarity. 9:874.
- Bottanelli, F., D.C. Gershlick, and J. Denecke. 2012. Evidence for sequential action of Rab5 and Rab7 GTPases in prevacuolar organelle partitioning. *Traffic*. 13:338-354.
- Boutté, Y., M. Frescatada-Rosa, S. Men, C.M. Chow, K. Ebine, A. Gustavsson, L. Johansson, T. Ueda, I. Moore, G. Jürgens, and M. Grebe. 2010. Endocytosis restricts Arabidopsis KNOLLE syntaxin to the cell division plane during late cytokinesis. *The EMBO Journal*. 29:546-558.
- Bradford, M.M. 1976. A rapid and sensitive method for the quantitation of microgram quantities of protein utilizing the principle of protein-dye binding. *Analytical Biochemistry*. 72:248-254.
- Brandizzi, F., and G.O. Wasteneys. 2013. Cytoskeleton-dependent endomembrane organization in plant cells: an emerging role for microtubules. *The Plant Journal*. 75:339-349.
- Brown, D.A., and E. London. 2000. Structure and function of sphingolipid-and cholesterol-rich membrane rafts. *Journal of Biological Chemistry*. 275:17221-17224.
- Burke, J.E., A.J. Inglis, O. Perisic, G.R. Masson, S.H. McLaughlin, F. Rutaganira, K.M. Shokat, and R.L. Williams. 2014. Structures of PI4KIII $\beta$  complexes show simultaneous recruitment of Rab11 and its effectors. *Science*. 344:1035-1038.
- Caudron, F., E. Denarier, J.-C. Thibout-Quintana, J. Brocard, A. Andrieux, and A. Fourest-Lieuvain. 2010. Mutation of Ser172 in yeast  $\beta$  tubulin induces defects in microtubule dynamics and cell division. *PLoS one*. 5:e13553.

- Chan, J., G. Calder, S. Fox, and C. Lloyd. 2005. Localization of the Microtubule End Binding Protein EB1 Reveals Alternative Pathways of Spindle Development in Arabidopsis Suspension Cells. *The Plant Cell*. 17:1737-1748.
- Chang-Jie, J., and S. Sonobe. 1993. Identification and preliminary characterization of a 65 kDa higher-plant microtubule-associated protein. *Journal of Cell Science*. 105:891-901.
- Cheng, Z., J.-F. Li, Y. Niu, X.-C. Zhang, O.Z. Woody, Y. Xiong, S. Djonović, Y. Millet, J. Bush, and B.J. McConkey. 2015. Pathogen-secreted proteases activate a novel plant immune pathway. *Nature*. 521:213-216.
- Cho, M.H., and W.F. Boss. 1995. Transmembrane signaling and phosphoinositides. In *Methods in cell biology*. Vol. 49. Elsevier. 543-554.
- Chow, C.-M., H. Neto, C. Foucart, and I. Moore. 2008. Rab-A2 and Rab-A3 GTPases Define a trans-Golgi Endosomal Membrane Domain in Arabidopsis That Contributes Substantially to the Cell Plate. *The Plant Cell*. 20:101-123.
- Clough, S.J., and A.F. Bent. 1998. Floral dip: a simplified method for *Agrobacterium*-mediated transformation of *Arabidopsis thaliana*. *The Plant Journal*. 16:735-743.
- Collings, D.A., L.K. Gebbie, P.A. Howles, U.A. Hurley, R.J. Birch, A.H. Cork, C.H. Hocart, T. Arioli, and R.E. Williamson. 2008. Arabidopsis dynamin-like protein DRP1A: a null mutant with widespread defects in endocytosis, cellulose synthesis, cytokinesis, and cell expansion. *Journal of Experimental Botany*. 59:361-376.
- Cristina, M.S., M. Petersen, and J. Mundy. 2010. Mitogen-activated protein kinase signaling in plants. *Annual review of plant biology*. 61:621-649.
- Curtis, M.D., and U. Grossniklaus. 2003. A Gateway Cloning Vector Set for High-Throughput Functional Analysis of Genes in *Planta*. *Plant Physiology*. 133:462-469.
- D'Avino, P.P., M.S. Savoian, and D.M. Glover. 2005. Cleavage furrow formation and ingression during animal cytokinesis: a microtubule legacy. *J Cell Sci*. 118:1549-1558.
- de Graaf, P., W.T. Zwart, R.A.J. van Dijken, M. Deneka, T.K.F. Schulz, N. Geijsen, P.J. Coffey, B.M. Gadella, A.J. Verkleij, P. van der Sluijs, and P.M.P. van Bergen en Henegouwen. 2004. Phosphatidylinositol 4-Kinase  $\beta$  Is Critical for Functional Association of rab11 with the Golgi Complex. *Molecular Biology of the Cell*. 15:2038-2047.
- Demmel, L., M. Beck, C. Klose, A.-L. Schlaitz, Y. Gloor, P.P. Hsu, J. Havlis, A. Shevchenko, E. Krause, Y. Kalaidzidis, and C. Walch-Solimena. 2008a. Nucleocytoplasmic Shuttling of the Golgi Phosphatidylinositol 4-Kinase Pik1 Is Regulated by 14-3-3 Proteins and Coordinates Golgi Function with Cell Growth. *Molecular Biology of the Cell*. 19:1046-1061.
- Demmel, L., M. Gravert, E. Ercan, B. Habermann, T. Müller-Reichert, V. Kukhtina, V. Haucke, T. Baust, M. Sohrmann, Y. Kalaidzidis, C. Klose, M.

- Beck, M. Peter, and C. Walch-Solimena. 2008b. The Clathrin Adaptor Gga2p Is a Phosphatidylinositol 4-phosphate Effector at the Golgi Exit. *Molecular Biology of the Cell*. 19:1991-2002.
- Dettmer, J., A. Hong-Hermesdorf, Y.-D. Stierhof, and K. Schumacher. 2006. Vacuolar H<sup>+</sup>-ATPase activity is required for endocytic and secretory trafficking in Arabidopsis. *The Plant Cell*. 18:715-730.
- Dhanasekaran, D., K. Kashef, C. Lee, H. Xu, and E. Reddy. 2007. Scaffold proteins of MAP-kinase modules. *Oncogene*. 26:3185-3202.
- Dhonukshe, P., F. Aniento, I. Hwang, D.G. Robinson, J. Mravec, Y.-D. Stierhof, and J. Friml. 2007. Clathrin-Mediated Constitutive Endocytosis of PIN Auxin Efflux Carriers in Arabidopsis. *Current Biology*. 17:520-527.
- Dhonukshe, P., F. Baluška, M. Schlicht, A. Hlavacka, J. Šamaj, J. Friml, and T.W.J. Gadella. 2006. Endocytosis of Cell Surface Material Mediates Cell Plate Formation during Plant Cytokinesis. *Developmental Cell*. 10:137-150.
- Di Paolo, G., and P. De Camilli. 2006. Phosphoinositides in cell regulation and membrane dynamics. *Nature*. 443:651-657.
- Di Rubbo, S., N.G. Irani, S.Y. Kim, Z.-Y. Xu, A. Gadeyne, W. Dejonghe, I. Vanhoutte, G. Persiau, D. Eeckhout, S. Simon, K. Song, J. Kleine-Vehn, J. Friml, G. De Jaeger, D. Van Damme, I. Hwang, and E. Russinova. 2013. The Clathrin Adaptor Complex AP-2 Mediates Endocytosis of BRASSINOSTEROID INSENSITIVE1 in Arabidopsis. *The Plant Cell*. 25:2986-2997.
- Djamei, A., A. Pitzschke, H. Nakagami, I. Rajh, and H. Hirt. 2007. Trojan horse strategy in Agrobacterium transformation: abusing MAPK defense signaling. *Science*. 318:453-456.
- DOWLER, S., R.A. CURRIE, D.G. CAMPBELL, D. Maria, G. KULAR, C.P. DOWNES, and D.R. ALESSI. 2000. Identification of pleckstrin-homology-domain-containing proteins with novel phosphoinositide-binding specificities. *Biochemical Journal*. 351:19-31.
- Drevensek, S., M. Goussot, Y. Duroc, A. Christodoulidou, S. Steyaert, E. Schaefer, E. Duvernois, O. Grandjean, M. Vantard, D. Bouchez, and M. Pastuglia. 2012. The Arabidopsis TRM1–TON1 Interaction Reveals a Recruitment Network Common to Plant Cortical Microtubule Arrays and Eukaryotic Centrosomes. *The Plant Cell*. 24:178-191.
- Ehrhardt, D.W., and S.L. Shaw. 2006. Microtubule dynamics and organization in the plant cortical array. *Annu. Rev. Plant Biol.* 57:859-875.
- Endler, A., C. Kesten, R. Schneider, Y. Zhang, A. Ivakov, A. Froehlich, N. Funke, and S. Persson. 2015. A Mechanism for Sustained Cellulose Synthesis during Salt Stress. *Cell*. 162:1353-1364.
- Fache, V., J. Gaillard, D. Van Damme, D. Geelen, E. Neumann, V. Stoppin-Mellet, and M. Vantard. 2010. Arabidopsis Kinetochore Fiber-Associated MAP65-4 Cross-Links Microtubules and Promotes Microtubule Bundle Elongation. *The Plant Cell*. 22:3804-3815.

- Fan, L., H. Hao, Y. Xue, L. Zhang, K. Song, Z. Ding, M.A. Botella, H. Wang, and J. Lin. 2013. Dynamic analysis of Arabidopsis AP2  $\sigma$  subunit reveals a key role in clathrin-mediated endocytosis and plant development. *Development*. 140:3826-3837.
- Fletcher, D.A., and R.D. Mullins. 2010. Cell mechanics and the cytoskeleton. *Nature*. 463:485-492.
- Fourest-Lieuvin, A., L. Peris, V. Gache, I. Garcia-Saez, C. Juillan-Binard, V. Lantez, and D. Job. 2006. Microtubule Regulation in Mitosis: Tubulin Phosphorylation by the Cyclin-dependent Kinase Cdk1. *Molecular Biology of the Cell*. 17:1041-1050.
- Fujimoto, M., Y. Suda, S. Vernhettes, A. Nakano, and T. Ueda. 2014. Phosphatidylinositol 3-kinase and 4-kinase have distinct roles in intracellular trafficking of cellulose synthase complexes in Arabidopsis thaliana. *Plant and Cell Physiology*. 56:287-298.
- Fujimoto, M., and T. Ueda. 2012. Conserved and plant-unique mechanisms regulating plant post-Golgi traffic. *Frontiers in plant science*. 3.
- Furt, F., S. König, J.-J. Bessoule, F. Sargueil, R. Zallot, T. Stanislas, E. Noirot, J. Lherminier, F. Simon-Plas, and I. Heilmann. 2010. Polyphosphoinositides are enriched in plant membrane rafts and form microdomains in the plasma membrane. *Plant Physiology*. 152:2173-2187.
- Gadeyne, A., C. Sánchez-Rodríguez, S. Vanneste, S. Di Rubbo, H. Zauber, K. Vanneste, J. Van Leene, N. De Winne, D. Eeckhout, G. Persiau, E. Van De Slijke, B. Cannoot, L. Vercruysse, Jonathan R. Mayers, M. Adamowski, U. Kania, M. Ehrlich, A. Schweighofer, T. Ketelaar, S. Maere, Sebastian Y. Bednarek, J. Friml, K. Gevaert, E. Witters, E. Russinova, S. Persson, G. De Jaeger, and D. Van Damme. 2014. The TPLATE Adaptor Complex Drives Clathrin-Mediated Endocytosis in Plants. *Cell*. 156:691-704.
- Galvão, Rafaelo M., U. Kota, Erik J. Soderblom, Michael B. Goshe, and Wendy F. Boss. 2008. Characterization of a new family of protein kinases from Arabidopsis containing phosphoinositide 3/4-kinase and ubiquitin-like domains. *Biochemical Journal*. 409:117-127.
- Garcia, P., R. Gupta, S. Shah, A.J. Morris, S.A. Rudge, S. Scarlata, V. Petrova, S. McLaughlin, and M.J. Rebecchi. 1995. The pleckstrin homology domain of phospholipase C-delta 1 binds with high affinity to phosphatidylinositol 4, 5-bisphosphate in bilayer membranes. *Biochemistry*. 34:16228-16234.
- Gaullier, J.-M., A. Simonsen, A. D'arrigo, B. Bremnes, H. Stenmark, and R. Aasland. 1998. FYVE fingers bind PtdIns (3) P. *Nature*. 394:432-433.
- Geldner, N., N. Anders, H. Wolters, J. Keicher, W. Kornberger, P. Muller, A. Delbarre, T. Ueda, A. Nakano, and G. Jürgens. 2003. The Arabidopsis GNOM ARF-GEF Mediates Endosomal Recycling, Auxin Transport, and Auxin-Dependent Plant Growth. *Cell*. 112:219-230.

- Geldner, N., V. Dénervaud-Tendon, D.L. Hyman, U. Mayer, Y.-D. Stierhof, and J. Chory. 2009. Rapid, combinatorial analysis of membrane compartments in intact plants with a multicolor marker set. *The Plant Journal*. 59:169-178.
- Gerth, K., F. Lin, W. Menzel, P. Krishnamoorthy, I. Stenzel, M. Heilmann, and I. Heilmann. 2017. Guilt by Association: A Phenotype-Based View of the Plant Phosphoinositide Network. *Annual Review of Plant Biology*. 68:349-374.
- Gloor, Y., M. Schöne, B. Habermann, E. Ercan, M. Beck, G. Weselek, T. Müller-Reichert, and C. Walch-Solimena. 2010. Interaction between Sec7p and Pik1p: The first clue for the regulation of a coincidence detection signal. *European Journal of Cell Biology*. 89:575-583.
- Godi, A., P. Pertile, R. Meyers, P. Marra, G. Di Tullio, C. Iurisci, A. Luini, D. Corda, and M.A. De Matteis. 1999. ARF mediates recruitment of PtdIns-4-OH kinase- $\beta$  and stimulates synthesis of PtdIns (4, 5) P<sub>2</sub> on the Golgi complex. *Nature cell biology*. 1.
- Godlee, C., and M. Kaksonen. 2013. From uncertain beginnings: Initiation mechanisms of clathrin-mediated endocytosis. *The Journal of Cell Biology*. 203:717-725.
- Gronnier, J., J.-M. Crowet, B. Habenstein, M.N. Nasir, V. Bayle, E. Hosy, M.P. Platre, P. Gouguet, S. Raffaele, D. Martinez, A. Grelard, A. Loquet, F. Simon-Plas, P. Gerbeau-Pissot, C. Der, E.M. Bayer, Y. Jaillais, M. Deleu, V. Germain, L. Lins, and S. Mongrand. 2017. Structural basis for plant plasma membrane protein dynamics and organization into functional nanodomains. *eLife*. 6:e26404.
- Group, M., K. Ichimura, K. Shinozaki, G. Tena, J. Sheen, Y. Henry, A. Champion, M. Kreis, S. Zhang, H. Hirt, C. Wilson, E. Heberle-Bors, B.E. Ellis, P.C. Morris, R.W. Innes, J.R. Ecker, D. Scheel, D.F. Klessig, Y. Machida, J. Mundy, Y. Ohashi, and J.C. Walker. 2002. Mitogen-activated protein kinase cascades in plants: a new nomenclature. *Trends in Plant Science*. 7:301-308.
- Gui, J., C. Liu, J. Shen, and L. Li. 2014. Grain setting defect1, encoding a remorin protein, affects the grain setting in rice through regulating plasmodesmatal conductance. *Plant physiology*. 166:1463-1478.
- Gurel, Pinar S., Anna L. Hatch, and Henry N. Higgs. Connecting the Cytoskeleton to the Endoplasmic Reticulum and Golgi. *Current Biology*. 24:R660-R672.
- Hao, H., L. Fan, T. Chen, R. Li, X. Li, Q. He, M.A. Botella, and J. Lin. 2014. Clathrin and Membrane Microdomains Cooperatively Regulate RbohD Dynamics and Activity in Arabidopsis. *The Plant Cell*.
- Hashimoto, T. 2003. Dynamics and regulation of plant interphase microtubules: a comparative view. *Current Opinion in Plant Biology*. 6:568-576.
- Hashimoto, T. 2015. Microtubules in Plants. *The Arabidopsis Book*:e0179.
- Hausser, A., G. Link, M. Hoene, C. Russo, O. Selchow, and K. Pfizenmaier.

2006. Phospho-specific binding of 14-3-3 proteins to phosphatidylinositol 4-kinase III  $\beta$  protects from dephosphorylation and stabilizes lipid kinase activity. *Journal of Cell Science*. 119:3613-3621.
- Hausser, A., P. Storz, S. Märtens, G. Link, A. Toker, and K. Pfizenmaier. 2005. Protein kinase D regulates vesicular transport by phosphorylating and activating phosphatidylinositol-4 kinase III $\beta$  at the Golgi complex. *Nature Cell Biology*. 7:880.
- Heilmann, I. 2016. Phosphoinositide signaling in plant development. *Development*. 143:2044-2055.
- Heilmann, M., and I. Heilmann. 2013. Mass Measurement of Polyphosphoinositides by Thin-Layer and Gas Chromatography. *In Plant Lipid Signaling Protocols*. T. Munnik and I. Heilmann, editors. Humana Press, Totowa, NJ. 25-32.
- Heilmann, M., and I. Heilmann. 2015. Plant phosphoinositides—complex networks controlling growth and adaptation. *Biochimica et Biophysica Acta (BBA) - Molecular and Cell Biology of Lipids*. 1851:759-769.
- Hempel, F., I. Stenzel, M. Heilmann, P. Krishnamoorthy, W. Menzel, R. Golbik, S. Helm, D. Dobritsch, S. Baginsky, J. Lee, W. Hoehenwarter, and I. Heilmann. 2017. MAPKs influence pollen tube growth by controlling the formation of phosphatidylinositol 4,5-bisphosphate in an apical plasma membrane domain. *The Plant Cell*.
- Hendricks, K.B., B. Qing Wang, E.A. Schnieders, and J. Thorner. 1999. Yeast homologue of neuronal frequenin is a regulator of phosphatidylinositol-4-OH kinase. *Nature cell biology*. 1.
- Higaki, T., N. Kutsuna, T. Sano, N. Kondo, and S. Hasezawa. 2010. Quantification and cluster analysis of actin cytoskeletal structures in plant cells: role of actin bundling in stomatal movement during diurnal cycles in Arabidopsis guard cells. *The Plant Journal*. 61:156-165.
- Hirst, J., L.D. Barlow, G.C. Francisco, D.A. Sahlender, M.N. Seaman, J.B. Dacks, and M.S. Robinson. 2011. The fifth adaptor protein complex. *PLoS biology*. 9:e1001170.
- Ho, C.-M.K., T. Hotta, F. Guo, R.W. Roberson, Y.-R.J. Lee, and B. Liu. 2011. Interaction of Antiparallel Microtubules in the Phragmoplast Is Mediated by the Microtubule-Associated Protein MAP65-3 in Arabidopsis. *The Plant Cell*. 23:2909-2923.
- Ho, C.-M.K., Y.-R.J. Lee, L.D. Kiyama, S.P. Dinesh-Kumar, and B. Liu. 2012. Arabidopsis microtubule-associated protein MAP65-3 cross-links antiparallel microtubules toward their plus ends in the phragmoplast via its distinct C-terminal microtubule binding domain. *The Plant Cell*. 24:2071-2085.
- Holmfeldt, P., M.E. Sellin, and M. Gullberg. 2009. Predominant regulators of tubulin monomer–polymer partitioning and their implication for cell polarization. *Cellular and molecular life sciences*. 66:3263.
- Hussey, P.J., T.J. Hawkins, H. Igarashi, D. Kaloriti, and A. Smertenko. 2002.

- The plant cytoskeleton: recent advances in the study of the plant microtubule-associated proteins MAP-65, MAP-190 and the *Xenopus* MAP215-like protein, MOR1. *Plant molecular biology*. 50:915-924.
- Ischebeck, T., S. Seiler, and I. Heilmann. 2010a. At the poles across kingdoms: phosphoinositides and polar tip growth. *Protoplasma*. 240:13-31.
- Ischebeck, T., I. Stenzel, and I. Heilmann. 2008. Type B Phosphatidylinositol-4-Phosphate 5-Kinases Mediate Arabidopsis and *Nicotiana tabacum* Pollen Tube Growth by Regulating Apical Pectin Secretion. *The Plant Cell*. 20:3312-3330.
- Ischebeck, T., L.H. Vu, X. Jin, I. Stenzel, C. Löffke, and I. Heilmann. 2010b. Functional Cooperativity of Enzymes of Phosphoinositide Conversion According to Synergistic Effects on Pectin Secretion in Tobacco Pollen Tubes. *Molecular Plant*. 3:870-881.
- Ito, E., M. Fujimoto, K. Ebine, T. Uemura, T. Ueda, and A. Nakano. 2012. Dynamic behavior of clathrin in *Arabidopsis thaliana* unveiled by live imaging. *The Plant Journal*. 69:204-216.
- Jarsch, I.K., and T. Ott. 2011. Perspectives on remorin proteins, membrane rafts, and their role during plant–microbe interactions. *Molecular plant-microbe interactions*. 24:7-12.
- Jensen, R.B., T. La Cour, J. Albrethsen, M. Nielsen, and K. Skriver. 2001. FYVE zinc-finger proteins in the plant model *Arabidopsis thaliana*: identification of PtdIns3P-binding residues by comparison of classic and variant FYVE domains. *Biochemical Journal*. 359:165-173.
- Jia, D.-J., X. Cao, W. Wang, X.-Y. Tan, X.-Q. Zhang, L.-Q. Chen, and D. Ye. 2009. GNOM-LIKE 2, Encoding an Adenosine Diphosphate-Ribosylation Factor-Guanine Nucleotide Exchange Factor Protein Homologous to GNOM and GNL1, is Essential for Pollen Germination in *Arabidopsis*. *Journal of Integrative Plant Biology*. 51:762-773.
- Jiang, W., G. Jimenez, N.J. Wells, T.J. Hope, G.M. Wahl, T. Hunter, and R. Fukunaga. 1998. PRC1: a human mitotic spindle-associated CDK substrate protein required for cytokinesis. *Molecular cell*. 2:877-885.
- Juang, Y.-L., J. Huang, J.-M. Peters, M.E. McLaughlin, C.-Y. Tai, and D. Pellman. 1997. APC-Mediated Proteolysis of Ase1 and the Morphogenesis of the Mitotic Spindle. *Science*. 275:1311-1314.
- Jürgens, G. 2005. Plant cytokinesis: fission by fusion. *Trends in cell biology*. 15:277-283.
- Kanaoka, M.M., L.J. Pillitteri, H. Fujii, Y. Yoshida, N.L. Bogenschutz, J. Takabayashi, J.-K. Zhu, and K.U. Torii. 2008. SCREAM/ICE1 and SCREAM2 specify three cell-state transitional steps leading to *Arabidopsis* stomatal differentiation. *The Plant Cell*. 20:1775-1785.
- Kanaseki, T., and K. Kadota. 1969. THE "VESICLE IN A BASKET". *The Journal of cell biology*. 42:202-220.
- Kang, B.H., E. Nielsen, M.L. Preuss, D. Mastrorarde, and L.A. Staehelin. 2011. Electron Tomography of RabA4b-and PI-4K $\beta$ 1-Labeled Trans Golgi

- Network Compartments in Arabidopsis. *Traffic*. 12:313-329.
- Kapp-Barnea, Y., L. Ninio-Many, K. Hirschberg, M. Fukuda, A. Jeromin, and R. Sagi-Eisenberg. 2006. Neuronal Calcium Sensor-1 and Phosphatidylinositol 4-Kinase  $\beta$  Stimulate Extracellular Signal-regulated Kinase 1/2 Signaling by Accelerating Recycling through the Endocytic Recycling Compartment. *Molecular Biology of the Cell*. 17:4130-4141.
- Kerk, D., J. Bulgrien, D.W. Smith, B. Barsam, S. Veretnik, and M. Gribskov. 2002. The complement of protein phosphatase catalytic subunits encoded in the genome of Arabidopsis. *Plant physiology*. 129:908-925.
- Kirik, A., D.W. Ehrhardt, and V. Kirik. 2012. TONNEAU2/FASS Regulates the Geometry of Microtubule Nucleation and Cortical Array Organization in Interphase Arabidopsis Cells. *The Plant Cell*. 24:1158-1170.
- Kleine-Vehn, J., P. Dhonukshe, R. Swarup, M. Bennett, and J. Friml. 2006. Subcellular Trafficking of the Arabidopsis Auxin Influx Carrier AUX1 Uses a Novel Pathway Distinct from PIN1. *The Plant Cell*. 18:3171-3181.
- Kleine-Vehn, J., Ł. Łangowski, J. Wiśniewska, P. Dhonukshe, P.B. Brewer, and J. Friml. 2008. Cellular and Molecular Requirements for Polar PIN Targeting and Transcytosis in Plants. *Molecular Plant*. 1:1056-1066.
- Koizumi, K., S. Naramoto, S. Sawa, N. Yahara, T. Ueda, A. Nakano, M. Sugiyama, and H. Fukuda. 2005. VAN3 ARF-GAP-mediated vesicle transport is involved in leaf vascular network formation. *Development*. 132:1699-1711.
- Kong, Q., N. Qu, M. Gao, Z. Zhang, X. Ding, F. Yang, Y. Li, O.X. Dong, S. Chen, X. Li, and Y. Zhang. 2012. The MEKK1-MKK1/MKK2-MPK4 Kinase Cascade Negatively Regulates Immunity Mediated by a Mitogen-Activated Protein Kinase Kinase Kinase in Arabidopsis. *The Plant Cell*. 24:2225-2236.
- König, S., M. Hoffmann, A. Mosblech, and I. Heilmann. 2008. Determination of content and fatty acid composition of unlabeled phosphoinositide species by thin-layer chromatography and gas chromatography. *Analytical Biochemistry*. 378:197-201.
- Konopka, C.A., S.K. Backues, and S.Y. Bednarek. 2008. Dynamics of Arabidopsis Dynamin-Related Protein 1C and a Clathrin Light Chain at the Plasma Membrane. *The Plant Cell*. 20:1363-1380.
- Kosetsu, K., S. Matsunaga, H. Nakagami, J. Colcombet, M. Sasabe, T. Soyano, Y. Takahashi, H. Hirt, and Y. Machida. 2010. The MAP kinase MPK4 is required for cytokinesis in Arabidopsis thaliana. *The Plant Cell*. 22:3778-3790.
- Krysan, P.J., P.J. Jester, J.R. Gottwald, and M.R. Sussman. 2002. An Arabidopsis mitogen-activated protein kinase kinase kinase gene family encodes essential positive regulators of cytokinesis. *The Plant Cell*. 14:1109-1120.
- Kurasawa, Y., W.C. Earnshaw, Y. Mochizuki, N. Dohmae, and K. Todokoro. 2004. Essential roles of KIF4 and its binding partner PRC1 in organized

- central spindle midzone formation. *The EMBO Journal*. 23:3237-3248.
- Lam, S.K., Y. Cai, Y.C. Tse, J. Wang, A.H.Y. Law, P. Pimpl, H.Y.E. Chan, J. Xia, and L. Jiang. 2009. BFA-induced compartments from the Golgi apparatus and trans-Golgi network/early endosome are distinct in plant cells. *The Plant Journal*. 60:865-881.
- Lampard, G.R., C.A. MacAlister, and D.C. Bergmann. 2008. Arabidopsis stomatal initiation is controlled by MAPK-mediated regulation of the bHLH SPEECHLESS. *Science*. 322:1113-1116.
- Latrasse, D., T. Jégu, H. Li, A. de Zelicourt, C. Raynaud, S. Legras, A. Gust, O. Samajova, A. Veluchamy, N. Rayapuram, J.S. Ramirez-Prado, O. Kulikova, J. Colcombet, J. Bigeard, B. Genot, T. Bisseling, M. Benhamed, and H. Hirt. 2017. MAPK-triggered chromatin reprogramming by histone deacetylase in plant innate immunity. *Genome Biology*. 18:131.
- Lee, G.-J., E.J. Sohn, M.H. Lee, and I. Hwang. 2004. The Arabidopsis Rab5 Homologs Rha1 and Ara7 Localize to the Prevacuolar Compartment. *Plant and Cell Physiology*. 45:1211-1220.
- Lee, J.S., S. Wang, S. Sritubtim, J.G. Chen, and B.E. Ellis. 2009. Arabidopsis mitogen-activated protein kinase MPK12 interacts with the MAPK phosphatase IBR5 and regulates auxin signaling. *The Plant Journal*. 57:975-985.
- Li, H., X. Zeng, Z.-Q. Liu, Q.-T. Meng, M. Yuan, and T.-L. Mao. 2009. Arabidopsis microtubule-associated protein AtMAP65-2 acts as a microtubule stabilizer. *Plant Molecular Biology*. 69:313-324.
- Li, R., P. Liu, Y. Wan, T. Chen, Q. Wang, U. Mettbach, F. Baluška, J. Šamaj, X. Fang, W.J. Lucas, and J. Lin. 2012. A Membrane Microdomain-Associated Protein, Arabidopsis Flot1, Is Involved in a Clathrin-Independent Endocytic Pathway and Is Required for Seedling Development. *The Plant Cell*. 24:2105-2122.
- Lingwood, D., and K. Simons. 2010. Lipid rafts as a membrane-organizing principle. *science*. 327:46-50.
- Lipka, E., A. Gadeyne, D. Stöckle, S. Zimmermann, G. De Jaeger, D.W. Ehrhardt, V. Kirik, D. Van Damme, and S. Müller. 2014. The Phragmoplast-Orienting Kinesin-12 Class Proteins Translate the Positional Information of the Preprophase Band to Establish the Cortical Division Zone in Arabidopsis thaliana. *The Plant Cell*. 26:2617-2632.
- Lipka, E., A. Herrmann, and S. Mueller. 2015. Mechanisms of plant cell division. *Wiley Interdisciplinary Reviews: Developmental Biology*. 4:391-405.
- Liu, P., R.L. Li, L. Zhang, Q.L. Wang, K. Niehaus, F. Baluška, J. Šamaj, and J.X. Lin. 2009. Lipid microdomain polarization is required for NADPH oxidase-dependent ROS signaling in Picea meyeri pollen tube tip growth. *The Plant Journal*. 60:303-313.
- Liu, Y., and S. Zhang. 2004. Phosphorylation of 1-aminocyclopropane-1-carboxylic acid synthase by MPK6, a stress-responsive mitogen-

- activated protein kinase, induces ethylene biosynthesis in Arabidopsis. *The Plant Cell*. 16:3386-3399.
- Löfke, C., K. Dünser, D. Scheuring, and J. Kleine-Vehn. 2015. Auxin regulates SNARE-dependent vacuolar morphology restricting cell size. *Elife*. 4:e05868.
- Löfke, C., T. Ischebeck, S. König, S. Freitag, and I. Heilmann. 2008. Alternative metabolic fates of phosphatidylinositol produced by phosphatidylinositol synthase isoforms in Arabidopsis thaliana. *Biochemical Journal*. 413:115-124.
- London, E., and D.A. Brown. 2000. Insolubility of lipids in triton X-100: physical origin and relationship to sphingolipid/cholesterol membrane domains (rafts). *Biochimica et Biophysica Acta (BBA)-Biomembranes*. 1508:182-195.
- Lou, Y., H. Ma, W.-H. Lin, Z.-Q. Chu, B. Mueller-Roeber, Z.-H. Xu, and H.-W. Xue. 2006. The highly charged region of plant  $\beta$ -type phosphatidylinositol 4-kinase is involved in membrane targeting and phospholipid binding. *Plant molecular biology*. 60:729-746.
- Lucas, J.R., S. Courtney, M. Hassfurder, S. Dhingra, A. Bryant, and S.L. Shaw. 2011. Microtubule-Associated Proteins MAP65-1 and MAP65-2 Positively Regulate Axial Cell Growth in Etiolated Arabidopsis Hypocotyls. *The Plant Cell*. 23:1889-1903.
- Lucas, J.R., and S.L. Shaw. 2012. MAP65-1 and MAP65-2 promote cell proliferation and axial growth in Arabidopsis roots. *The Plant Journal*. 71:454-463.
- Mansour, S.J., J. Skaug, X.-H. Zhao, J. Giordano, S.W. Scherer, and P. Melançon. 1999. p200 ARF–GEP1: A Golgi-localized guanine nucleotide exchange protein whose Sec7 domain is targeted by the drug brefeldin A. *Proceedings of the National Academy of Sciences of the United States of America*. 96:7968-7973.
- Mao, T., L. Jin, H. Li, B. Liu, and M. Yuan. 2005. Two microtubule-associated proteins of the Arabidopsis MAP65 family function differently on microtubules. *Plant physiology*. 138:654-662.
- McMahon, H.T., and E. Boucrot. 2011. Molecular mechanism and physiological functions of clathrin-mediated endocytosis. *Nat Rev Mol Cell Biol*. 12:517-533.
- McMichael, C.M., and S.Y. Bednarek. 2013. Cytoskeletal and membrane dynamics during higher plant cytokinesis. *new phytologist*. 197:1039-1057.
- Men, S., Y. Boutté, Y. Ikeda, X. Li, K. Palme, Y.-D. Stierhof, M.-A. Hartmann, T. Moritz, and M. Grebe. 2008. Sterol-dependent endocytosis mediates post-cytokinetic acquisition of PIN2 auxin efflux carrier polarity. *Nature Cell Biology*. 10:237.
- Meskiene, I., and H. Hirt. 2000. MAP kinase pathways: molecular plug-and-play chips for the cell. *Plant Molecular Biology*. 42:791-806.

- Miart, F., T. Desprez, E. Biot, H. Morin, K. Belcram, H. Höfte, M. Gonneau, and S. Vernhettes. 2014. Spatio-temporal analysis of cellulose synthesis during cell plate formation in Arabidopsis. *The Plant Journal*. 77:71-84.
- Mollinari, C., J.-P. Kleman, W. Jiang, G. Schoehn, T. Hunter, and R.L. Margolis. 2002. PRC1 is a microtubule binding and bundling protein essential to maintain the mitotic spindle midzone. *The Journal of Cell Biology*. 157:1175-1186.
- Mueller-Roeber, B., and C. Pical. 2002. Inositol Phospholipid Metabolism in Arabidopsis. Characterized and Putative Isoforms of Inositol Phospholipid Kinase and Phosphoinositide-Specific Phospholipase C. *Plant Physiology*. 130:22-46.
- Müller, I., W. Wagner, A. Völker, S. Schellmann, P. Nacry, F. Küttner, Z. Schwarz-Sommer, U. Mayer, and G. Jürgens. 2003. Syntaxin specificity of cytokinesis in Arabidopsis. *Nature Cell Biology*. 5:531.
- Müller, J., M. Beck, U. Mettbach, G. Komis, G. Hause, D. Menzel, and J. Šamaj. 2010. Arabidopsis MPK6 is involved in cell division plane control during early root development, and localizes to the pre-prophase band, phragmoplast, trans-Golgi network and plasma membrane. *The Plant Journal*. 61:234-248.
- Müller, S., and G. Jürgens. 2016. Plant cytokinesis—No ring, no constriction but centrifugal construction of the partitioning membrane. *Seminars in Cell & Developmental Biology*. 53:10-18.
- Müller, S., A. Smertenko, V. Wagner, M. Heinrich, P.J. Hussey, and M.-T. Hauser. 2004. The Plant Microtubule-Associated Protein AtMAP65-3/PLE Is Essential for Cytokinetic Phragmoplast Function. *Current Biology*. 14:412-417.
- Munnik, T., and E. Nielsen. 2011. Green light for polyphosphoinositide signals in plants. *Current Opinion in Plant Biology*. 14:489-497.
- Munnik, T., and J.E.M. Vermeer. 2010. Osmotic stress-induced phosphoinositide and inositol phosphate signalling in plants. *Plant, Cell & Environment*. 33:655-669.
- Murata, T., T. Sano, M. Sasabe, S. Nonaka, T. Higashiyama, S. Hasezawa, Y. Machida, and M. Hasebe. 2013. Mechanism of microtubule array expansion in the cytokinetic phragmoplast. *Nature Communications*. 4:1967.
- Murray, M.G., and W.F. Thompson. 1980. Rapid isolation of high molecular weight plant DNA. *Nucleic Acids Research*. 8:4321-4326.
- Nakagami, H., H. Soukupová, A. Schikora, V. Zárský, and H. Hirt. 2006. A mitogen-activated protein kinase kinase mediates reactive oxygen species homeostasis in Arabidopsis. *Journal of Biological Chemistry*. 281:38697-38704.
- Naramoto, S., J. Kleine-Vehn, S. Robert, M. Fujimoto, T. Dainobu, T. Paciorek, T. Ueda, A. Nakano, M.C.E. Van Montagu, H. Fukuda, and J. Friml. 2010. ADP-ribosylation factor machinery mediates endocytosis in plant cells.

- Proceedings of the National Academy of Sciences*. 107:21890-21895.
- Naramoto, S., M.S. Otegui, N. Kutsuna, R. de Rycke, T. Dainobu, M. Karampelias, M. Fujimoto, E. Feraru, D. Miki, H. Fukuda, A. Nakano, and J. Friml. 2014. Insights into the Localization and Function of the Membrane Trafficking Regulator GNOM ARF-GEF at the Golgi Apparatus in Arabidopsis. *The Plant Cell*. 26:3062-3076.
- Naramoto, S., S. Sawa, K. Koizumi, T. Uemura, T. Ueda, J. Friml, A. Nakano, and H. Fukuda. 2009. Phosphoinositide-dependent regulation of VAN3 ARF-GAP localization and activity essential for vascular tissue continuity in plants. *Development*. 136:1529-1538.
- Nishihama, R., M. Ishikawa, S. Araki, T. Soyano, T. Asada, and Y. Machida. 2001. The NPK1 mitogen-activated protein kinase kinase kinase is a regulator of cell-plate formation in plant cytokinesis. *Genes & Development*. 15:352-363.
- Nishihama, R., T. Soyano, M. Ishikawa, S. Araki, H. Tanaka, T. Asada, K. Irie, M. Ito, M. Terada, H. Banno, Y. Yamazaki, and Y. Machida. 2002. Expansion of the Cell Plate in Plant Cytokinesis Requires a Kinesin-like Protein/MAPKKK Complex. *Cell*. 109:87-99.
- Nomura, K., S. DebRoy, Y.H. Lee, N. Pumplin, J. Jones, and S.Y. He. 2006. A Bacterial Virulence Protein Suppresses Host Innate Immunity to Cause Plant Disease. *Science*. 313:220-223.
- Ohashi-Ito, K., and D.C. Bergmann. 2006. Arabidopsis FAMA controls the final proliferation/differentiation switch during stomatal development. *The Plant Cell*. 18:2493-2505.
- Okazaki, K., S.-y. Miyagishima, and H. Wada. 2015. Phosphatidylinositol 4-Phosphate Negatively Regulates Chloroplast Division in Arabidopsis. *The Plant Cell*. 27:663-674.
- Ookata, K., S.-i. Hisanaga, M. Sugita, A. Okuyama, H. Murofushi, H. Kitazawa, S. Chari, J.C. Bulinski, and T. Kishimoto. 1997. MAP4 Is the in Vivo Substrate for CDC2 Kinase in HeLa Cells: Identification of an M-Phase Specific and a Cell Cycle-Independent Phosphorylation Site in MAP4. *Biochemistry*. 36:15873-15883.
- Ortiz-Zapater, E., E. Soriano-Ortega, M.J. Marcote, D. Ortiz-Masiá, and F. Aniento. 2006. Trafficking of the human transferrin receptor in plant cells: effects of tyrphostin A23 and brefeldin A. *The Plant Journal*. 48:757-770.
- Otto, G.P., and B.J. Nichols. 2011. The roles of flotillin microdomains – endocytosis and beyond. *Journal of Cell Science*. 124:3933-3940.
- Paez Valencia, J., K. Goodman, and M.S. Otegui. 2016. Endocytosis and Endosomal Trafficking in Plants. *Annual Review of Plant Biology*. 67:309-335.
- Park, J.-S., S.K. Steinbach, M. Desautels, and S.M. Hemmingsen. 2009. Essential Role for *Schizosaccharomyces pombe* pik1 in Septation. *PLOS ONE*. 4:e6179.
- Park, M., and G. Jürgens. 2012. Membrane Traffic and Fusion at Post-Golgi

- Compartments. *Frontiers in Plant Science*. 2.
- Park, M., S. Touihri, I. Müller, U. Mayer, and G. Jürgens. 2012. Sec1/Munc18 Protein Stabilizes Fusion-Competent Syntaxin for Membrane Fusion in Arabidopsis Cytokinesis. *Developmental Cell*. 22:989-1000.
- Pearse, B.M.F. 1975. Coated vesicles from pig brain: Purification and biochemical characterization. *Journal of Molecular Biology*. 97:93-98.
- Pellman, D., M. Bagget, Y. Tu, G.R. Fink, and H. Tu. 1995. Two microtubule-associated proteins required for anaphase spindle movement in *Saccharomyces cerevisiae*. *The Journal of Cell Biology*. 130:1373-1385.
- Petersen, M., P. Brodersen, H. Naested, E. Andreasson, U. Lindhart, B. Johansen, H.B. Nielsen, M. Lacy, M.J. Austin, J.E. Parker, S.B. Sharma, D.F. Klessig, R. Martienssen, O. Mattsson, A.B. Jensen, and J. Mundy. 2000. Arabidopsis MAP Kinase 4 Negatively Regulates Systemic Acquired Resistance. *Cell*. 103:1111-1120.
- Peyroche, A., B. Antony, S. Robineau, J. Acker, J. Cherfils, and C.L. Jackson. 1999. Brefeldin A Acts to Stabilize an Abortive ARF-GDP-Sec7 Domain Protein Complex: Involvement of Specific Residues of the Sec7 Domain. *Molecular Cell*. 3:275-285.
- Piper, R.C., and D.J. Katzmann. 2007. Biogenesis and Function of Multivesicular Bodies. *Annual Review of Cell and Developmental Biology*. 23:519-547.
- Polevoy, G., H.-C. Wei, R. Wong, Z. Szentpetery, Y.J. Kim, P. Goldbach, S.K. Steinbach, T. Balla, and J.A. Brill. 2009. Dual roles for the Drosophila PI 4-kinase Four wheel drive in localizing Rab11 during cytokinesis. *The Journal of Cell Biology*. 187:847-858.
- Preuss, M.L., A.J. Schmitz, J.M. Thole, H.K.S. Bonner, M.S. Otegui, and E. Nielsen. 2006. A role for the RabA4b effector protein PI-4K $\beta$ 1 in polarized expansion of root hair cells in *Arabidopsis thaliana*. *The Journal of Cell Biology*. 172:991-998.
- Qi, X., M. Kaneda, J. Chen, A. Geitmann, and H. Zheng. 2011. A specific role for Arabidopsis TRAPP II in post-Golgi trafficking that is crucial for cytokinesis and cell polarity. *The Plant Journal*. 68:234-248.
- Qi, X., and H. Zheng. 2013. Rab-A1c GTPase Defines a Population of the Trans-Golgi Network that Is Sensitive to Endosidin1 during Cytokinesis in Arabidopsis. *Molecular Plant*. 6:847-859.
- Qiu, J.-L., L. Zhou, B.-W. Yun, H.B. Nielsen, B.K. Fiil, K. Petersen, J. MacKinlay, G.J. Loake, J. Mundy, and P.C. Morris. 2008. Arabidopsis mitogen-activated protein kinase kinases MKK1 and MKK2 have overlapping functions in defense signaling mediated by MEKK1, MPK4, and MKS1. *Plant physiology*. 148:212-222.
- Raffaele, S., E. Bayer, D. Lafarge, S. Cluzet, S.G. Retana, T. Boubekur, N. Leborgne-Castel, J.-P. Carde, J. Lherminier, and E. Noirot. 2009. Remorin, a solanaceae protein resident in membrane rafts and plasmodesmata, impairs potato virus X movement. *The Plant Cell*.

- 21:1541-1555.
- Rasmussen, C.G., B. Sun, and L.G. Smith. 2011. Tangled localization at the cortical division site of plant cells occurs by several mechanisms. *Journal of Cell Science*. 124:270-279.
- Rasmussen, C.G., A.J. Wright, and S. Müller. 2013. The role of the cytoskeleton and associated proteins in determination of the plant cell division plane. *The Plant Journal*. 75:258-269.
- Reichardt, I., D. Slane, F. El Kasmi, C. Knöll, R. Fuchs, U. Mayer, V. Lipka, and G. Jürgens. 2011. Mechanisms of Functional Specificity Among Plasma-Membrane Syntaxins in Arabidopsis. *Traffic*. 12:1269-1280.
- Reichardt, I., Y.-D. Stierhof, U. Mayer, S. Richter, H. Schwarz, K. Schumacher, and G. Jürgens. 2007. Plant Cytokinesis Requires De Novo Secretory Trafficking but Not Endocytosis. *Current Biology*. 17:2047-2053.
- Richter, S., N. Geldner, J. Schrader, H. Wolters, Y.-D. Stierhof, G. Rios, C. Koncz, D.G. Robinson, and G. Jurgens. 2007. Functional diversification of closely related ARF-GEFs in protein secretion and recycling. *Nature*. 448:488-492.
- Richter, S., M. Kientz, S. Brumm, M.E. Nielsen, M. Park, R. Gavidia, C. Krause, U. Voss, H. Beckmann, U. Mayer, Y.-D. Stierhof, and G. Jürgens. 2014. Delivery of endocytosed proteins to the cell–division plane requires change of pathway from recycling to secretion. *eLife*. 3:e02131.
- Richter, S., L.M. Muller, Y.-D. Stierhof, U. Mayer, N. Takada, B. Kost, A. Vieten, N. Geldner, C. Koncz, and G. Jurgens. 2012. Polarized cell growth in Arabidopsis requires endosomal recycling mediated by GBF1-related ARF exchange factors. *Nat Cell Biol*. 14:80-86.
- Roth, T.F., and K.R. Porter. 1964. YOLK PROTEIN UPTAKE IN THE OOCYTE OF THE MOSQUITO AEDES AEGYPTI. L. *The Journal of Cell Biology*. 20:313-332.
- Rybak, K., A. Steiner, L. Synek, S. Klaeger, I. Kulich, E. Facher, G. Wanner, B. Kuster, V. Zarsky, S. Persson, and Farhah F. Assaad. 2014. Plant Cytokinesis Is Orchestrated by the Sequential Action of the TRAPP II and Exocyst Tethering Complexes. *Developmental Cell*. 29:607-620.
- Šamaj, J., F. Baluška, B. Voigt, M. Schlicht, D. Volkmann, and D. Menzel. 2004. Endocytosis, Actin Cytoskeleton, and Signaling. *Plant Physiology*. 135:1150-1161.
- Šamaj, J., M. Ovecka, A. Hlavacka, F. Lecourieux, I. Meskiene, I. Lichtscheidl, P. Lenart, J. Salaj, D. Volkmann, L. Bögre, F. Baluška, and H. Hirt. 2002. Involvement of the mitogen-activated protein kinase SIMK in regulation of root hair tip growth. *The EMBO Journal*. 21:3296-3306.
- Sanderfoot, A.A., V. Kovaleva, D.C. Bassham, and N.V. Raikhel. 2001. Interactions between syntaxins identify at least five SNARE complexes within the Golgi/prevacuolar system of the Arabidopsis cell. *Molecular Biology of the Cell*. 12:3733-3743.
- Santiago-Tirado, F.H., and A. Bretscher. 2011. Membrane-trafficking sorting

- hubs: cooperation between PI4P and small GTPases at the trans-Golgi network. *Trends in cell biology*. 21:515-525.
- Santiago-Tirado, F.H., A. Legesse-Miller, D. Schott, and A. Bretscher. 2011. PI4P and Rab Inputs Collaborate in Myosin-V-Dependent Transport of Secretory Compartments in Yeast. *Developmental Cell*. 20:47-59.
- Sasabe, M., V. Boudolf, L. De Veylder, D. Inzé, P. Genschik, and Y. Machida. 2011a. Phosphorylation of a mitotic kinesin-like protein and a MAPKKK by cyclin-dependent kinases (CDKs) is involved in the transition to cytokinesis in plants. *Proceedings of the National Academy of Sciences*. 108:17844-17849.
- Sasabe, M., K. Kosetsu, M. Hidaka, A. Murase, and Y. Machida. 2011b. Arabidopsis thaliana MAP65-1 and MAP65-2 function redundantly with MAP65-3/PLEIADE in cytokinesis downstream of MPK4. *Plant signaling & behavior*. 6:743-747.
- Sasabe, M., and Y. Machida. 2012. Regulation of organization and function of microtubules by the mitogen-activated protein kinase cascade during plant cytokinesis. *Cytoskeleton*. 69:913-918.
- Sasabe, M., T. Soyano, Y. Takahashi, S. Sonobe, H. Igarashi, T.J. Itoh, M. Hidaka, and Y. Machida. 2006. Phosphorylation of NtMAP65-1 by a MAP kinase down-regulates its activity of microtubule bundling and stimulates progression of cytokinesis of tobacco cells. *Genes & development*. 20:1004-1014.
- Šašek, V., M. Janda, E. Delage, J. Puyaubert, A. Guivarc'h, E. López Maseda, P.I. Dobrev, J. Caius, K. Bóka, O. Valentová, L. Burketová, A. Zachowski, and E. Ruelland. 2014. Constitutive salicylic acid accumulation in pi4kIIIβ1β2 Arabidopsis plants stunts rosette but not root growth. *New Phytologist*. 203:805-816.
- Sauer, M., T. Paciorek, E. Benková, and J. Friml. 2006. Immunocytochemical techniques for whole-mount in situ protein localization in plants. *Nature Protocols*. 1:98.
- Scheuring, D., C. Viotti, F. Krüger, F. Künzl, S. Sturm, J. Bubeck, S. Hillmer, L. Frigerio, D.G. Robinson, P. Pimpl, and K. Schumacher. 2011. Multivesicular Bodies Mature from the Trans-Golgi Network/Early Endosome in Arabidopsis. *The Plant Cell*. 23:3463-3481.
- Sciorra, V.A., A. Audhya, A.B. Parsons, N. Segev, C. Boone, and S.D. Emr. 2005. Synthetic Genetic Array Analysis of the PtdIns 4-kinase Pik1p Identifies Components in a Golgi-specific Ypt31/rab-GTPase Signaling Pathway. *Molecular Biology of the Cell*. 16:776-793.
- Seguí-Simarro, J.M., J.R. Austin, E.A. White, and L.A. Staehelin. 2004. Electron tomographic analysis of somatic cell plate formation in meristematic cells of Arabidopsis preserved by high-pressure freezing. *The Plant Cell*. 16:836-856.
- Shiina, N., and S. Tsukita. 1999. Mutations at Phosphorylation Sites of XenopusMicrotubule-associated Protein 4 Affect Its Microtubule-binding

- Ability and Chromosome Movement during Mitosis. *Molecular biology of the cell*. 10:597-608.
- Shirakawa, M., H. Ueda, T. Shimada, Y. Koumoto, T.L. Shimada, M. Kondo, T. Takahashi, Y. Okuyama, M. Nishimura, and I. Hara-Nishimura. 2010. Arabidopsis Qa-SNARE SYP2 proteins localized to different subcellular regions function redundantly in vacuolar protein sorting and plant development. *The Plant Journal*. 64:924-935.
- Simon, M.L.A., M.P. Platre, S. Assil, R. Wijk, W.Y. Chen, J. Chory, M. Dreux, T. Munnik, and Y. Jaillais. 2014. A multi-colour/multi-affinity marker set to visualize phosphoinositide dynamics in Arabidopsis. *The Plant Journal*. 77:322-337.
- Simon, M.L.A., M.P. Platre, M.M. Marquès-Bueno, L. Armengot, T. Stanislas, V. Bayle, M.-C. Caillaud, and Y. Jaillais. 2016. A PtdIns (4) P-driven electrostatic field controls cell membrane identity and signalling in plants. *Nature plants*. 2:16089.
- Simons, K., and D. Toomre. 2000. Lipid rafts and signal transduction. *Nature reviews Molecular cell biology*. 1.
- Smertenko, A., N. Saleh, H. Igarashi, H. Mori, I. Hauser-Hahn, C.-J. Jiang, S. Sonobe, C.W. Lloyd, and P.J. Hussey. 2000. A new class of microtubule-associated proteins in plants. *Nat Cell Biol*. 2:750-753.
- Smertenko, A.P., H.-Y. Chang, S. Sonobe, S.I. Fenyk, M. Weingartner, L. Bögre, and P.J. Hussey. 2006. Control of the AtMAP65-1 interaction with microtubules through the cell cycle. *Journal of Cell Science*. 119:3227-3237.
- Smertenko, A.P., H.-Y. Chang, V. Wagner, D. Kaloriti, S. Fenyk, S. Sonobe, C. Lloyd, M.-T. Hauser, and P.J. Hussey. 2004. The Arabidopsis microtubule-associated protein AtMAP65-1: molecular analysis of its microtubule bundling activity. *The Plant Cell*. 16:2035-2047.
- Smertenko, A.P., D. Kaloriti, H.-Y. Chang, J. Fiserova, Z. Opatrny, and P.J. Hussey. 2008. The C-terminal variable region specifies the dynamic properties of Arabidopsis microtubule-associated protein MAP65 isoforms. *The Plant Cell*. 20:3346-3358.
- Sousa, E., B. Kost, and R. Malhó. 2008. Arabidopsis Phosphatidylinositol-4-Monophosphate 5-Kinase 4 Regulates Pollen Tube Growth and Polarity by Modulating Membrane Recycling. *The Plant Cell*. 20:3050-3064.
- Soyano, T., R. Nishihama, K. Morikiyo, M. Ishikawa, and Y. Machida. 2003. NQK1/NtMEK1 is a MAPKK that acts in the NPK1 MAPKKK-mediated MAPK cascade and is required for plant cytokinesis. *Genes & Development*. 17:1055-1067.
- Spinner, L., A. Gadeyne, K. Belcram, M. Goussot, M. Moison, Y. Duroc, D. Eeckhout, N. De Winne, E. Schaefer, E. Van De Slijke, G. Persiau, E. Witters, K. Gevaert, G. De Jaeger, D. Bouchez, D. Van Damme, and M. Pastuglia. 2013. A protein phosphatase 2A complex spatially controls plant cell division. *Nature Communications*. 4:1863.

- Stanislas, T., A. Hüser, I.C. Barbosa, C.S. Kiefer, K. Brackmann, S. Pietra, A. Gustavsson, M. Zourelidou, C. Schwechheimer, and M. Grebe. 2015. Arabidopsis D6PK is a lipid domain-dependent mediator of root epidermal planar polarity. *Nature plants*. 1:15162.
- Steiner, A., L. Müller, K. Rybak, V. Vodermaier, E. Facher, M. Thellmann, R. Ravikumar, G. Wanner, M.-T. Hauser, and F.F. Assaad. 2016a. The membrane-associated Sec1/Munc18 KEULE is required for phragmoplast microtubule reorganization during cytokinesis in Arabidopsis. *Molecular plant*. 9:528-540.
- Steiner, A., K. Rybak, M. Altmann, H.E. McFarlane, S. Klaeger, N. Nguyen, E. Facher, A. Ivakov, G. Wanner, and B. Kuster. 2016b. Cell cycle-regulated PLEIADE/AtMAP65-3 links membrane and microtubule dynamics during plant cytokinesis. *The Plant Journal*. 88:531-541.
- Stevenson-Paulik, J., J. Love, and W.F. Boss. 2003. Differential Regulation of Two Arabidopsis Type III Phosphatidylinositol 4-Kinase Isoforms. A Regulatory Role for the Pleckstrin Homology Domain. *Plant Physiology*. 132:1053-1064.
- Stevenson, J.M., I.Y. Perera, and W.F. Boss. 1998. A Phosphatidylinositol 4-Kinase Pleckstrin Homology Domain That Binds Phosphatidylinositol 4-Monophosphate. *Journal of Biological Chemistry*. 273:22761-22767.
- Stöckle, D., A. Herrmann, E. Lipka, T. Lauster, R. Gavidia, S. Zimmermann, and S. Müller. 2016. Putative RopGAPs impact division plane selection and interact with kinesin-12 POK1. *Nature Plants*. 2:16120.
- Strompen, G., F. El Kasmi, S. Richter, W. Lukowitz, F.F. Assaad, G. Jürgens, and U. Mayer. 2002. The Arabidopsis HINKEL gene encodes a kinesin-related protein involved in cytokinesis and is expressed in a cell cycle-dependent manner. *Current Biology*. 12:153-158.
- Suarez-Rodriguez, M.C., L. Adams-Phillips, Y. Liu, H. Wang, S.-H. Su, P.J. Jester, S. Zhang, A.F. Bent, and P.J. Krysan. 2007. MEKK1 is required for flg22-induced MPK4 activation in Arabidopsis plants. *Plant physiology*. 143:661-669.
- Szumanski, A.L., and E. Nielsen. 2010. Phosphatidylinositol 4-Phosphate is Required for Tip Growth in Arabidopsis thaliana. In *Lipid Signaling in Plants*. T. Munnik, editor. Springer Berlin Heidelberg, Berlin, Heidelberg. 65-77.
- Takahashi, Y., T. Soyano, K. Kosetsu, M. Sasabe, and Y. Machida. 2010. HINKEL kinesin, ANP MAPKKs and MKK6/ANQ MAPKK, which phosphorylates and activates MPK4 MAPK, constitute a pathway that is required for cytokinesis in Arabidopsis thaliana. *Plant and cell physiology*. 51:1766-1776.
- Tanaka, H., M. Ishikawa, S. Kitamura, Y. Takahashi, T. Soyano, C. Machida, and Y. Machida. 2004. The AtNACK1/HINKEL and STUD/TETRASPORE/AtNACK2 genes, which encode functionally redundant kinesins, are essential for cytokinesis in Arabidopsis. *Genes*

- to Cells*. 9:1199-1211.
- Tanaka, H., S. Kitakura, R. De Rycke, R. De Groot, and J. Friml. 2009. Fluorescence Imaging-Based Screen Identifies ARF GEF Component of Early Endosomal Trafficking. *Current Biology*. 19:391-397.
- Tanaka, H., S. Kitakura, H. Rakusová, T. Uemura, M.I. Feraru, R. De Rycke, S. Robert, T. Kakimoto, and J. Friml. 2013. Cell polarity and patterning by PIN trafficking through early endosomal compartments in *Arabidopsis thaliana*. *PLoS genetics*. 9:e1003540.
- Tang, Y., C.-Y. Zhao, S.-T. Tan, and H.-W. Xue. 2016. Arabidopsis Type II Phosphatidylinositol 4-Kinase PI4Ky5 Regulates Auxin Biosynthesis and Leaf Margin Development through Interacting with Membrane-Bound Transcription Factor ANAC078. *PLoS Genetics*. 12:e1006252.
- Tejos, R., M. Sauer, S. Vanneste, M. Palacios-Gomez, H. Li, M. Heilmann, R. van Wijk, J.E. Vermeer, I. Heilmann, and T. Munnik. 2014. Bipolar plasma membrane distribution of phosphoinositides and their requirement for auxin-mediated cell polarity and patterning in *Arabidopsis*. *The Plant Cell*. 26:2114-2128.
- Thole, J.M., J.E. Vermeer, Y. Zhang, T.W. Gadella, and E. Nielsen. 2008. Root hair defective4 encodes a phosphatidylinositol-4-phosphate phosphatase required for proper root hair development in *Arabidopsis thaliana*. *The Plant Cell*. 20:381-395.
- Traub, L.M. 2009. Tickets to ride: selecting cargo for clathrin-regulated internalization. *Nat Rev Mol Cell Biol*. 10:583-596.
- Tulin, A., S. McClerklin, Y. Huang, and R. Dixit. 2012. Single-Molecule Analysis of the Microtubule Cross-Linking Protein MAP65-1 Reveals a Molecular Mechanism for Contact-Angle-Dependent Microtubule Bundling. *Biophysical Journal*. 102:802-809.
- Uemura, T., M.T. Morita, K. Ebine, Y. Okatani, D. Yano, C. Saito, T. Ueda, and A. Nakano. 2010. Vacuolar/pre-vacuolar compartment Qa-SNAREs VAM3/SYP22 and PEP12/SYP21 have interchangeable functions in *Arabidopsis*. *The Plant Journal*. 64:864-873.
- Unger, T., Y. Jacobovitch, A. Dantes, R. Bernheim, and Y. Peleg. 2010. Applications of the Restriction Free (RF) cloning procedure for molecular manipulations and protein expression. *Journal of Structural Biology*. 172:34-44.
- Ungewickell, E., and D. Branton. 1981. Assembly units of clathrin coats. *Nature*. 289:420-422.
- Valencia, J.P., K. Goodman, and M.S. Otegui. 2016. Endocytosis and Endosomal Trafficking in Plants. *Annual Review of Plant Biology*. 67:309-335.
- Van Damme, D., S. Coutuer, R. De Rycke, F.-Y. Bouget, D. Inzé, and D. Geelen. 2006. Somatic cytokinesis and pollen maturation in *Arabidopsis* depend on TPLATE, which has domains similar to coat proteins. *The Plant Cell*. 18:3502-3518.

- Van Damme, D., K. Van Poucke, E. Boutant, C. Ritzenthaler, D. Inzé, and D. Geelen. 2004. In Vivo Dynamics and Differential Microtubule-Binding Activities of MAP65 Proteins. *Plant Physiology*. 136:3956-3967.
- Van Damme, D., M. Vanstraelen, and D. Geelen. 2007. Cortical division zone establishment in plant cells. *Trends in Plant Science*. 12:458-464.
- Vermeer, J.E.M., J.M. Thole, J. Goedhart, E. Nielsen, T. Munnik, and T.W.J. Gadella Jr. 2009. Imaging phosphatidylinositol 4-phosphate dynamics in living plant cells. *The Plant Journal*. 57:356-372.
- Viotti, C., J. Bubeck, Y.-D. Stierhof, M. Krebs, M. Langhans, W. van den Berg, W. van Dongen, S. Richter, N. Geldner, J. Takano, G. Jürgens, S.C. de Vries, D.G. Robinson, and K. Schumacher. 2010. Endocytic and Secretory Traffic in Arabidopsis Merge in the Trans-Golgi Network/Early Endosome, an Independent and Highly Dynamic Organelle. *The Plant Cell*. 22:1344-1357.
- Vos, J.W., M. Dogterom, and A.M.C. Emons. 2004. Microtubules become more dynamic but not shorter during preprophase band formation: A possible “search-and-capture” mechanism for microtubule translocation. *Cell Motility and the Cytoskeleton*. 57:246-258.
- Walch-Solimena, C., and P. Novick. 1999. The yeast phosphatidylinositol-4-OH kinase pik1 regulates secretion at the Golgi. *Nature cell biology*. 1:523-525.
- Wandosell, F., L. Serrano, and J. Avila. 1987. Phosphorylation of alpha-tubulin carboxyl-terminal tyrosine prevents its incorporation into microtubules. *Journal of Biological Chemistry*. 262:8268-8273.
- Wang, Y.J., J. Wang, H.Q. Sun, M. Martinez, Y.X. Sun, E. Macia, T. Kirchhausen, J.P. Albanesi, M.G. Roth, and H.L. Yin. 2003. Phosphatidylinositol 4 Phosphate Regulates Targeting of Clathrin Adaptor AP-1 Complexes to the Golgi. *Cell*. 114:299-310.
- Wattelet-Boyer, V., L. Brocard, K. Jonsson, N. Esnay, J. Joubès, F. Domergue, S. Mongrand, N. Raikhel, R.P. Bhalerao, P. Moreau, and Y. Boutté. 2016. Enrichment of hydroxylated C24- and C26-acyl-chain sphingolipids mediates PIN2 apical sorting at trans-Golgi network subdomains. 7:12788.
- Weisshart, K., J. Fuchs, and V. Schubert. 2016. Structured Illumination Microscopy (SIM) and Photoactivated Localization Microscopy (PALM) to analyze the abundance and distribution of RNA Polymerase II molecules on flow-sorted Arabidopsis nuclei. *Bio-protocol*. 6:e1725.
- Wloga, D., and J. Gaertig. 2010. Post-translational modifications of microtubules. *Journal of Cell Science*. 123:3447-3455.
- Wu, C., L. Tan, M. Hooren, X. Tan, F. Liu, Y. Li, Y. Zhao, B. Li, Q. Rui, and T. Munnik. 2017. Arabidopsis EXO70A1 recruits Patellin3 to the cell membrane independent of its role as exocyst subunit. *Journal of Integrative Plant Biology*.
- Wunderlich, W., I. Fialka, D. Teis, A. Alpi, A. Pfeifer, R.G. Parton, F. Lottspeich,

- and L.A. Huber. 2001. A Novel 14-Kilodalton Protein Interacts with the Mitogen-Activated Protein Kinase Scaffold Mp1 on a Late Endosomal/Lysosomal Compartment. *The Journal of Cell Biology*. 152:765-776.
- Xue, H.-W., C. Pical, C. Brearley, S. Elge, and B. Müller-Röber. 1999. A Plant 126-kDa Phosphatidylinositol 4-Kinase with a Novel Repeat Structure: CLONING AND FUNCTIONAL EXPRESSION IN BACULOVIRUS-INFECTED INSECT CELLS. *Journal of Biological Chemistry*. 274:5738-5745.
- Yamamoto, W., S. Wada, M. Nagano, K. Aoshima, D.E. Siekhaus, J.Y. Toshima, and J. Toshima. 2018. Distinct roles for plasma membrane PtdIns(4)P and PtdIns(4,5)P<sub>2</sub> during receptor-mediated endocytosis in yeast. *Journal of Cell Science*. 131.
- Yamaoka, S., Y. Shimono, M. Shirakawa, Y. Fukao, T. Kawase, N. Hatsugai, K. Tamura, T. Shimada, and I. Hara-Nishimura. 2013. Identification and Dynamics of Arabidopsis Adaptor Protein-2 Complex and Its Involvement in Floral Organ Development. *The Plant Cell*. 25:2958-2969.
- Yang, Z. 2008. Cell Polarity Signaling in Arabidopsis. *Annual Review of Cell and Developmental Biology*. 24:551-575.
- Yasuhara, H., S. Sonobe, and H. Shibaoka. 1993. Effects of Taxol on the Development of the Cell Plate and of the Phragmoplast in Tobacco BY-2 Cells. *Plant and Cell Physiology*. 34:21-29.
- Young, A. 2007. Structural insights into the clathrin coat. *Seminars in Cell & Developmental Biology*. 18:448-458.
- Yu, L., J. Nie, C. Cao, Y. Jin, M. Yan, F. Wang, J. Liu, Y. Xiao, Y. Liang, and W. Zhang. 2010. Phosphatidic acid mediates salt stress response by regulation of MPK6 in Arabidopsis thaliana. *New Phytologist*. 188:762-773.
- Zeng, Q., J.-G. Chen, and B.E. Ellis. 2011. AtMPK4 is required for male-specific meiotic cytokinesis in Arabidopsis. *The Plant Journal*. 67:895-906.
- Zhang, H., and R.K. Dawe. 2011. Mechanisms of plant spindle formation. *Chromosome Research*. 19:335-344.
- Zhang, Y., S. Persson, J. Hirst, M.S. Robinson, D. van Damme, and C. Sánchez-Rodríguez. 2015. Change your Tplate, change your fate: plant CME and beyond. *Trends in Plant Science*. 20:41-48.
- Zhao, Y., A. Yan, J.A. Feijó, M. Furutani, T. Takenawa, I. Hwang, Y. Fu, and Z. Yang. 2010. Phosphoinositides Regulate Clathrin-Dependent Endocytosis at the Tip of Pollen Tubes in Arabidopsis and Tobacco. *The Plant Cell*. 22:4031-4044.
- Zhu, C., and W. Jiang. 2005. Cell cycle-dependent translocation of PRC1 on the spindle by Kif4 is essential for midzone formation and cytokinesis. *Proceedings of the National Academy of Sciences of the United States of America*. 102:343-348.

- Zhu, C., E. Lau, R. Schwarzenbacher, E. Bossy-Wetzel, and W. Jiang. 2006. Spatiotemporal control of spindle midzone formation by PRC1 in human cells. *Proceedings of the National Academy of Sciences*. 103:6196-6201.
- Zhu, Y., L.M. Traub, and S. Kornfeld. 1998. ADP-Ribosylation Factor 1 Transiently Activates High-Affinity Adaptor Protein Complex AP-1 Binding Sites On Golgi Membranes. *Molecular Biology of the Cell*. 9:1323-1337.

## 7. Appendix

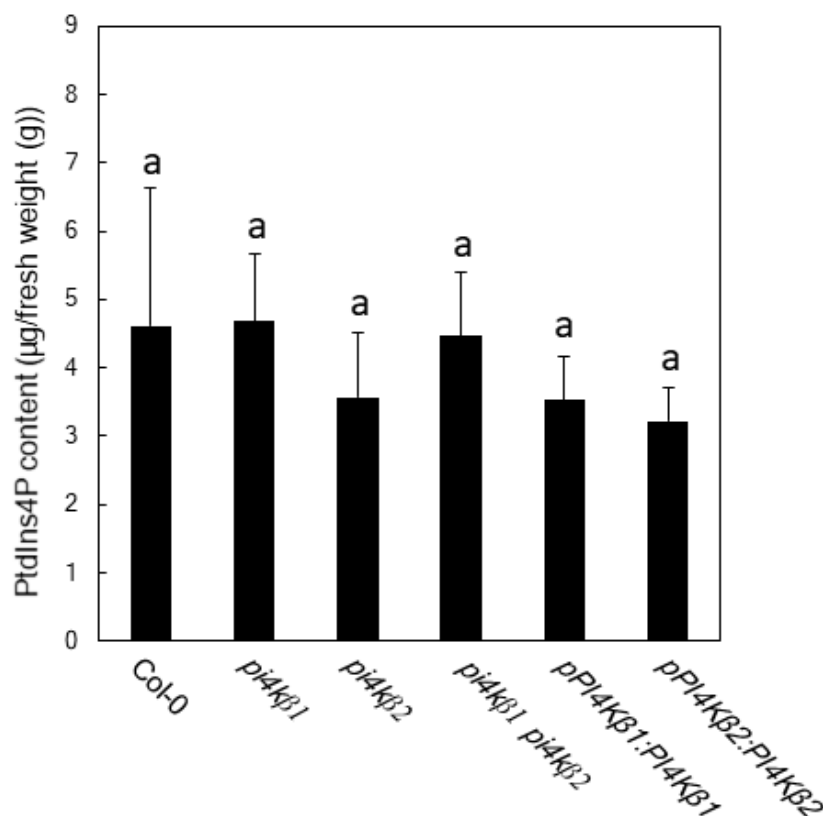


**Fig 7.1. PtdIns4P level is not changed in the *pi4kβ1 pi4kβ2* double mutant.** Two-week-old seedlings were subjected to PtdIns4P analysis. The *pi4kβ1 pi4kβ2* double mutant did not show any difference for PtdIns4P level determined by one-way ANOVA using LSD multiple comparisons with 95% confidence interval. Data represent the mean  $\pm$  SD. The experiment was performed once by Dr. Mareike Heilmann with three replicates for each genotypes.

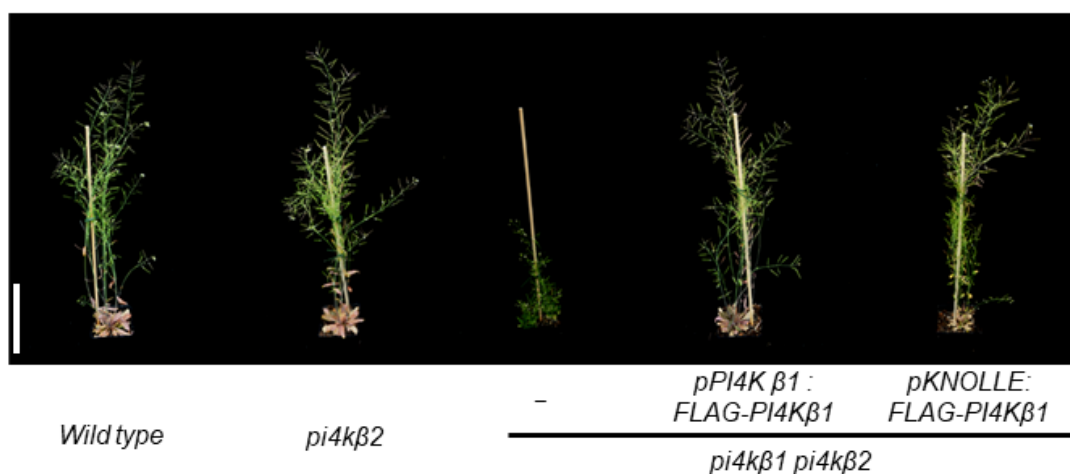


**Figure 7.2. The *pi4kβ1 pi4kβ2* phenotype is rescued by a *FLAG-PI4Kβ1* driven by *KNOLLE* cis-regulatory sequences.** Transgenic lines and controls, as indicated. 50-day-old plants are shown. Bar, 10 cm

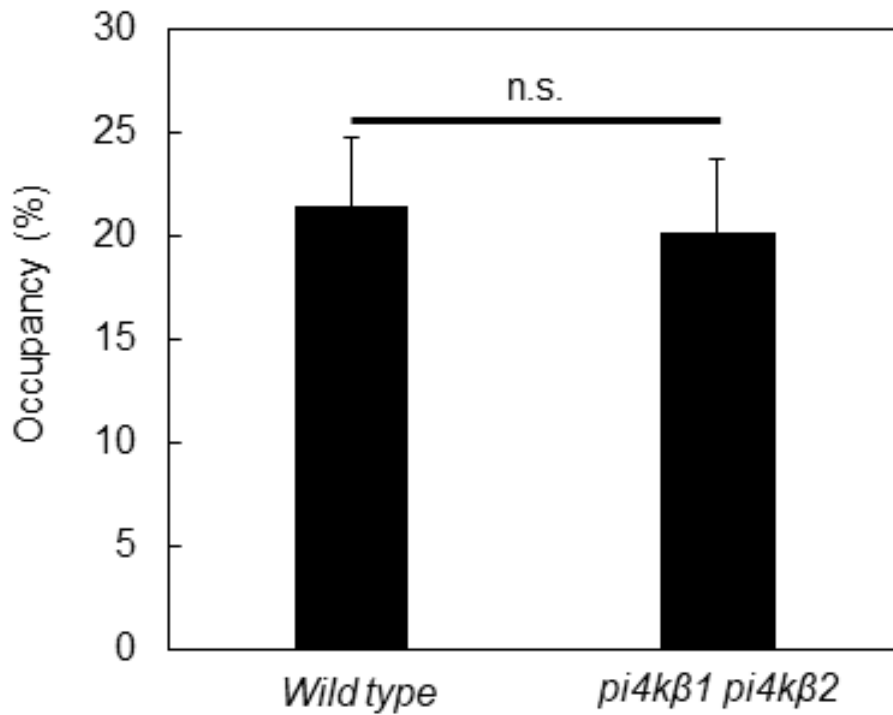


**Figure 7.3. Quantification of cortical microtubule density in five-day-old root elongation zones.** Data represent the mean  $\pm$  SD. n.s., not significant. N = 11 cells of 11 seedlings for wild type, while n = 7 cells of 7 *pi4kβ1 pi4kβ2* double mutant were used for quantification.

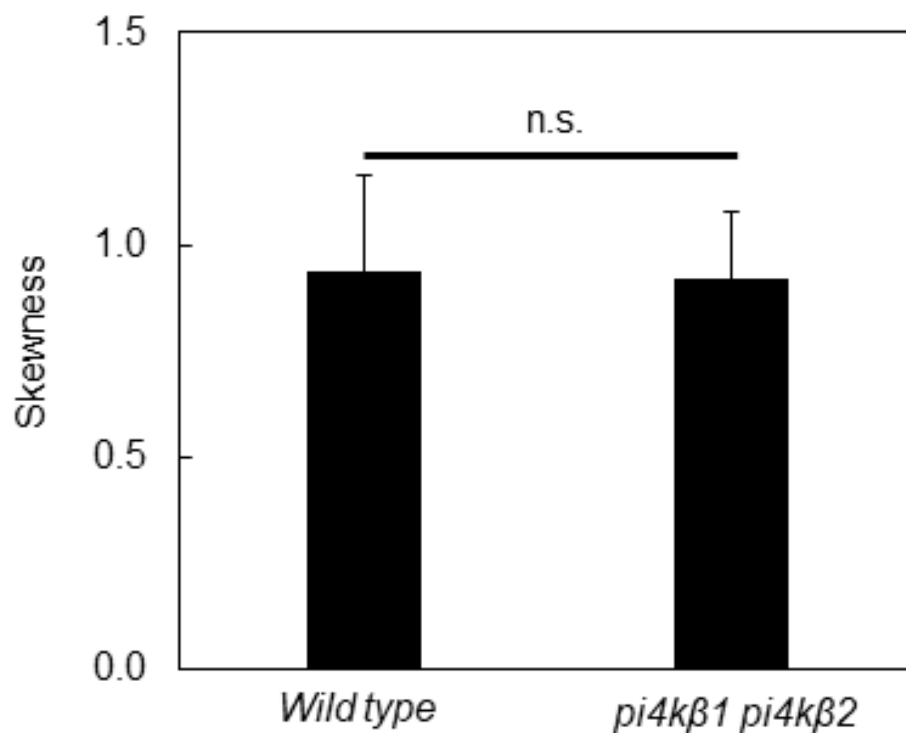


**Figure 7.4. Quantification of cortical microtubule bundling in five-day-old root elongation zones.** Data represent the mean  $\pm$  SD. n.s., not significant. N = 11 cells of 11 seedlings for wild type, while n = 7 cells of 7 *pi4kβ1 pi4kβ2* double mutant were used for quantification.

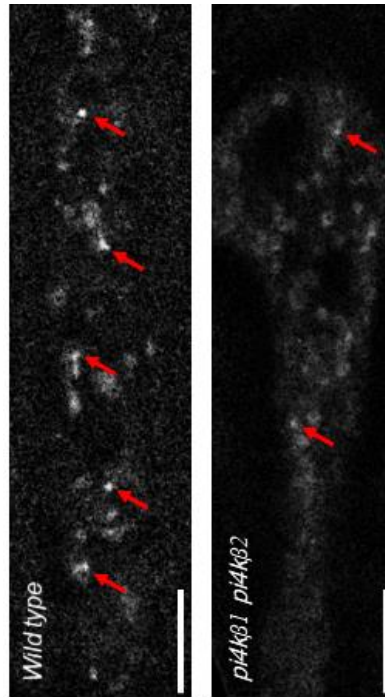


**Figure 7.5. MPK4 affects localization of mCherry-PI4K $\beta$ 1.** Five-day-old roots of *wild type* (10 cells, 10 roots) and *mpk4-2* (6 cells, 6 roots) expressing mCherry-PI4K $\beta$ 1 were imaged by spinning disc microscope. Bright dots (red arrows) which were present in *wild type* reduced in *mpk4-2*. Bars are 10  $\mu$ m.

**Table 7.1 Offspring of self-pollinated  $pi4k\beta1^{-/-} \times \beta2^{+/-} \times mpk4-2^{+/-}$** 

Genotype	Number observed	Number expected
$pi4k\beta1^{-/-} \times \beta2^{+/+} \times mpk4-2^{+/+}$	35 (19 %)	11 (6 %)
$pi4k\beta1^{-/-} \times \beta2^{+/-} \times mpk4-2^{+/+}$	19 (10 %)	23 (13 %)
$pi4k\beta1^{-/-} \times \beta2^{-/-} \times mpk4-2^{+/+}$	11 (6 %)	11 (6 %)
$pi4k\beta1^{-/-} \times \beta2^{+/+} \times mpk4-2^{+/-}$	54 (30 %)	23 (13 %)
$pi4k\beta1^{-/-} \times \beta2^{+/-} \times mpk4-2^{+/-}$	20 (11 %)	46 (25 %)
$pi4k\beta1^{-/-} \times \beta2^{-/-} \times mpk4-2^{+/-}$	9 (5 %)	23 (13 %)
$pi4k\beta1^{-/-} \times \beta2^{+/+} \times mpk4-2^{-/-}$	29 (16 %)	11 (6 %)
$pi4k\beta1^{-/-} \times \beta2^{+/-} \times mpk4-2^{-/-}$	4 (2 %)	23 (13 %)
$pi4k\beta1^{-/-} \times \beta2^{-/-} \times mpk4-2^{-/-}$	0 (0 %)	11 (6 %)
Total number	181	-
P-value	-	2.49526E-33 <0.0001*

The genotypes of 181 progeny were determined based on PCR results. Expected values were calculated using Mendelian law. P-value was calculated by chi-squared test. An asterisk indicates a significant P-value in comparison with expected number.

**Table 7.2 Primers used for genotyping**

Name	Sequence	Length of product
pi4kbeta1-intron-RP	AGTGCCTGTGCTTGCTA TTGTCC	<i>PI4Kβ1</i> : 1434 bp <i>pi4kβ1</i> : about 1000 bp
pi4kbeta1-intron-exon-LP	GAATAGAAGCCTGCAGG AAGGG	(LB6316+ pi4kbeta1-intron-RP)
pi4kbeta2-intron-RP	GTAAAGTGCCTGTGTCC TGCTTGAT	<i>PI4Kβ2</i> : 1693 bp <i>pi4kβ2</i> : about 1200 bp
pi4kbeta2-intron-LP	CATGGTGTACATCTCA CACAATTTGC	(LB6316+ pi4kbeta2-intron-RP)
K4WT_S	GTGACAATGCAAGAAGA TACGTTAGACAGC	MPK4: 1077 bp

**Table 7.2 Primers used for genotyping**

K4WT_R	CTTGAAATATCTACAGAG TTGGTGTG	<i>mpk4</i> : about 800 bp (LB6316+K4WT_R)
gPI4Kbeta1-LP	TCCAGTCCCTAGACATG ATTTGTCTGTA	For genotyping of <i>pi4kβ1×β2+mCherry-gPI4Kbeta1</i>
gPI4Kbeta1-RP	ATGGAAAGTTACCTGGTT GGGACC	<i>gPI4Kβ1</i> : 5100 bp <i>gpi4kβ1</i> : about 500 bp
mCherry-F	ATGCGGCGCGCCtATGG TGAGCAAGGGCGAGGA GG	(LB6316+ gPI4Kbeta1- RP) <i>mCherry-gPI4Kbeta1</i> : 1800 bp
pi4kbeta1-1-R	CTGAATTTGCACCCAATT CC	
pi4kbeta1-intron-RP	AGTGCCTGTGCTTGCTA TTGTCC	For genotyping of <i>pi4kβ1×β2+ pPI4Kβ1-FLAG-PI4Kβ1</i>
pi4kbeta1-intron-exon-LP	GAATAGAAGCCTGCAGG AAGGG	<i>PI4Kβ1</i> : 1434 bp <i>pi4kβ1</i> : about 1000 bp
FLAG-pi4kbeta1-genotyping-f	CGCCTCGGCCATGGACT ACAAGGATG	(LB6316+ pi4kbeta1- intron-RP)
pi4kbeta1-1-R	CTGAATTTGCACCCAATT CC	<i>FLAG-PI4Kβ1</i> :1100 bp
pi4kbeta1-intron-RP	AGTGCCTGTGCTTGCTA TTGTCC	For genotyping of <i>pi4kβ1×β2+ pPI4Kβ1-PI4Kβ1</i>
pi4kbeta1-intron-exon-LP	GAATAGAAGCCTGCAGG AAGGG	<i>PI4Kβ1</i> : 1434 bp

**Table 7.2 Primers used for genotyping**

pi4k beta1-sal1-F	ATGCGTCGACATGCCGA TGGGACGCTTTCTAT	<i>pi4kβ1</i> : about 1000 bp (LB6316+ pi4kbeta1- intron-RP)
pi4k beta1-bamh1-R	ATGCGGATCCTCACAATA TTCCATTTAAGAC	<i>PI4Kβ1</i> transgene:3300 bp
pi4kbeta2-intron-RP	GTAAAGTGCCTGTGTCC TGCTTGAT	For genotyping of <i>pi4kβ1×β2+ pPI4Kβ2-</i> <i>PI4Kβ2</i>
pi4kbeta2-intron-LP	CATGGTGTACATCTCA CACAAATTTGC	<i>PI4Kβ2</i> : 1693 bp
pi4k beta2-sal1-F	ATGCGTCGACATGCAGA TGGCACAGTTTCT	<i>pi4kβ2</i> : about 1200 bp (LB6316+ pi4kbeta2- intron-RP)
pi4k beta2-bamh1-R	ATGCGGATCCTCATCGTA TTCCATTCAACAC	<i>PI4Kβ2</i> transgene:3300 bp

**Table 7.3 Primers used for cloning**

Name	Sequence	Length of product
PI4Kβ1-F	ATGCGT <u>CGAC</u> ATGCCGATGGGACGCTTT CTAT (underlined, Sall)	3366 bp
PI4Kβ1-R	ATGCGGAT <u>CCT</u> CACAATATTCCATTTAAGA C (underlined, BamHI)	
PI4Kβ2-F	ATGCGT <u>CGAC</u> ATGCAGATGGCACAGTTTC T (underlined, Sall)	3351 bp

PI4K $\beta$ 2-R	ATGCGGATCCTCATCGTATTCCATTCAAC AC (underlined, BamHI)	
pPI4K $\beta$ 1-F	ATGCGGCCATTACGGCCATGTTTTCTCTC ACACCCTCATA (underlined, Sfil)	1360 bp
pPI4K $\beta$ 1-R	ATGCGGCCGAGGCGGCCCTAATCAGCC AAGCATAAAAAGC (underlined, Sfil)	
pPI4K $\beta$ 2-F	ATGCGGCCATTACGGCCCAACCGTCGGT GTTCTCGTAA (underlined, Sfil)	1198 bp
pPI4K $\beta$ 2-R	ATGCGGCCGAGGCGGCCCTTTTGATGATC AGTCTTAGAATAA (underlined, Sfil)	
pKNOLLE-F	ATGCGGCCATTACGGCCCTTAGGATGGA GAGCCTTGCAGC (underlined, Sfil)	3013 bp
pKNOLLE-R	ATGCGGCCGAGGCGGCCCTTTTTACCT GAAAGTCAAC (underlined, Sfil)	
RF-pi4kbeta1-F1	CAACTTTGTACAAAAAAGCAGGGCCTCCT TCTTCAGGGAACGATGGAT	5040 bp
RF-pi4kbeta1-R1	CGTCTCGCATATCTCATTAAAGCAGCCTA ACTTCCTCCATGGCAACAGTAC	
RF-pi4kbeta1-F2	GTACTGTTGCCATGGAGGAAGTTAGG	2026 bp
RF-pi4kbeta1-R2	GCCAACTTTGTACAAGAAAGCTGAGTACC TGCAGAAGGTAACAGACCAAAG	
RF-pi4kbeta1-F3	CTTTGGTCTGTTACCTTCTGCAGG	1909 bp

RF-pi4kbeta1- R3	GCCAACTTTGTACAAGAAAGCTGAGTAGT AAACAGCGAGAGTAAACGGTAGACT	
RF-pi4kbeta1- F4	AGTCTACCGTTTACTCTCGCTGTTTAC	1689 bp
RF-pi4kbeta1- R4	GCCAACTTTGTACAAGAAAGCTGAGTAGG ATCCGAGTTAGTTACCGGG- TAAATCAGGAGG	
mCherry- gPI4Kb1-F	GGGCTTTTTATGCTTGGCTGATTAGGATG GTGAGCAAGG-GCGAGGAGGA	711 bp
mCherry- SGPSG- gPI4Kb1-R	AGATAGAAAGCGTCCCATCGGCAT <u>ACCA-</u> <u>GATGGACCAGACTT</u> GTACAGCTCGTCCAT GCCGC (underlined, SGPSG)	
PI4K $\beta$ <sub>1422-1121</sub> -F	ATG <u>CCCCGGG</u> TAGGGAGGGTTTTTCAA AAATTC (unerlined, XmaI)	2097 bp
PI4K $\beta$ <sub>1422-1121</sub> -R	ATG <u>CGGATCC</u> CTCACAATATTCCATTTAAG ACCC (underlined, BamHI)	
PI4K $\beta$ <sub>11-566</sub> -F	ATG <u>CCCCGGG</u> TATGCCGATGGGACGCTTT CTATC (underlined, XmaI)	1698 bp
PI4K $\beta$ <sub>11-566</sub> -R	ATG <u>CGGATCC</u> CATATGACGTTTCACATAAC GC (underlined, BamHI)	
MPK4-F	ATG <u>CCCATGG</u> GAGATGTCCGGCGGAGAGTT GTTTCG (undelined, NcoI)	1131 bp
MPK4-R	ATG <u>CGGATCC</u> CTCACACTGAGTCTTGAGG ATTGA (underlined, BamHI)	

**Table 7.4 Chemicals used in this thesis**

<b>Name</b>	<b>Supplier</b>	<b>Solvent</b>	<b>Stock concentration</b>	<b>Working concentration</b>
Carbenicillin	Duchefa	H <sub>2</sub> O	100 mg/ml	100 µg/ml
Kanamycin	Duchefa	H <sub>2</sub> O	50 mg/ml	50 µg/ml
Rifampicin	Duchefa	methanol	50 mg/ml	50 µg/ml
Phosphinothricin	Duchefa	H <sub>2</sub> O	10 mg/ml	10 µg/ml
Glufosinate ammonium	Sigma	H <sub>2</sub> O	10 mg/ml	10 µg/ml
SynaptoRed C2 (FM 4-64)	Sigma	H <sub>2</sub> O	2 mM	20 µM
Brefeldin A (BFA)	Sigma	DMSO	50 mM	50 µM
Cycloheximide (CHX)	Sigma	DMSO	50 mM	50 µM
Albumin Fraktion V (BSA)	Roth	PBS	-	3-5 %
DMSO	Sigma	-	-	-
cOmplete protease inhibitor cocktail	Roche	Corresponding buffer		1 ×
PhosSTOP phosphatase inhibitor cocktail	Sigma	Corresponding buffer	-	1 ×

Propidium iodide (PI)	Sigma	H <sub>2</sub> O	1 mg/ml	10 µg/ml
DAPI	Sigma	H <sub>2</sub> O	1 mg/ml	1 µg/ml
Calcofluor White M2R	Sigma	0.1 M Tris-HCl (pH 9.0)	3.5 mg/ml	3.5 µg/ml
Myelin basic protein (MBP)	Sigma		10 µg/µl	0.25 µg/µl
Macerozyme R-10	Serva	PEM		2 %
Isopropyl-β-D-thiogalactopyranosid (IPTG)	Thermo	H <sub>2</sub> O	1 M	1 mM
Paraformaldehyde	Sigma	PEM		4 %
Sodium orthovanadate (Na <sub>3</sub> VO <sub>4</sub> )	Sigma	H <sub>2</sub> O	200 mM	1 mM
Sodium fluoride (NaF)	Sigma	H <sub>2</sub> O	0.5 M	10 mM
β-glycerophosphate	Sigma	H <sub>2</sub> O	0.5 M	50 mM

**Table 7.5 Microorganism used in this dissertation**

Organism	Strain	Purpose
----------	--------	---------

<i>Escherichia coli</i>	DH5 $\alpha$	Cloning
<i>Saccharomyces cerevisiae</i>	Y2H Gold	Yeast two hybrid
<i>Agrobacterium tumefaciens</i>	AGL0	Plant transformation

**Table 7.6 Vectors used in this thesis**

Vectors	Resistance	Provided by	Description
pEntry E	Ampicilin	Dr. Mareike Heilmann, MLU Halle-Wittenberg	It contains <i>attL1</i> and <i>attL2</i> recombination sites which mediate LR reaction of Gateway
pMDC123	Kanamycin (in bacterium) Basta (in plants)	Curtis and Grossniklaus, 2003(Curtis and Grossniklaus, 2003)	Binary destination vector which has <i>attR1</i> and <i>attR2</i> sites that mediate LR reaction.
pGADT7	Ampicilin	Clontech	Prey vector that has a activation domain of transcription factor GAL4
pGBKT7	kanamycin	Clontech	Bait vector which has a DNA-binding domain of GAL4
pGADT7-T	Ampicilin	Clontech	Positive control plasmid which encodes the GAL4

---

			activation domain fused with SV40 large T-antigen
pGBKT7-53	kanamycin	Clontech	Positive control encodes the GAL4 DNA-Binding domain fused with murine p53

---

**Table 7.7 Antibodies used for immunoblotting in this thesis**


---

Name	Supplier	Host	Dilution
anti-AtPI4K $\beta$ 1	Eurogentec	Rabbit	1:250
Anti-myc	M4439, Sigma	Mouse	1:2000
Anti-mouse IgG (H + L) conjugated with horseradish peroxidase (HRP)	A4416, Sigma	Goat	1:15,000
anti-Rabbit IgG light chain conjugated with HRP	MAB201P, Merck Millipore	Mouse	1:15,000

---

**Table 7.8 Antibodies used for immunostaining in this thesis**


---

Name	Supplier	Host	Dilution
Anti- $\alpha$ -tubulin	clone YOL 1/34, Abcam	Rat	1:1000
Anti-KNOLLE	Gift from Prof. Gerd Jürgens	Rabbit	1:2000
Anti-GFP	A11122, Invitrogen	Rabbit	1:2000
Anti-mCHerry	ab167453, Abcam	Rabbit	1:2000

---

Alexa Flour® 555 anti-rat IgG (H + L)	A21434, Invitrogen	Goat	1:2000
Alexa Flour® 488 anti-rabbit IgG (H + L)	A21206, Invitrogen	Donkey	1:2000

---

**8. Abbreviations**

<i>A.thaliana</i>	<i>Arabidopsis thaliana</i>
ANTH	AP180 N-terminal homology
APC	anaphase-promoting Complex
APS	ammonium persulfate
AP-2	adaptor protein 2
ARF-GAP	ARF-specific GTPase activating protein
ARF1	ADP-ribosylation factor 1
Ase1	Anaphase spindle elongation 1
AUX1	AUXIN-RESISTANT 1
BAR	Bin–amphiphysin–Rvs
BFA	Brefeldin A
BIG	Brefeldin A-inhibited guanine nucleotide-exchange protein
BRI1	BRASSINOSTEROID INSENSITIVE1
CAP1	clathrin assembly protein 1
CBB	Coomassie Brilliant Blue
CCV	clathrin-coated vesicle
CDK	cyclin-dependent kinase
CDP-DAG	cytidine diphosphate diacylglycerol
CDS	cortical division site
CDTA	<i>trans</i> -1,2-diaminocyclohexaneN,N,N',N'-tetraacetic acid
CDZ	cortical division zone
CESA3	cellulose synthase subunit A3
CHX	cycloheximide

CKL6	casein kinase 1-like 6
CLSM	confocal laser scanning microscopy
CME	clathrin-mediated endocytosis
COP1	coat protein 1
DAPI	4',6-diamidino-2-phenylindole
DMSO	dimethyl sulfoxide
DRM	detergent-resistant membrane
DRP	dynamamin-related protein
DSP	dual-specificity phosphatase
DTT	dithiothreitol
EB	ethidium bromide
ECA4	epsin-like clathrin adaptor 4
EE	early endosome
EGTA	ethylene glycol-bis( $\beta$ -aminoethyl ether)-N,N,N',N'-tetraacetic acid
EH	EPS15 homology
EPS15	epidermal growth factor receptor pathway substrate 15
ESCRT	endosomal sorting complex required for transport
FAPP1	phosphatidylinositol-four-phosphate adaptor protein-1
FCHO	FES-CIP4 homology domain only
FM 4-64	N-(3-triethylammoniumpropyl)-4-(6-(4-(diethylamino) phenyl) hexatrienyl) pyridinium dibromide
GaAsP	gallium Arsenide phosphide
GBF	Golgi-specific brefeldin A-resistance guanine nucleotide exchange factor

---

GEF	guanosine nucleotide exchange factor
GNL1	GNOM-LIKE 1
HCl	hydrogen chloride
HSC70	ATPase heat shock cognate 70
IMTs	interdigitating microtubules
JNK1	c-Jun N-terminal kinase1
LB	lysogeny broth
LDL	low-density-lipoprotein
LE	late endosome
LiAc	lithium acetate
LKU	lipid kinase unique
LOLITA	Longin-like protein interacting with TPLATE adaptor
LRP1	low-density-lipoprotein receptor-related protein 1
MAP	microtubule-associated proteins
MAPK	mitogen-activated protein kinase
MBP	myelin basic protein
MgCl <sub>2</sub>	magnesium chloride
MTB	microtubule binding region
MVB	multivesicular bodies
NACK	<u>N</u> PK1- <u>a</u> ctivating <u>k</u> inesin-like protein
NEK6	NIMA-related kinase 6
NH domain	novel homology domain
nIMTs	noninterdigitating microtubules
NPK1	nucleus- and phragmoplast-localized protein kinase 1
NaF	sodium fluoride
Na <sub>3</sub> VO <sub>4</sub>	sodium orthovanadate

## ABBREVIATIONS

---

PCR	polymerase chain reaction
PH domain	pleckstrin homology domain
PHS1	PROPYZAMIDE HYPERSENSITIVE 1
PIN1	auxin efflux transporters-PIN- FORMED 1
PIPES	piperazine-N,N' -bis(2- ethanesulfonic acid)
PIP5K5	phosphatidylinositol-4-phosphate 5- kinase 5
PIS	phosphatidylinositol synthase
PI4K	phosphatidylinositol 4-OH kinase
PM	plasma membrane
POK	phragmoplast-orienting kinesin
PPB	preprophase band
PPC domain	plant PI4K charged domain
PPI	polyphosphoinositides
PRC1	PROTEIN REGULATING CYTOKINESIS 1
PtdIns	phosphatidylinositol
PtdIns4P	phosphatidylinositol 4-phosphate
PtdOH	phosphatidic acid
PTP	Protein tyrosine phosphatase
PVC	prevacuolar compartment
PBS	phosphate buffered saline
PMSF	phenylmethane sulfonyl fluoride
RACK1	receptor for activated C kinase 1
RF cloning	restriction free (RF) cloning
RHD4	ROOT HAIR DEFECTIVE4

## ABBREVIATIONS

---

R-SNARE	R- <u>s</u> oluble <u>N</u> SF (N-ethylmaleimide-sensitive factor) <u>a</u> ttachment protein <u>r</u> eceptors
SAC	suppressor of actin
SD meida	synthetic dropout media
SDS-PAGE	sodium dodecyl sulfat polyacrylamide gel electrophoresis
SH3	Src-homology 3
SYP	Syntaxin of Plants
TAE	Tris-acetate-EDTA
TASH3	TPLATE-associated Src-homology 3
TEMED	tetramethylethylenediamine
TGN	<i>trans</i> -Golgi network
TML	TPLATE complex muniscin-like
TPC	TPLATE complex
TRAPP II	Transport Protein Particle II (TRAPP II)
μHD	μ homology domain
VAMP711	vesicle-associated membrane protein 711
VHA-a1	vacuolar H <sup>+</sup> -ATPase subunit a1
3D-SIM	3D-structured illumination microscopy

**Publications**

1. Lin F, Krishnamoorthy P, Schubert V, Heilmann I. Cell plate-associated PI4K $\beta$  is essential for cytokinesis in Arabidopsis. (in preparation)
2. Gerth K, Lin F, Daamen F, Menzel W, Heinrich F, Heilmann M (2017) Arabidopsis phosphatidylinositol 4-phosphate 5-kinase 2 contains a functional nuclear localization sequence and interacts with alpha-importins. Plant J 92: 862-878. doi: 10.1111/tpj.13724
3. Gerth K, Lin F, Menzel W, Krishnamoorthy P, Stenzel I, Heilmann M, Heilmann I (2017) Guilt by Association: A Phenotype-Based View of the Plant Phosphoinositide Network. Annu Rev Plant Biol 68: 349-374. doi: 10.1111/tpj.13724

**Acknowledgements**

I would like to express my thanks to all of people who helped me during my PhD study and thesis writing.

Foremost, I am deeply grateful to my supervisor Prof. Dr. Ingo Heilmann. I would like to thank him for accepting me as his PhD student, having regular discussion during my PhD study to give me ideals, suggestions and helping me solve problems so that I could further my research so smoothly without encountering overwhelming difficulties, always being so easy-going when I went to his office and not pushing me, his criticism on science, always being patient to listen to my talking and improving my pronunciation of English, spending much time on correcting my paper and thesis and sometimes even scarifying his weekends. Without his help and supervision, I could not finish my PhD study.

I also want to thank all of members of AG Heilmann group those who has already left or still be here for their help, discussions, and suggestions. I am extremely thankful to my friend Katharina Gerth. During my PhD study, she always helped me translate German protocols to English protocols and taught me how to do those such as plant transformation, qPCR, and so on. We were usually the last two person who left the lab so that we talked and shared lots of things which was a good way to alleviate pressure. I may her succeed in defending her upcoming PhD degree and making a great grade.

I also would like to give thanks to Dr. Mareike Heilmann for helping me perform lipid analysis, ordering antibodies, giving me suggestions, and of course sharing her protocols and materials. I am also thankful to Dr. Praveen Krishnamoorthy for telling me how to use Fiji which I never used before, giving me lots of *A. thaliana* markers, teaching me how to use spinning disc microscope, helping me do some experiments and analyze some data for my paper, and sometimes accompanying me to the Chinese restaurant in Halle.

I also would like to give my great appreciation to Prof. Dr. Bettina Hause (Leibniz Institute of Plant Biochemistry, IPB) for sharing space for my plant growth, and helping me perform immunostaining against FLAG-PI4K $\beta$ 1 line. I would not submit my paper without her help. Although immunostaining was not successful, I still want to thank her for sparing her time to do it. Similarly, I am grateful to Dr. Gerd Hause (MLU Biocenter) for performing electron microscopy studies on some of my samples.

In addition, much thanks to Prof. Gerd Jürgens (University of Tübingen, Germany ) for providing the KNOLLE antibody, and to Dr. Farhah F. Assaad (Technische Universität München, Germany) and Prof. Marie-Theres Hauser (University of Natural Resources and Life Sciences, Vienna (BOKU), Austria) for the GFP-MAP65-3 marker line, Dr. Jean Colcombet (Université Paris-Sud, INRA, France) for kindly sharing the MPK4-YFP, MPK4-myc lines, Prof. Dr. Staffan Persson and Dr. Rene Schneider (University of Melbourne, VIC, AU) for providing the mCherry-TUA5 line and a Fiji macro to analyze microtubule dynamics, Prof. Kirsten Bacia (Martin-Luther-University Halle-Wittenberg, Germany) for access to the spinning disc microscope, PD Dr. Magret Köck and Karin Klar (Martin-Luther-University Halle-Wittenberg, Germany) for access to the isotope laboratories, Dr. Veit Schubert (Leibniz Institute of Plant Genetics and Crop Plant Research, IPK, Germany) for help take images using 3-D SIM.

I also profusely thank China Scholarship Council (CSC) for supporting my four-year stay in Germany, and German Research Foundation (DFG, grant He3424/6 and CRC648 TP B10 for giving access to carry out my experiments.

I also thank all of my Chinese friends who I met during my stay in Halle. We played together, communicated quite often which made me always feel like I was in China and not so lonely.

I would like to specifically appreciate long time waiting, understanding, constant support and encouragement from Dr. Lixia Wang throughout my PhD study. Without those, I could not hold on to end. Will you marry me?

## ACKNOWLEDGEMENTS

---

Last but not least, I would like to give my huge appreciation to my sister, brother, and my parents for encouraging me to finish my PhD study and making me get success. I love you!

**Curriculum vitae**

Name, given name: Lin, Feng  
Gender: Male  
Nationality: Chinese  
Date of birth: 1<sup>st</sup> April, 1986  
Birthplace: Guannan, Jiangsu Province, China  
Work address: Martin-Luther-University Halle-Wittenberg  
Institute for Biochemistry and Biotechnology  
Department of Cellular Biochemistry  
Kurt-Mothes-Str. 3  
06120 Halle (Saale)  
Germany  
Email: feng.lin@biochemtech.uni-halle.de  
Current address: Richard-Paulick-Str.13, 06124 Halle (Saale)

**Education**

09. 2006 - 06. 2010 Bachelor, Nanjing Agricultural University  
09. 2010 - 06. 2013 Master, Nanjing Agricultural University  
02.2014 - present PhD, Martin-Luther-University Halle-Wittenberg  
(CSC scholarship from China). Supervisor, Prof. Dr. Ingo Heilmann.  
Title of Project: The molecular function of cell plate-associated phosphoinositides during plant somatic cytokinesis

**Publications**

1. Gerth K, Lin F, Daamen F, Menzel W, Heinrich F, Heilmann M (2017) Arabidopsis phosphatidylinositol 4-phosphate 5-kinase 2 contains a functional nuclear localization sequence and interacts with alpha-importins.

Plant J 92: 862-878. doi: 10.1111/tpj.13724

2. Gerth K, Lin F, Menzel W, Krishnamoorthy P, Stenzel I, Heilmann M, Heilmann I (2017) Guilt by Association: A Phenotype-Based View of the Plant Phosphoinositide Network. *Annu Rev Plant Biol* 68: 349-374. doi: 10.1111/tpj.13724
3. Lin F, Qu Y, Zhang Q (2014) Phospholipids: molecules regulating cytoskeletal organization in plant abiotic stress tolerance. *Plant Signal Behav* 9(3):e28337. doi: 10.4161/psb.28337.
4. Jiang Y, Wu K, Lin F, Qu Y, Liu X, Zhang Q (2014) Phosphatidic acid integrates calcium signaling and microtubule dynamics into regulating ABA-induced stomatal closure in Arabidopsis. *Planta* 239(3):565-75. doi: 10.1007/s00425-013-1999-5.
5. Zhang Q, Lin F, Mao T, Nie J, Yan M, Yuan M, Zhang W (2012) Phosphatidic acid regulates microtubule organization by interacting with MAP65-1 in response to salt stress in Arabidopsis. *Plant Cell* 24(11):4555-76. doi: 10.1105/tpc.

---

Datum / date

Unterschrift des Antragstellers / Signature of the applicant

**Erklärung/Declaration under Oath**

Ich erkläre hiermit, dass ich die Arbeit selbstständig und ohne fremde Hilfe verfasst, keine anderen als die von mir angegebenen Quellen und Hilfsmittel benutzt und die den benutzten Werken wörtlich oder inhaltlich entnommenen Stellen als solche kenntlich gemacht habe.

I declare that this thesis is my own work entirely and has been written without any help from other people. I used only the sources mentioned and included all the citations correctly both in word or content.

---

Datum / date

---

Unterschrift des Antragstellers / Signature of the applicant